

eScholarship@UMassChan

Neural Diversity in the *Drosophila* Olfactory Circuitry: A Dissertation

Item Type	Doctoral Dissertation
Authors	Lai, Sen-Lin
DOI	10.13028/0tc8-tg27
Publisher	University of Massachusetts Medical School
Rights	Copyright is held by the author, with all rights reserved.
Download date	2026-05-18 13:30:42
Link to Item	https://hdl.handle.net/20.500.14038/31658

A Dissertation Presented

By

Sen-Lin Lai

Submitted to the Faculty of the

University of Massachusetts

Graduate School of Biomedical Sciences, Worcester

in partial fulfillment of the requirements for the degree of

DOCTOR OF PHILOSOPHY

July 31st, 2007

NEURAL DIVERSITY IN THE DROSOPHILA OLFACTORY CIRCUITRY
A Dissertation Presented

By

Sen-Lin Lai

Approval as to style and content by:

Tzumin Lee, M.D., Ph.D., Thesis Advisor

Marc. R. Freeman Ph.D., Chair of Committee

Vivian Budnik, Ph.D., Member of Committee

Paul Garrity, Ph.D., Member of Committee

Gregory Pazour, Ph.D., Member of Committee

Scott Waddell, Ph.D., Member of Committee

Anthony Carruthers, Ph.D.,
Dean of the Graduate School of Biomedical Sciences

Program in Neuroscience

July 31st, 2007

Dedications

To my mom and sisters for their support along the way.

&

To Chien-Hui for her encouragement, support, and endless love.

Acknowledgements

I would like to thank my advisor Dr. Tzumin Lee for not only his guidance and support but also sharing his knowledge and passion of science. I would also like to thank my committee members Dr. Vivian Budnik, Dr. Akira Chiba, Dr. Marc Freeman, Dr. Paul Garrity, Dr. Julia George, Dr. Richard Kollmar, Dr. Gregory Pazour, Dr. Hugh Robertson, Dr. Charles Sagerström and Dr. Scott Waddell for their suggestions on this project. I thank Dr. Steve Hanes for sending the plasmid pSH18-34, Dr. Jun Ma for pBTM116, Dr. Gary Struhl for GF51, and Dr. Norbert Perrimon for P[GawB]; Dr. Liqun Luo for the fly strains *GAL4-GH146* and *Acj6-GAL4*, Dr. Leslie Vosshall for *Or83b-GAL4*, Dr. Reinhard Stocker for *GAL4-GH298*, Dr. Gero Miesenböck for *GAL4-KL107*, and Dr. Kei Ito for *GAL4-MZ699*, *GAL4-NP6115*, *GAL4-NP7175*, and Bloomington Stock Center for various alleles. Thanks current and former Lee lab members for helpful discussions and technical supports.

Abstract

Different neurons and glial cells in the *Drosophila* olfactory circuitry have distinct functions in olfaction. The mechanisms to generate most of diverse neurons and glial cells in the olfactory circuitry remain unclear due to the incomprehensive study of cell lineages. To facilitate the analyses of cell lineages and neural diversity, two independent binary transcription systems were introduced into *Drosophila* to drive two different transgenes in different cells. A technique called 'dual-expression-control MARCM' (mosaic analysis with a repressible cell marker) was created by incorporating a GAL80-suppressible transcription factor LexA::GAD (GAL4 activation domain) into the MARCM. This technique allows the induction of UAS- and lexAop- transgenes in different patterns among the GAL80-minus cells. Dual-expression-control MARCM with a ubiquitous driver *tubP-LexA::GAD* and various subtype-specific GAL4s which express in antennal lobe neurons (ALNs) allowed us to characterize diverse ALNs and their lineage relationships. Genetic studies showed that ALN cell fates are determined by spatial identities rooted in their precursor cells and temporal identities based on their birth timings within the lineage, and then finalized through cell-cell interactions mediated by Notch signaling. Glial cell lineage analyses by MARCM and dual-expression-control MARCM show that diverse post-embryonic born glial cells are lineage specified and independent of neuronal lineage. Specified glial lineages expand their glial population by symmetrical division and do not further diversify glial cells. Construction of a GAL4-insensitive transcription factor LexA::VP16 (VP16 acidic activation domain) allows the independent induction of lexAop transgenes in the entire mushroom body (MB) and labeling of

individual MB neurons by MARCM in the same organism. A computer algorithm is developed to perform morphometric analysis to assist the study of MB neuron diversity.

Table of contents

Chapter I..... Introduction.....	1
Chapter II..... Establishment of the LexA-based binary transcriptional system.....	14
Chapter III..... Lineage analysis of antennal lobe neurons.....	41
Chapter IV..... Gliogenesis in the postembryonic Drosophila brain.....	74
Chapter V..... Morphometric analysis of the Drosophila mushroom bodies.....	91
Chapter VI..... Conclusion.....	105
Reference.....	108
Appendix.....	118

List of tables

Tabel I.....	Characterizations of ALN-GAL4s.....	64
--------------	-------------------------------------	----

List of figures

Figure 1.....	MARCM (mosaic analysis with a repressible cell marker).....	12
Figure 2.....	The Drosophila olfactory circuitry and brain atlas.....	13
Figure 3.....	Dual-expression-control MARCM and LexA-based binary transcriptional systems.....	33
Figure 4.....	GAL4- versus LexA-based binary transcription systems.....	34
Figure 5.....	Comparison of LexA::GAD/lexAop with GAL4/UAS.....	35
Figure 6.....	Differential expression of distinct transgenes in ORNs versus PNs.....	36
Figure 7.....	Labeling of GAL80-minus neurons and glia by dual-expression-control MARCM.....	37
Figure 8.....	Dual-expression-control MARCM with tubP-LexA::GAD and GAL4-GH146.....	39
Figure 9.....	Dual-expression-control MARCM.....	65
Figure 10.....	Characterization of antennal-lobe-neuron-GAL4s.....	66
Figure 11.....	Single cell analysis of antennal lobe neurons.....	68
Figure 12.....	Simultaneous reduction of mPN and type I IN in the later-induced MARCM Nb clone.....	69
Figure 13.....	Notch signaling is involved in the generation of IALN neuronal diversity.....	70
Figure 14.....	Sequential generation of different types of PN in the ventral lineage...	72
Figure 15.....	Hypothetic proliferation model of lateral ALN lineage.....	73
Figure 16.....	Independent labeling of surface and neuropile glial clones.....	87
Figure 17.....	Separated antennal lobe glial lineages.....	88
Figure 18.....	Surface glial MARCM clone analysis	89
Figure 19.....	Proliferation models of gliogenesis.....	90
Figure 20.....	247-LexA::VP16-labeled MB.....	102
Figure 21.....	Generation of a virtual standard MB.....	103
Figure 22.....	Deviation chart of MB.....	103
Figure 23.....	Spatial mapping of core α/β neurons in MBs.....	104

Abbreviations

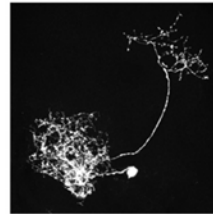
adALN anterodorsal antennal lobe neuron	IN local interneuron
adPN anterodorsal projection neuron;	IALN lateral antennal lobe neuron
AL antennal lobes	lexAop LexA operator
ALN antennal lobe neuron	LG-GH146 LexA::GAD-GH146
ALN antennal lobe neuron	LH lateral horn
ALN-GAL4	LH lateral horn
antennal-lobe-neuron-GAL4	IPN lateral projection neuron
AMMC antennal mechanosensory and motor center	mACT middle antennal-cerebral tract
AN antennal nerve	MARCM mosaic analysis with a repressible cell marker
aPN atypical projection neuron	MB mushroom body
B-PN bilateral projection neurons	MBN mushroom body neuron
de deutocerebrum;	mPN monoglomerular projection neuron
eIN excitatory interneuron	MZ699-vPNGAL4-MZ699 -positive ventral projection neuron
FLP flipase	N neuron
GAD GAL4-activation domain	NGB neuroglioblast
GB glioblast	NP6115-PN GAL4-NP6115-positive projection neuron
GC great commissure;	oACT outer antennal-cerebral tract
GH146-adPN GAL4-GH146-positive anterodorsal projection neuron	oPN oligoglomerular projection neuron
GH146-IPN GAL4-GH146-positive lateral projection neuron	ORN olfactory receptor neuron
GH146-PN GAL4-GH146-positive projection neuron	pilpr posterior inferior lateral protocerebrum
GH146-vPN GAL4-GH146-positive ventral projection neuron	pimpr posterior inferior medial protocerebrum;
GMC ganglion mother cell	pipr posterior inferior protocerebrum
iACT inner antennal-cerebral tract	PN projection neuron
iIN inhibitory interneuron	pPN polyglomerular projection neuron
in ant con inter antennal connective	SOG sub-oesophageal ganglion;
IN local interneuron	type I Acj6-ALN type I Acj6-positive antennal lobe neuron

type I IN type I interneuron
type II *Acj6*-ALN type II *Acj6*-positive
antennal lobe neuron
type II IN type II interneuron
type III *Acj6*-N type III *Acj6*-positive
neuron
UAS upstream activating sequence
vALN ventral antennal lobe neuron
vlpr ventral lateral protocerebrum
vlpr ventral lateral protocerebrum

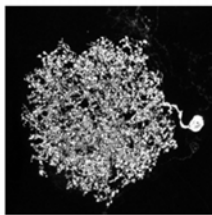
Nomenclature of Neurons



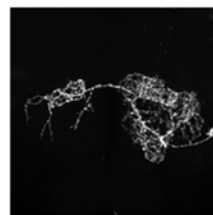
Monoglomerular
projection neuron
(mPN)



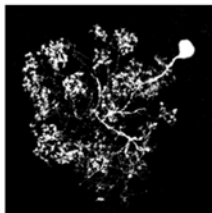
Type I Acj6-positive
antennal lobe neuron
(Type I Acj6-ALN)



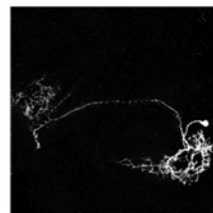
Type I interneuron
(Type I IN)



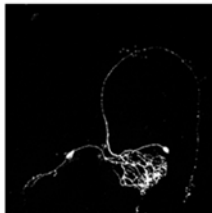
Type II Acj6-positive
antennal lobe neuron
(Type II Acj6-ALN)



Type II interneuron
(Type II IN)



Type III Acj6-positive
neuron
(Type III Acj6-N)



Atypical projection
neuron
(aPN)



Ventrall projection
neuron
(vPN)

CHAPTER I

INTRODUCTION

Neural diversity

Diverse neurons and glial cells in the nervous systems form various structures and numerous synaptic connections as the foundation of our perception, emotion, learning, memory, and movement. Different types of cells in various nervous systems have their unique functions; and depending on different criteria, the cell types in the nervous systems range from hundreds to thousands. Neurons and glial cells can be first classified by their spatial location and connectivity, then be divided based on their general morphologies, and further characterized by the detailed elaboration patterns of their processes. They can also be distinguished by different molecular markers, including various combinations of transcription factors they express during development to acquire their cell fates, and neurotransmitters, receptors and ion channels they use after maturation to propagate information (Anderson, 1992; Jessell and Sanes, 2000). Detailed descriptions of diverse cellular morphologies, their molecular properties and their connectivity should provide insights into different nervous systems work.

The *Drosophila* olfactory circuitry as a model system to study neural diversity

To study the neural diversity, the *Drosophila* olfactory circuitry (Figure 1) can serve as a good model system. The olfactory circuitry comprises peripheral and central nervous systems and both systems are composed of diverse neurons and glial cells (reviewed in Jefferis and Hummel, 2006). The olfactory pathway conveys information from olfactory receptor neurons (ORNs) which are located in the antennae and maxillary palps (Stocker et al., 1990). Each ORN expresses one of 60 odorant receptors, and different odors elicit different combinations of ORNs (reviewed in Hallem and Carlson, 2004). The ORNs expressing the same odorant receptors have convergent axon projections to one of 50 topographically fixed glomeruli in the primary brain structure antennal lobes (AL) where they form synapses with antennal lobe neurons (ALN), including projection neurons (PN) and local interneurons (IN) (Stocker et al., 1990; Stocker et al., 1997; Gao et al., 2000; Vosshall et al., 2000). The PNs target dendrites to one or multiple glomeruli in the AL and extend axons to higher olfactory centers, the mushroom bodies (MB) and lateral horn (LH) (Stocker et al., 1990; Jefferis et al., 2001). The PNs which innervate only one glomerulus form synapses with a single class of ORNs, and they are suggested to transmit the excitatory activity from specific ORNs to the MB and the LH areas (Jefferis et al., 2001; Marin et al., 2002; Wong et al., 2002; Wang et al., 2003; Jefferis et al., 2007; Lin et al., 2007). INs are classified as excitatory INs (eIN) and inhibitory INs (iIN) based on their physiological functions. Both eINs and iINs have extensive arborization of their neurites to ramify the entire AL. These INs were shown to modulate PNs' activity and transform odor code (Wilson and Laurent, 2005;

Olsen et al., 2007; Shang et al., 2007). There are at least four distinct types of MB neurons, γ neurons, α'/β' neurons, pioneer α/β neurons and α/β neurons (Lee et al., 1999; Zhu et al., 2003; Zhu et al., 2006). Each type of MB neurons elaborates dendrites in a particular pattern to form synapses with the axons projected by particular subsets of PNs, and project axons into a unique lobe structure in the MB (Zhu et al., 2006; Jefferis et al., 2007; Lin et al., 2007). Functional studies suggested that different types of MB neuron have different functions during olfactory associated learning and memory (Krashes et al., 2007). The LH is formed by multiple types of neurons and is suggested to integrate excitatory and inhibitory signals from the AL (Tanaka et al., 2004; Jefferis et al., 2007). Besides, various types of glial cells which wrap around different neuropiles also play important supportive roles in the circuitry (Freeman and Doherty, 2006). The specific connections from ORNs through PNs to MB neurons indicate that the odor information is encoded as a spatial profile (topographic map) and transmitted to the brain in totality for interpretations (Vosshall et al., 2000; Gao et al., 2000). Recent studies from excitatory INs have suggested that a temporal profile created in the AL is more crucial for the odor recognition in the brain (Olsen et al., 2007; Shang et al., 2007). These studies demonstrate that characterizations of more distinct types of neurons and glial cells in the olfactory circuitry and identifying how they connect to each other will facilitate our understandings of olfaction.

From lineage to neural diversity

How are diverse cells in the olfactory circuit generated? What are the underlying

molecular and cellular mechanisms to control the generation of neural diversity? Two axes of information, spatial and temporal factors, have been shown to contribute to the generation of neural diversity during development (Pearson and Doe, 2004).

Newly-derived precursor cells acquire their spatial identities based on their anterior-posterior and dorsal-ventral locations in the nervous systems, and use intrinsic or extrinsic temporally regulated cues to produce distinct progeny over times. Consequently, each progeny is determined by its spatial identity rooted in its precursor cell and its temporal identity based on its birth-order and birth timing within the lineage (Pearson and Doe, 2004). Furthermore, the cell-cell interaction between the progeny is also involved in the determination of final cell fate (Artavanis-Tsakonas et al., 1999). Different cell identities are then translated as different genetic expression profiles for cells to obtain distinct cellular morphologies and physiological properties. Therefore, to understand how spatial factors, temporal factors and cell-cell interactions are integrated to diversify cell identities in the nervous systems, it is requisite to acquire the knowledge of neural lineages to establish the ground for experimental studies.

A cell lineage is a pattern of cell divisions and cell fates (Greenwald, 1985). The description of a cell lineage includes the precursor and its descendants, the cell compositions, the birth timing and birth order of the progenies, and the development of the cells (Anderson, 1992). Several methods have been used for cell lineage analysis in different studies, such as direct observation of embryos (Sulston et al., 1983; Sternberg and Horvitz, 1984; Tagher and Goodman, 1984; Doe and Technau, 1993) and ablation of progenitor cells by chemicals or laser to determine their progeny by analyzing structural

deficiencies (Lohs-Schardin et al., 1979; Underwood et al., 1980; Doe and Goodman, 1985a; Doe and Goodman 1985b; Stocker et al., 1997; Armstrong et al., 1998). The progenitor cells can also be injected with different dyes to trace their progeny (Jacobson and Hirose, 1978; Weisblat et al., 1978; Gimlich and Cooke, 1983; Godement et al., 1987; Sanes, 1989; Frank and Sanes, 1991).

Genetic clonal analysis is another commonly used approach to analyze cell lineage. This method often involves the labeling of a patch (or clone) of genetically identical cells derived from a common precursor (reviewed in Blair, 2003; Zugates and Lee, 2004). Induction of recombinases to mediate mitotic recombination between homologous chromosomes in the heterozygous precursor to generate homozygous daughter cells is largely used now for clonal analysis (Golic and Lindquist, 1989; Orban et al., 1992). The inducible system can be coupled with various labeling strategies, such as GAL4/UAS system in *Drosophila* or double markers system in mice, for cell lineage analysis (reviewed in Luo, 2007). The MARCM (mosaic analysis with a repressible cell marker) system was developed for easier clonal analysis. It is a useful and versatile tool to study cell lineage and morphology at single-cell resolution in the *Drosophila* CNS. In MARCM, only one of the two homozygous daughter cells lacks the GAL4 repressor GAL80, has active GAL4 and thus expresses a reporter gene (Figure 2A) (Lee and Luo, 1999; Lee and Luo 2001; Zugates and Lee, 2005). Through mitotic recombination, MARCM can positively label a clone of cells that are derived from a common GAL80-minus precursor cell (Lee and Luo, 1999; Lee et al., 1999) (Figure 2B). Numerous cell-subtype-specific GAL4 drivers, which are controlled by genomic

regulatory sequences, restrictedly express in specific cells (Lee et al, 1999; Jefferis et al., 2001). These GAL4s can selectively label the cells of interest and serve as markers for cell identities (Calleja et al., 1996; Bourbon et al., 2002; Zhu et al., 2006). Moreover, UAS-membrane or cytosolic markers can label the cell morphologies to assist characterization of neural diversity (Yeh et al., 1995; Ito et al., 1997b; Lee et al., 2000b; Wang et al., 2004). In addition, by controlling the timing of mitotic recombination during development, MARCM can also be used to determine the timing of cell birth and the birth order of different cells within any given lineage (Lee et al., 1999; Jefferis et al, 2001; Zhu et al., 2006).

Comprehensive cell lineage analyses of ORNs, PNs and MB neurons (MBN) by the MARCM system with different subtype-specific GAL4s have helped to characterize the cellular and molecular mechanisms to generate neural diversity (Lee et al., 1999; Jefferis et al., 2001; Endo et al., 2007). For example, lineage analysis showed that each ORN selectively expresses specific odorant receptor based on their lineages and cell-cell interactions with their sibling ORNs mediated by notch signaling (Reddy et al., 1997; Goulding et al., 2000; Jhaveri et al., 2000). With the characterization of an enhancer trap line *GAL4-GHI46*, three clusters of PNs that position anterodorsally, laterally and ventrally to the AL are identified (Stocker et al., 1997). The MARCM system revealed that each cluster of *GAL4-GHI46*-positive PNs (GH146-PN) is derived from distinct lineages and the dendrites from different lineages innervate specific subsets of AL glomeruli (Jefferis et al., 2001). Detailed single-cell analysis showed that *GHI46*-PNs which are derived from the same lineages and born at the same developmental stages

target their dendrite to one of the lineage-specified glomeruli in the AL and exhibit stereotyped axon arborization patterns in the MB and LH (Jefferis et al., 2001; Marin et al., 2002; Wong et al., 2002; Jefferis et al., 2007; Lin et al., 2007). Recent studies further demonstrated that their precise targeting are controlled by a unique combination of various cell fate determinants, such as *Acj6*, *drifter*, *chip*, *islet*, *lim1* and *cut* (Komiyama et al., 2003; Komiyama and Luo, 2007). The MB is derived from four identical precursor cells (Ito et al., 1997a; Lee et al., 1999). Studies by MARCM showed that each precursor cell sequentially generates the four types of MBNs, γ neurons, α'/β' neurons, pioneer α/β neurons and α/β neurons, at different stages through larval and pupal development (Lee et al., 1999; Zhu et al., 2003; Zhu et al., 2006). The MBN cell fates are temporally determined by the Chinmo protein concentration gradient during neurogenesis, and the shift of protein concentration gradient can alter the birth timing of different types of neurons (Zhu et al., 2006). These studies have demonstrated how cell lineage analysis contributes to the understandings of the generation of neural diversity. Furthermore, comparisons of ORN, PN and MB neuron lineages show that different lineages use different combinations of temporal factors, spatial factors and cell-cell interactions to diversify their progeny. How other lineages in the olfactory circuitry integrate these factors to diversify their progeny remains unknown.

Study of neural diversity with dual binary transcriptional systems in *Drosophila*

In the olfactory circuitry, although the neural diversity and its underlying mechanisms to diversify cells have been studied in some lineages, several questions

remain unclear. For example, earlier studies estimated that there exist about 150 PNs around the AL but only 90 *GHI46*-PNs have been identified so far, and the rest of them are poorly characterized (Stocker et al., 1997; Jefferis et al., 2001). Studies with Golgi impregnation have demonstrated that many more distinct types of cells also participate in the formation of the AL. Where those cells originate and how they acquire their cell fates remains unknown (Stocker et al., 1990; Stocker, 1994). Besides, within each MB lobes, neurons project their axons and dendrites parallel to each other. There are no obvious morphological differences, and few subtype-specific GAL4s or cell markers can distinguish those MBNs (Tanaka et al., 2004). Connectivity studies have demonstrated that each larval MBN dendrites form stereotyped glomerular structures in the MB calyx and connect to distinct types of PNs (Masuda-Nakagawa et al., 2005). These findings lead us to ask if the same types of MBNs also have distinct spatial distribution in the MB in the adults. In addition, does each of them form specific connections with particular sets of cells?

These questions, however, could not be answered by the MARCM technique due to several limitations of the system. First, the MARCM technique uses subtype-specific GAL4s (e.g. Brand and Perrimon, 1993; Yang et al., 1995; Manseau et al., 1997) to label the cells of interest. Since not all the time all the progeny derived from a single GAL80-minus precursor cell can be detected in MARCM, it is insufficient for a comprehensive lineage analysis. Second, the MARCM system relies on a single binary transcriptional system (GAL4/UAS) and it is impossible to express different UAS transgenes in different types of cells in the same animals, which also prevents us from

studying different types of cells simultaneously. In addition, the original MARCM system cannot label the cells of interest at the single-cell resolution and mark entire neuropile simultaneously with the same GAL4, because the involvement of GAL80 in MARCM limits the concurrent use of another GAL4-based genetic method. For example, without labeling individual MBNs and MB's entire morphology simultaneously or the MB neurons and their connecting cells in the same brain, it is difficult to recognize the neural diversity based on their spatial location and connectivity.

Having another widely applicable noninterfering ectopic binary transcriptional system would provide solutions to some of these limitations. Two independent binary transcriptional systems could permit the targeted expression of distinct transgenes in different patterns in the same organism. If the new system is made GAL80 suppressible, distinct types of GAL80-minus cells can be labeled in different colors at the same time. Furthermore, the incorporation of a GAL4-independent binary transcriptional system with a ubiquitous driver into conventional MARCM would permit a more thorough mosaic or lineage analysis of the cells of interest in the complex CNS. Alternatively, if the new system is insensitive to GAL80, one can control transgene induction independently of MARCM.

In this thesis work, I developed a GAL4-independent binary transcriptional system and demonstrated how the concurrent use of the dual binary transcription systems may facilitate the study of neural diversity in the *Drosophila* olfactory circuitry. In this system, transgenes were put under control of a basal promoter LexA operator (lexAop). By fusing LexA with the strong viral transactivation domain from VP16 or the GAL4-activation

domain (GAD), GAL80-insensitive and GAL80-suppressible transcriptional factors were generated that efficiently drive the expression of *lexAop*-controlled transgenes *in vivo*. The induction of *LexA/lexAop* is comparable to the *GAL4/UAS* in quality and quantity.

Construction of *LexA::VP16* driver allows the expression of *lexAop*-transgenes independently of induction of MARCM clones. By incorporating *LexA::GAD* drivers into MARCM, a new technique called ‘dual-expression-control MARCM’ was developed. Different subtype-specific *GAL4*s and *LexA::GAD* drivers can simultaneously induce the expression of *UAS*- and *lexAop*- transgenes in different patterns among the *GAL80*-minus cells. Incorporation of the ubiquitous driver *tubP-LexA::GAD* in the dual-expression-control MARCM allows us to label all *GAL80*-minus progeny and distinguish the *GAL4*-positive *GAL80*-minus cells at the same time. Also, the entire mosaic pattern and the *GAL4*-negative *GAL80*-minus progeny can be observed in the *GAL80*-minus clones (Chapter II).

By using different enhancer trap *GAL4* lines in MARCM, various types of ALNs were characterized. The concurrent use of these *GAL4* lines and the ubiquitous drivers *tubP-LexA::GAD* in the dual-expression-control MARCM determined the lineage relationships of these ALNs. From one single precursor cell, located at the lateral side of the AL, several distinct types of ALNs are generated. The ALNs derived from the lateral precursor cell are sequentially produced at specific developmental stages. Furthermore, cell-cell interactions between sibling ALNs also affect the cell fate determination (Chapter III).

The other type of cells in the nervous system, glia, also display huge diversity based on their location, morphology and molecular markers (reviewed in Freeman and Doherty, 2006). Cell lineage analysis by MARCM with a glial-specific driver *Repo-GAL4* shows that diverse post-embryonic born glial cells in the central brain region are specified on the basis of their lineages. Dual-expression-control MARCM with *Repo-LexA::GAD* and the drivers specifically expressing in neurons further demonstrates that glial cells are generated from the precursors independent of neuronal lineages (Chapter VI).

Construction of a MB-specific line *247-LexA::VPI6* allows the induction of *lexAop* transgenes in the entire MB and labeling of individual MB neurons by MARCM in the same organism. A computer algorithm was developed to perform morphometric analysis to assist the determination of the spatial location of MB neurons in the neuropile (Chapter V) (Guétat et al., 2006).

These newly developed methods in this thesis work greatly facilitate the analysis of neural diversity in the complex neural lineages, and the results establish the foundation for future genetic and molecular experiments to uncover the underlying cellular and molecular mechanisms governing the generation of neural diversity.

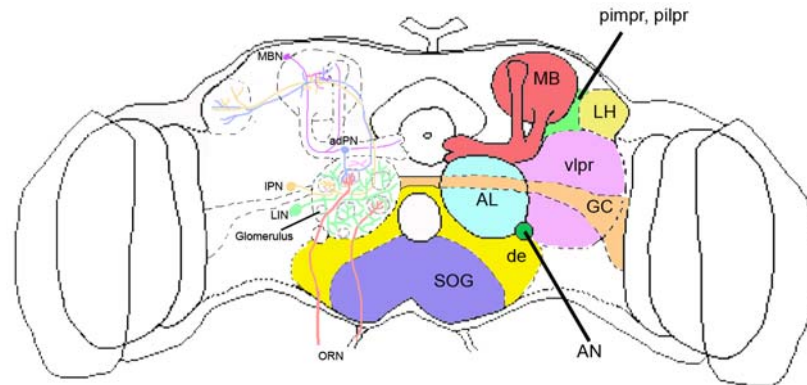


Figure 1. The *Drosophila* olfactory circuitry and brain atlas

Schematic of the olfactory circuitry (left hemisphere) and brain structures (right hemisphere) in the adult *Drosophila*. The olfactory circuitry is exemplified by representative olfactory receptor neurons (red), antennal lobe neurons which includes projection neurons (blue and orange) and interneurons (green), and mushroom body neurons (purple). Various brain structures are outlined by solid- or dash-lines and imposed with different colors. The naming of brain structures follows Otsuna and Ito (2006). Abbreviations: adPN, anterodorsal projection neuron; AN, antennal nerve; AL, antennal lobe; IPN, lateral projection neuron; IN, local interneuron; de, deutocerebrum; GC, great commissure; LH, lateral horn; MB, mushroom body; MBN, mushroom body neuron; pilpr, posterior inferior lateral protocerebrum; pimpr, posterior inferior medial protocerebrum; SOG, sub-oesophageal ganglion; vlpr, ventral lateral protocerebrum.

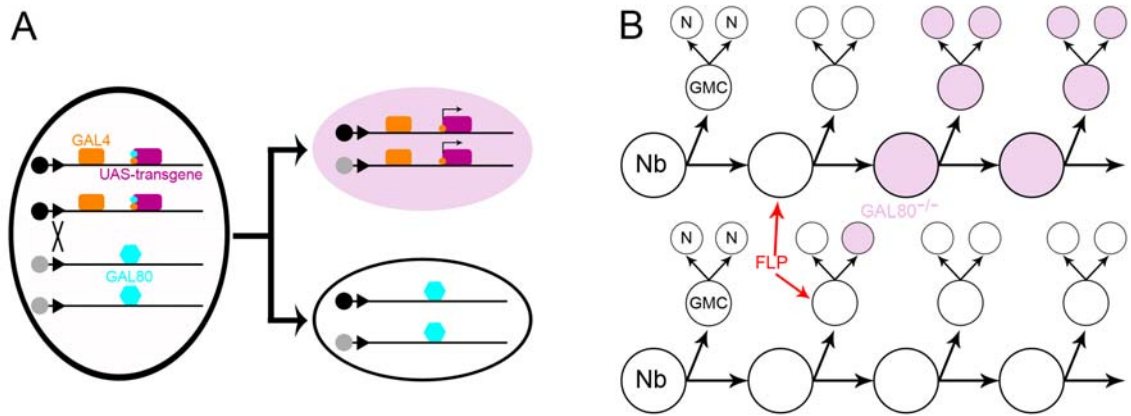


Figure 2. MARCM (mosaic analysis with a repressible cell marker)

(A) Schematic illustration of genetic basis of MARCM. Mitotic recombination mediated by flipase (FLP) in the heterozygous mother cell leads to the loss of GAL80 in one of the two homozygous daughter cells, which allows GAL4 to drive expression of the UAS-fused reporter gene and label the GAL80^{-/-} cell (pink oval). (B) Illustrations of the sizes of MARCM clones. During neurogenesis in the *Drosophila* CNS, a neuroblast (Nb) generates a series of ganglion mother cells (GMC) and renews itself for next cycle of proliferation via asymmetrical division. Each GMC then divides once to produce two post-mitotic neurons (N). The labeled neurons (pink circles in the top panel) in a multicellular Nb clone are derived from a GAL80-minus Nb after FLP-mediated mitotic recombination. Note that if the GMC becomes GAL80-negative after mitotic recombination, the two derived neurons will be labeled as a two-cell clone (not shown). If the mitotic recombination occurs in the dividing GMC, only one of the two daughter cells will be labeled (pink circle in the bottom panel).

CHAPTER II

ESTABLISHMENT OF THE LEXA-BASED BINARY TRANSCRIPTIONAL SYSTEM

Introduction

Genetic mosaic analysis can generate homozygous mutant cells from heterozygous precursors, and it is widely used to determine a gene's functions in an intact organism (Xu and Rubin, 1993; Lee and Luo, 1999; Zugates and Lee, 2004; Zong et al., 2005). MARCM was developed for easier mosaic analysis in the *Drosophila* CNS (Lee and Luo, 1999; Lee and Luo 2001). It is a useful and versatile tool to study both lineage and morphology at single-cell resolution. Through mitotic recombination, MARCM can positively label a clone of cells which are derived from a common GAL80-minus precursor cell (Lee and Luo, 1999; Lee et al., 1999) (Figure 1B). Numerous cell-subtype-specific GAL4 drivers, which are controlled by genomic regulatory sequences, express in specific cells (Lee et al, 1999; Jefferis et al., 2001). These GAL4s can selectively label the cells of interest and serve as markers for cell identities (Calleja et al., 1996; Bourbon et al., 2002; Zhu et al., 2006). Besides, distinct UAS-markers (such as nuclear or membrane marker) can be used independently or jointly to label entire

morphologies as well as different cellular compartments to elucidate more detailed features of the neurons (Yeh et al., 1995; Ito et al., 1997b; Lee et al., 2000b; Wang et al., 2004). By controlling the timing of mitotic recombination during development, MARCM can also be used to determine the timing of cell birth and the birth order of different cells within any given lineage (Lee et al., 1999; Jefferis et al., 2001; Zhu et al., 2006). Moreover, MARCM can label the cells with homozygous mutant genes in unstained heterozygous tissues and help to investigate cell-autonomous functions of the gene (Lee et al., 2000a; Lee et al., 2000b; Wang et al., 2002; Zheng et al., 2003; Wang et al., 2004; Zhu et al., 2006).

However, using subtype-specific GAL4s (e.g. Brand and Perrimon, 1993; Yang et al., 1995; Manseau et al., 1997) to label MARCM clones has potential problems. Because clones are usually generated in a non-tissue-specific manner, MARCM cannot label all GAL80-minus cells without using a ubiquitous GAL4 driver (Figure 3A, left panel). Therefore, it is difficult to distinguish cell-autonomous from non-autonomous phenotypes by examining subsets of mosaic patterns. Since not all the time all the progeny derived from a single GAL80-minus progenitor can be detected in MARCM, it is insufficient for a comprehensive lineage analysis. In addition, most fly genetic or transgenic tools, including MARCM, rely on a single binary transcriptional system (GAL4/UAS) and it is impossible to express different UAS transgenes in different types of cells in the same animals, which prevents us from studying different types of cells simultaneously. The involvement of GAL80 in MARCM further limits the co-application of other GAL4-based genetic and transgenic methods.

Having another widely applicable noninterfering ectopic binary transcriptional system would provide solutions to some of these limitations. Two independent binary transcriptional systems could permit the targeted expression of distinct transgenes in different patterns in the same organism. If the new system is made insensitive to GAL80, one can control transgene induction independently of MARCM. Alternatively, one could label distinct types of GAL80-minus cells in different colors at the same time when both binary transcriptional systems are rendered GAL80 suppressible. Furthermore, the incorporation of a GAL4-independent binary transcriptional system with a ubiquitous driver into conventional MARCM would permit a more thorough mosaic or lineage analysis of the cells of interest in the complex CNS (Figure 3A, right panel).

Here a GAL4-independent binary transcriptional system (Kidd et al., 1998; Szuts and Bienz, 2000) was introduced into the *Drosophila*. How concurrent use of two independent binary transcriptional systems can facilitate various studies in the *Drosophila* nervous system is demonstrated. In this system, transgenes of interest are put under the control of a basal promoter containing eight LexA-binding sites (lexAop) (Estojak et al., 1995). By fusing LexA (Brent and Ptashne, 1985) with VP16 (Triezenberg et al., 1985) or GAD (Ma and Ptashne, 1987), GAL80-insensitive and GAL80-suppressible transcriptional factors are generated and both can efficiently drive the expression of lexAop-controlled transgenes *in vivo* (Figure 3B). The induction of LexA/lexAop is comparable to the GAL4/UAS in quality and quantity. Three distinct LexA drivers are used to demonstrate how combinations of GAL4-dependent genetic tools and LexA-based binary transcriptional systems may help to dissect intricate cellular and molecular

networks in the *Drosophila* CNS. Construction of an *Or83b-LexA::VP16* line allows us to drive the expression of *lexAop* transgenes in olfactory receptor neurons (ORNs) independently of MARCM analysis of their synaptic partners, the projection neurons (PNs) (Stocker et al., 1990; Jefferis et al., 2001). By incorporating LexA::GAD drivers into MARCM, a new technology called ‘dual-expression-control MARCM’ is developed. It permits the induction of distinct transgenes in different patterns among GAL80-minus cells in mosaic tissues. Use of *Repo-LexA::GAD* in dual-expression-control MARCM permits the simultaneous but differential labeling of GAL80-minus neurons and glial cells in intact brains. Lineage analysis with this dual-expression-control MARCM technique suggests the presence of neuroglioblasts in the developing optic lobes but does not support the production of glia by postembryonic mushroom body neuronal precursors. In addition, dual-expression-control MARCM with *tubP-LexA::GAD* allows us to simultaneously label all GAL80-minus cells while marking the GAL4-positive, GAL80-minus cells differentially. One can, thus, detect the entire mosaic patterns and start to visualize GAL4-negative progeny in GAL80-minus clones. Using this approach, we have identified many *GAL4-GHI46*-negative neurons in previously characterized PN lineages.

Material and Methods

New transgenes

(i) *Or83b-LexA::VP16* in *pCaSpeR4*. The *Or83b* promoter region (Wang et al., 2003) was amplified by polymerase chain reaction (PCR) to remove an endogenous Xba I site and subcloned with Kpn I and Not I into *pCaSpeR4* within which the SV40 poly A

region had been inserted. The LexA::VP16 ORF was assembled by subcloning LexA (with Hind III & EcoRI) and VP16 (with EcoRI) (Invitrogen) sequentially into pBS. LexA::VP16 was then subcloned into the *Or83b* promoter-carrying pCaSpeR4 vector with Not I and Xba I as the cloning sites.

(ii) *Repo-GAL4 in pCaSpeR4*. An 8.5-kb genomic fragment immediately upstream of the *Repo* ORF (Xiong and Montell, 1995) was amplified by PCR, and then subcloned into the SV40 poly A region-bearing pCaSpeR4 with Kpn I and Not I to create the pCaSpeR4-*Repo*-poly A vector. *GAL4* was subcloned from pCaSpeR4-tubP-GAL4-poly A (Lee and Luo, 1999) into the pCaSpeR4-*Repo*-poly A with Not I and Xba I.

(iii) *Repo-LexA::GAD in pCaSpeR4*. The GAL4 activation domain (GAD) from amino acid 768 to 881 (Ma and Ptashne, 1987) was amplified by PCR with the primers TTGAATTCGCCAATTTTAATCAAAGTGG and CTGGATCCTTACTCTTTTTTTGGGTTGG and subcloned into pBTM116 (Vojtek et al., 1993) in frame to the 3' of LexA. The fused LexA::GAD was then subcloned into the pCaSpeR4-*Repo*-poly A with Not I and Nhe I/Xba I.

(iv) *tubP-LexA::GAD in pCaSpeR4*. LexA::GAD was subcloned from pBTM116-LexA::GAD into the pCaSpeR4-tubP-poly A (Lee and Luo, 1999) with Not I and Nhe I/Xba I as the cloning sites.

(v) *UAS-mCD8 in pUAST*. The PCR product encoding mouse CD8 (Lee and Luo, 1999) was subcloned into pUAST with Xho I and Xba I as the cloning sites.

(vi) *rCD2::GFP in pLOT*. The *lexA* operator (*lexAop*), amplified from pSH18-34 (Estojak et al., 1995) with the primers of AGCGGATCCTAATCTTACCTCGACTGC and

CAGCAAGCTTATCATCCCTCGACGTAC was ligated with another PCR product containing pUAST's *hsp70* TATA box, multiple cloning sites and SV40 poly A region. The fused fragment was inserted into the BamH I-digested pUAST (Brand and Perrimon, 1993) to create the LexA-responding cloning vector pLOT. rCD2, amplified from GF51 (Wong et al., 2002), was subcloned into the GFP-containing pBS (Lee and Luo, 1999) with KpnI and BamHI as cloning sites, and then pLOT-rCD2::GFP was constructed by subcloning rCD2::GFP into pLOT with EcoR I and Not I.

All constructs were injected into a y^{-},w^{-} strain to generate transgenic flies according to standard procedures (Spradling and Rubin, 1982).

Fly culture, histology and microscopy

Dissection, immunostaining and mounting of larval CNS and adult brains were carried out as described (Lee and Luo, 1999). Primary antibodies used in the study include rat antibody to mCD8 (1:100, Caltag), rabbit antibody to GFP (1:100, Molecular Probes), and mouse monoclonal antibody to Elav (1:100, DSHB) and Repo (1:100, DSHB). Immunofluorescent signals were collected by confocal microscopy and the images were then processed using Adobe Photoshop. The percentages of *GAL4-GHI46*-negative cells in the PN neuroblast clones were calculated by first counting both *GAL4-GHI46*-positive (doubly labeled) and *GAL4-GHI46*-negative (green only) cell bodies from individual focal plans and then obtaining the ratios of the total numbers of cell bodies.

Western blot analysis

For a given experimental condition, ten adult fly brains were homogenized in 50 μ L β -mercaptoethanol-contained Laemmli sample buffer (Bio-Rad). One tenth of the homogenate was analyzed by the SDS-polyacrylamide gel electrophoresis (Laemmli, 1970) and separated proteins were transferred to poly(vinylidene difluoride) (PVDF) membrane (Bio-Rad). The resultant membrane was sequentially incubated with 5% nonfat dry milk in TTBS (Tris-buffered saline with 0.5% Tween 20) at room temperature for 30 min, with rabbit anti-GFP Ab (1:1,000, Molecular Probes) at 4 °C overnight, with HRP-conjugated sheep anti-rabbit Ab (1:5,000, Amersham) at room temperature for two hours, and detected with ECL Western Blotting Detection Reagents (Amersham). The same membrane was then stripped with stripping buffer (2% SDS and 7 μ L/mL β -mercaptoethanol in TBS) at room temperature for 30 minutes and probed with anti-mouse- α -tubulin Ab (1:4,000, Sigma). GFP-containing proteins and tubulin were, respectively, quantified by NIH ImageJ for analysis of western blot results. The averaged relative expression level of GFP from four independent experiments was determined by GFP amount normalized to tubulin amount.

Results

Generation of LexA/lexAop binary transcriptional system

A typical transcriptional activator consists of two separable functional domains, the DNA-binding domain and the transactivating domain (Ptashne, 1988). The activator binds to specific nucleotide sequences via the DNA-binding domain and subsequently activates transcription when the transactivating domain recruits transcription machinery

(Ptashne, 1988). The newly introduced binary transcriptional system is established on *E. coli* protein LexA and LexA-binding sequences, the lexA operator (lexAop). LexA was fused with the viral transcriptional factor VP16 acidic domain (VP16) or GAL4 activation domain (GAD) to generate two chimeric transcriptional factors to control the expression of lexAop-fused transgenes (lexAop-transgene) in *Drosophila* (Figure 3B).

Comparison of LexA/lexAop and GAL4/UAS

To compare the induction ability of LexA/lexAop binary transcriptional system with the GAL4/UAS system in *Drosophila* CNS, four new transgenes, Or83b-LexA::VP16, Repo-GAL4, Repo-LexA::GAD (Figure 4A) and lexAop-rCD2::GFP (Figure 4B), were introduced into the fly genome; Or83b-GAL4 flies were also used (Wang et al., 2003). Or83b-LexA::VP16 was generated by fusing LexA::VP16 with the Or83b promoter, which has been characterized to drive transgene expressed in ORNs (Wang et al., 2003). Repo-GAL4 and Repo-LexA::GAD were generated by fusing different transcription factors with the Repo promoter, an 8.5-kilobase (kb) genomic fragment upstream of the glia-specific gene Repo (Xiong and Montell, 1995). The lexAop-rCD2::GFP reporter was constructed by subcloning the rCD2::GFP open reading frame (ORF) into pLOT, a modified pUAST vector (Brand and Perrimon, 1993) in which the GAL4 upstream activating sequences (UAS) had been replaced with eight repeats of LexA binding sites (lexAop) (Figure 4B). The expression pattern and induction level of UAS-mCD8::GFP (Lee and Luo, 1999) driven by GAL4 and lexAop-rCD2::GFP by LexA::VP16 or LexA::GAD were examined by fluorescent

microscopy and western blot.

Or83b-GAL4 selectively drove the expression of UAS-mCD8::GFP in most olfactory receptor neurons (ORNs) (Wang et al., 2003) and resulted in specific labeling of antennal lobes in the central brain where ORN axons form synapses with the dendrites of projection neuron (PN) (Figure 4C). When LexA::VP16 was fused with the Or83b promoter and induced the expression of *lexAop-rCD2::GFP*, most ORNs were labeled and comparable expression pattern in the antennal lobes was observed (Figure 4D). Endogenous Repo expresses in most glial cells (Xiong and Montell, 1995), and the transgenes fused with the Repo promoter were expected to exclusively express in glial cells. When a nuclear-marker (UAS-nlsGFP) (Shiga et al., 1996) was expressed under the control of Repo-GAL4, nlsGFP specifically labeled Repo-positive glial cells (data not shown). Repo-GAL4 was then used to drive expression of membrane-targeted reporter gene UAS-mCD8::GFP, and mCD8::GFP labeled fluorescent matrixes outlining individual neuropils and their complex sub-compartments in the *Drosophila* CNS (Figure 4F). An analogous glial matrix was observed when *Repo-LexA::GAD* was used to drive expression of *lexAop-rCD2::GFP* (Figure 4G). One goal to introduce LexA/lexAop into flies was to develop GAL80-insensitive or GAL80-suppressible binary transcriptional systems and incorporate it into MARCM to study cell-cell interactions or facilitate complex neuronal lineage analysis. To determine the effects of GAL80 on LexA::VP16 and LexA::GAD, inductions of *lexAop-rCD2::GFP* by Or83b-LexA::VP16 or *Repo-LexA::GAD* in the presence of *tubP-GAL80* (Figure 4E&H, respectively) were examined. *tubP-GAL80*-mediated ubiquitous expression of GAL80 effectively suppresses

most GAL4 drivers in *Drosophila* (Lee and Luo, 1999; Lee et al., 2000a; Lee et al., 200b; Zheng et al., 2003; Wang et al., 2004) and it has been shown that GAL80 blocks GAL4 activity by binding to GAD (Ma and Ptashne, 1985). Consistent with this notion, GAL80 fully suppressed *Repo-LexA::GAD* (Figure 4E) but did not inhibit *Or83b-LexA::VP16* (Figure 4H). Therefore, *LexA::VP16* drives transgene expression irrespective of the presence of GAL80 while *LexA::GAD* and GAL4 can activate transgene expression only in GAL80-minus cells.

The induction levels of GAL4/UAS and *LexA::GAD/lexAop* were then quantitatively compared by analyzing the expression of *UAS-mCD8::GFP* versus *lexAop-rCD2::GFP* in the presence or absence of either *Repo-GAL4* or *Repo-LexA::GAD* (Figure 5). Six independent transgenic lines, three *UAS-mCD8::GFPs* plus three *lexAop-rCD2::GFPs*, were examined. Basal expression patterns of individual lines in the absence of drivers were determined by detecting green fluorescence directly in whole-mount brains (Figure 5A–F), and the levels of driver-dependent induction were quantified by western blot analysis (Figure 5G&H). Compared with the UAS promoter, *lexAop* exhibited higher basal activity (Figure 5G). However, like UAS-transgenes, individual *lexAop* lines exhibited distinct patterns of leaky expression, eliminating the concern that some endogenous transcriptional factors might weakly interact with the *lexAop* promoter (Figure 5A-F). Besides, upon proper induction, the *LexA/lexAop* appeared more potent than GAL4/UAS. Almost two-fold higher induction in the *LexA* system was quantified when various independent reporters were combined with the same driver (Figure 5G), and similar results were obtained with multiple independent drivers

(Figure 5H). In addition, this quantitative analysis confirmed no cross-activation between GAL4/UAS and LexA::GAD/lexAop (Figure 3G).

These results showed that exogenous LexA/lexAop binary transcriptional system, similar to GAL4/UAS, could also be controlled by tissue-specific promoters to target transgenes expressing in specific tissues, and effectively operate as a GAL4/UAS-independent binary transgene induction system.

MARCM-independent transgene induction with LexA::VP16

GAL80-insensitive LexA::VP16 was subsequently examined whether it can work independently of MARCM. ORNs form synapses with PNs in the ALs (Stocker et al., 1990). A single adult *Drosophila* AL consists of 40-50 identifiable glomeruli (Laissue et al., 1999), through which stereotyped synaptic connections are made between different ORNs and distinct PNs (Figure 6A) (Stocker et al., 1990; Jefferis et al, 2001). Using *GAL4-GHI46* (Stocker et al., 1997) in MARCM, one can selectively label GAL80-minus PNs in mosaic brains. When *Or83b-LexA::VP16* and *lexAop-rCD2::GFP* were introduced into such mosaic organisms, most ORNs were consistently and strongly labeled by GFP regardless of the PN mosaic patterns (Figure 6B&C; n = 56). These results demonstrated that LexA::VP16 can mediate MARCM-independent binary transgene induction in mosaic organisms.

Analyses of neurogenesis and gliogenesis with dual-expression-control MARCM

Since GAL4 and LexA::GAD can drive different transgenes at the same time but only in the absence of GAL80, it was possible to concurrently use GAL4 and LexA::GAD in MARCM to differentially label distinct types of GAL80-minus cells in mosaic tissues (example illustrated in Figure 7A). When GAL4 and LexA::GAD exist in a mutually exclusive manner, loss of GAL80 spontaneously leads to expression of UAS-marker gene and lexAop-reporter gene in different cells. Thus, complex mosaic tissues can be analyzed in a more thorough way, permitting direct identification of distinct clones and/or different clonal cells based on their cell fates. For simplicity, the term “dual-expression-control MARCM” is used to describe MARCM with independent controls over two distinct sets of transgenes in GAL80-minus cells.

Dual-expression-control MARCM was then tested to see whether and how it could facilitate mosaic analysis in the complex *Drosophila* CNS. Neurons and glial cells both acquire intricate morphologies and their processes often interweave extensively. To resolve them simultaneously in mosaic brains, *Repo-LexA::GAD* and *lexAop-rCD2::GFP* were incorporated into a neuronal GAL4-based MARCM. Loss of GAL80 should result in the de-inhibition of GAL4 and LexA::GAD activity in neurons and glial cells, respectively, leading to the expression of distinct marker genes in GAL80-minus neurons and GAL80-minus glial cells. Two complex fly stocks were established and subsequently crossed to produce the progeny that carried eight transgenic elements, including two *FRT^{G13}* sites, *hs-FLP*, *GAL4-OK107* (Connolly et al., 1996), *UAS-mCD8*, *tubP-GAL80*, *Repo-LexA::GAD* and *lexAop-rCD2::GFP*. All adult brain cells labeled with *GAL4-OK107* are positive for the neuronal marker Elav (Robinow and White, 1991), and

they mainly constitute the insect olfactory learning and memory center, the mushroom bodies (Connolly et al., 1996; Lee et al., 1999) and the optic lobes (data not shown). In contrast, *Repo-LexA::GAD* exclusively labeled Repo-positive glial cells. After the induction of mitotic recombination during development of these flies, specifically labeled GAL80-minus brain cells in an otherwise unlabeled background were obtained ($n = 115$). No cell was observed doubly labeled with mCD8 and rCD2::GFP (Figure 7B), supporting the notion that *GAL4-OK107*-dependent expression of mCD8 remained restricted to neurons whereas rCD2::GFP driven by *Repo-LexA::GAD* marked only GAL80-minus glial cells (Figure 7C). Despite extensive interlacing of neuronal and glial processes, dual-color labeling made it possible to resolve them unambiguously (Figure 7D). The result shows that concurrent use of two independent GAL80-suppressible drivers in MARCM permits the simultaneous mosaic analysis of distinct types of cells in complex tissues.

To investigate how such dual-expression-control MARCM may help in the lineage analysis of complex tissues, mosaic fly brains with differentially labeled GAL80-minus neurons and GAL80-minus glial cells were further analyzed. Given that isolated multicellular clones are probably derived from single GAL80-minus progenitors (Lee and Luo, 1999; Zong et al., 2005), the identification and analysis of such large clones should provide information about the lineage relationships of distinct brain cells. To investigate if large *GAL4-OK107*-positive neuronal clones would consistently contain certain GAL80-minus *Repo-LexA::GAD*-expressing glial cells, isolated multicellular clones were selectively generated by inducing mitotic recombination weakly at the early first-instar stage. The analysis was focused on the mushroom body and optic lobe regions

where large neuronal clones could be frequently observed. One adult mushroom body is derived from four indistinguishable neuroblasts (Truman and Bate, 1988; Ito et al., 1997a; Zhu et al., 2003). During development, mushroom body neuroblasts repeatedly undergo asymmetric divisions and continuously give rise to postmitotic cells until eclosion (Ito and Hotta, 1992; Lee et al., 1999). Twenty-nine mushroom body neuroblast clones which were specifically labeled with dual-expression-control MARCM were collected and analyzed (for example, Figure 7E-G). Rarely were observed the rCD2::GFP-positive cells in such clones (4 of 29 clones). In addition, large central brain glial clones could sometimes be obtained without the induction of any mushroom body neuronal clone in the same region (for example, Figure 7F) or even throughout the brain ($n = 8$; data not shown) ($n = 8$). In contrast, the large optic lobe clones always consisted of both mCD8-labeled neurons and rCD2::GFP-marked glial cells ($n = 93$; Figure 7H-J). This observation was consistent with the notion that some optic lobe neuropils and glial cells are possibly derived from common precursors, as evidenced by the frequent co-labeling of local neurons and glial cells after flipping out an FRT cassette (Dearborn and Kunes, 2004). These results suggested the possible involvement of neuroglioblasts in optic lobe development, but revealed no glial cell production by postembryonic mushroom body neuroblasts.

Dual-expression-control MARCM with a ubiquitous driver

Use of a subtype-specific GAL4 in conventional MARCM greatly simplifies mosaic analysis of complex nervous systems, but substantially limits what can be

detected. To help resolve this dilemma, an ubiquitous LexA::GAD driver was incorporated into dual-expression-control MARCM to selectively label specific clones (or subsets of daughter cells) and detect the entire mosaic patterns (or all the progeny) at the same time (Figure 3A). Such dual-expression-control MARCM was applied to study antennal lobe PNs (Figure 8A).

Current knowledge about the *Drosophila* antennal lobe PNs and their connectivity is largely derived from the characterization of three clusters of *GAL4-GHI46*-positive PNs around each of the paired antennal lobes (Jefferis et al., 2001). There are about 50, 35 and 6 cell bodies positioned dorsally, laterally and ventrally to the antennal lobe (Jefferis et al., 2001). Conventional MARCM has revealed that each cluster is derived from distinct lineages. Notably, those neurite projection patterns are prespecified based on both the lineages and the timings of birth, as evidenced by the labeling of different stereotyped antennal lobe glomeruli in the PN clones derived from different origins or at different developmental stages (Jefferis et al., 2001). However, many PNs are thought to be negative for *GAL4-GHI46* and remain poorly characterized (Stocker et al., 1990; Stocker et al., 1997; Jefferis et al., 2001). To help identify such *GAL4-GHI46*-negative PNs, *GAL4-GHI46* and *tubP-LexA::GAD* were used in dual-expression-control MARCM. Mitotic recombination was induced at the early first-instar larval stage, and adult brains were examined for their mosaic patterns by dual-expression-control MARCM. In those collected brains, *GAL4-GHI46*-dependent expression of UAS-mCD8 exclusively marked those previously characterized PN clones, whereas *tubP-LexA::GAD*-driven expression of *lexAop-rCD2::GFP* apparently labeled all GAL80-minus cells ($n = 23$ brains; Figure

8B). Further analyzing those tubP-LexA::GAD-positive clones adjacent to antennal lobes, three of them constantly contained GAL4-GH146-positive neuroblast clones ($n = 28$), and had neurites innervating antennal lobes. These neuroblast clones were located dorsal, lateral and ventral to the antennal lobes (Figure 8B). Within each clone, the previously undetected cells (tubP-LexA::GAD-positive GAL4-GH146-negative cells) constituted approximately 39%, 78% and 88% of the dorsal ($n = 7$), lateral ($n = 4$) and ventral ($n = 3$) neuroblast clones, respectively.

Among the dorsal, lateral and ventral neuroblast clones, the lateral ones were most prominent, occupying most of the space between the dorsal and ventral clones (Figure 8C–E). The lateral clones contained many *GAL4-GH146*-negative cell bodies and appeared to innervate all antennal lobe glomeruli (Figure 8D&E). Nevertheless, in the mushroom body calyx where PNs' axons form synapses with MB neurons, few neurites were derived from GAL4-GH146-negative cells (data not shown), while in lateral horns where PNs' axons terminate, some neurites were only labeled by tubP-LexA::GAD (Figure 8F). These observations suggested that the *GAL4-GH146*-negative cells of the lateral clone were possibly antennal lobe interneurons or obtained atypical neurites projection pattern compared to GAL4-GH146-positive PNs. The dorsal clone (Figure 8G-I), in contrast, clearly contained *GAL4-GH146*-negative PNs, as evidenced by the presence of specific green-only glomerular targets in the antennal lobes, such as DA2, DL2, DP11, VC3, VC4, and Vm5v (for example, asterisk in Figure 8H) (Laissue et al., 1999; Couto et al., 2005) and many green-only neurites in the MB calyx (data not shown) and lateral horns (double arrows in Figure 8J).

GAL4-GH146-positive ventral-PNs have their dendrites innervating entire antennal lobes and their axons bypassing MB calyx and terminating at the lateral horns (Jefferis et al., 2001). The entire ventral clone (labeled by tubP-LexA::GAD) also targeted their dendrites to entire antennal lobes and projected their axons directly to the lateral horns (data not shown). These results showed how dual-expression-control MARCM can provide essential information for detailed lineage analysis involving multiple cell fates.

Discussion

Targeted expression can label cells of interest and manipulate gene functions in various controlled manners in intact tissues, and has become a powerful genetic tool to dissect complex cellular and molecular networks in the brain (Duffy, 2002). Two independent binary transcriptional systems (GAL4/UAS and LexA/lexAop), which are used together, can independently induce the expression of distinct transgenes in the same organism. The predictable expression governed by LexA-containing transcriptional factors (Figure 2C-H) and the fact that no cross-activation exists between LexA/lexAop and GAL4/UAS (Figure 5-8) encourage the development of LexA/lexAop as a second widely applicable binary transcriptional system in *Drosophila*. In addition, this dual expression control allows various new types of genetic mosaic studies (Figures 6-8). In particular, the incorporation of a ubiquitous LexA::GAD driver into conventional MARCM permits a more thorough mosaic and lineage analysis in the *Drosophila* CNS (Figures 7 and 8). The recent success in the genetic mosaic analysis of mouse brains with MADM (mosaic

analysis with double markers) (Zong et al., 2005) indicates that advanced fly genetic and transgenic tools could facilitate analogous studies in higher model organisms.

Dual expression control may assist the study of complex biological processes. For instance, a second binary induction system can work independently of existing genetic and transgenic tools, as exemplified by LexA::VP16-mediated, MARCM-independent transgene induction (Fig. 6). In this case, one may spatially control mitotic recombination using LexA::VP16 in combination with *lexAop-FLP*, while analyzing mosaic patterns by MARCM. Additional possibilities include LexA::VP16-governed manipulation of gene functions, followed by MARCM-based single-cell analysis of either autonomous or nonautonomous phenotypes depending on the involved GAL4 driver. Furthermore, one might wish to establish the LexA versions of some GAL4-based genetic and transgenic systems and/or develop future tools based on LexA, instead, for easier coapplication of multiple techniques.

In addition, by incorporating a second binary induction system into existing tools (for example, MARCM), new genetic and transgenic technologies (like dual-expression-control MARCM) can be developed (Figures 7 and 8). Several new modes of mosaic analysis are made possible by dual-expression-control MARCM. For instance, any given mosaic pattern can now be analyzed in two-color channels such that additional information (such as cell fates, clones' real sizes and even the entire mosaic pattern) can be obtained (for example, Figures 7 and 8). A subtype-specific GAL4 should, hereafter, be supplemented with a ubiquitous LexA::GAD driver for thorough analysis of mosaic patterns by MARCM. This is particularly important for distinguishing cell-autonomous

from nonautonomous phenotypes, as well as for the comprehensive analysis of complex lineages. If desired, one can also manipulate gene functions differentially in distinct types of cells within the clones by the independent induction of distinct dominant transgenes. In summary, dual expression control should foster the creation of a new generation of genetic and transgenic tools, which should allow further elucidation of various cellular and molecular networks that govern the generation of neural diversity.

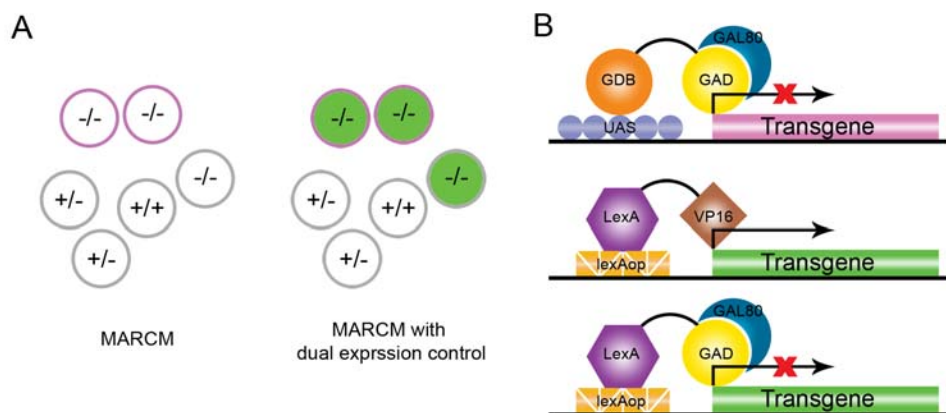


Figure 3. Dual-expression-control MARCM and LexA-based binary transcriptional systems

(A) Schematic illustrations of labeling of specific GAL80-minus cells ($-/-$) (magenta-outlined circles) in conventional MARCM (left) versus identification of both GAL80-minus cells of interest (magenta-outlined green circles) and the entire mosaic pattern (green circles) using MARCM with dual expression control (right). (B) Schematic illustrations of GAL4/UAS and LexA/lexAop binary transcriptional systems. GDB, GAL4 DNA binding domain; GAD, GAL4 activation domain; UAS, upstream activation sequence; lexAop, LexA operator.

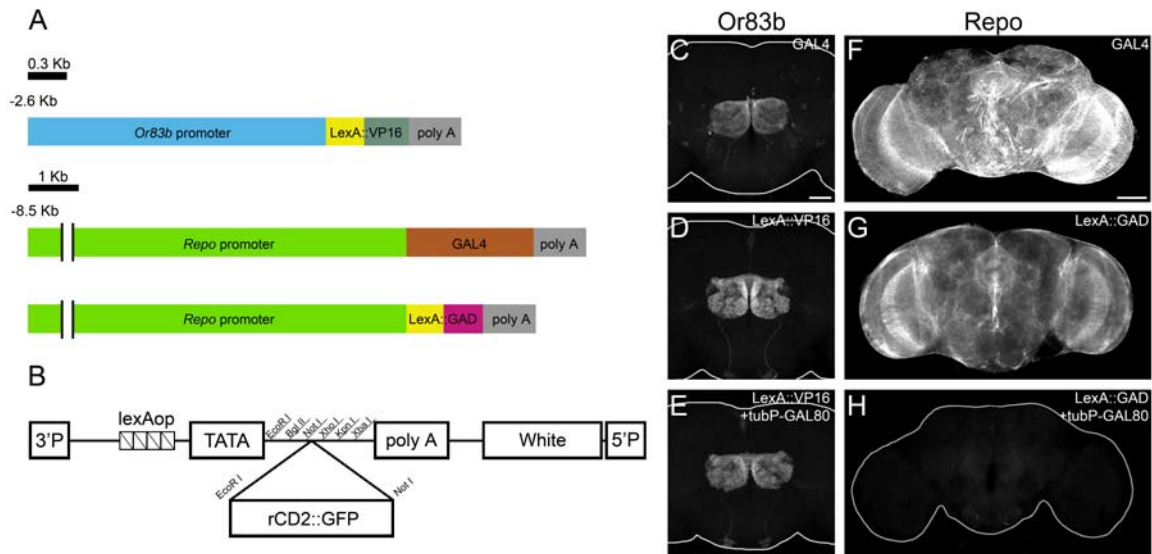


Figure 4. GAL4- versus LexA-based binary transcription systems

(A–B) Schematic illustrations of constructs used to compare GAL4- and LexA-based binary systems. The *Or83b* and *Repo* promoters (cyan and green boxes, respectively) were fused with the ORFs of various bipartite transcriptional factors. In addition, *rCD2::GFP* was put under the control of eight LexA-binding sites (*lexAop*) to generate a reporter gene for LexA-containing transcriptional factors (B). (C–H) Composite confocal images of adult brains showing induction of *UAS-mCD8::GFP* by *Or83b-GAL4* (C) or *Repo-GAL4* (F), and induction of *lexAop-rCD2::GFP* by *Or83b-LexA::VP16* (D, E) or *Repo-LexA::GAD* (G, H). In the absence of tubP-GAL80, the *Or83b* and *Repo* drivers effectively turned on GFP expression in the antennal lobes (C, D) and throughout the glia (F, G). But GAD-containing bipartite transcriptional factors were unable to activate reporter gene expression in the presence of GAL80 (H). In contrast, GAL80 exerted no effect on the induction of *lexAop-rCD2::GFP* by *Or83b-LexA::VP16* (E). Scale bar, 50 μ m in C–E and 100 μ m in F–H.

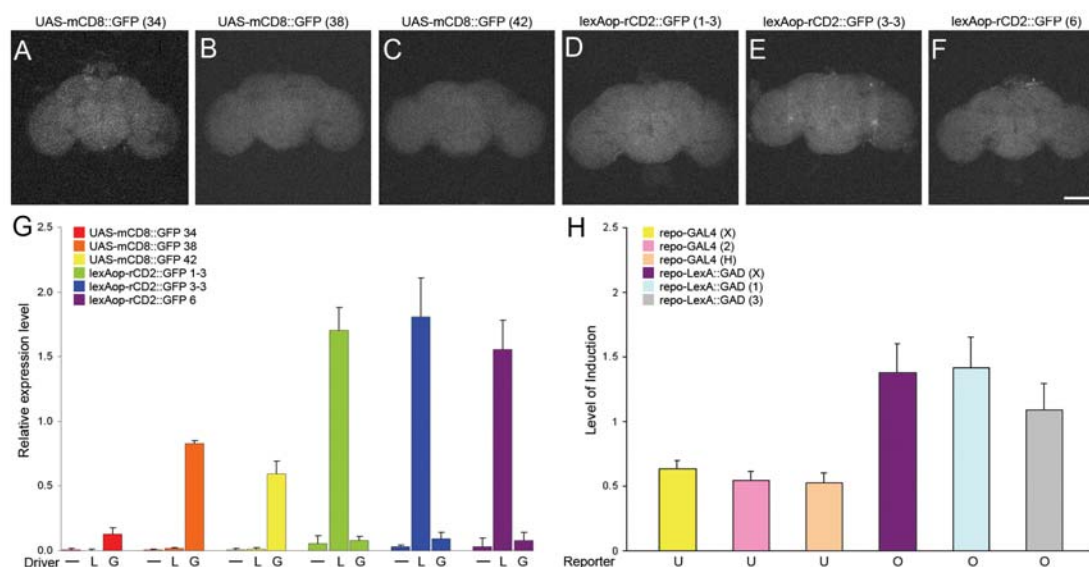


Figure 5. Comparison of LexA::GAD/lexAop with GAL4/UAS.

(A-F) Basal expression of various reporter genes in whole-mount adult brains. (G-H) Quantification of levels of expression by western blot analysis. (G) Six independent reporter genes were tested with different drivers. Reporter genes existed alone (—) or with Repo-LexA::GAD(X) (L) or Repo-GAL4(X) (G). (H) Independent Repo-GAL4 lines and Repo-LexA::GAD lines were used to drive expression of UAS-mCD8::GFP(42) (U) and lexAop-rCD2::GFP(6) (O), respectively. Note that the relative expression level in G was determined by the amount of GFP-containing protein normalized to the amount of endogenous tubulin, and the level of induction in h was derived by subtracting basal expressions from total expressions. Error bars represent standard deviation.

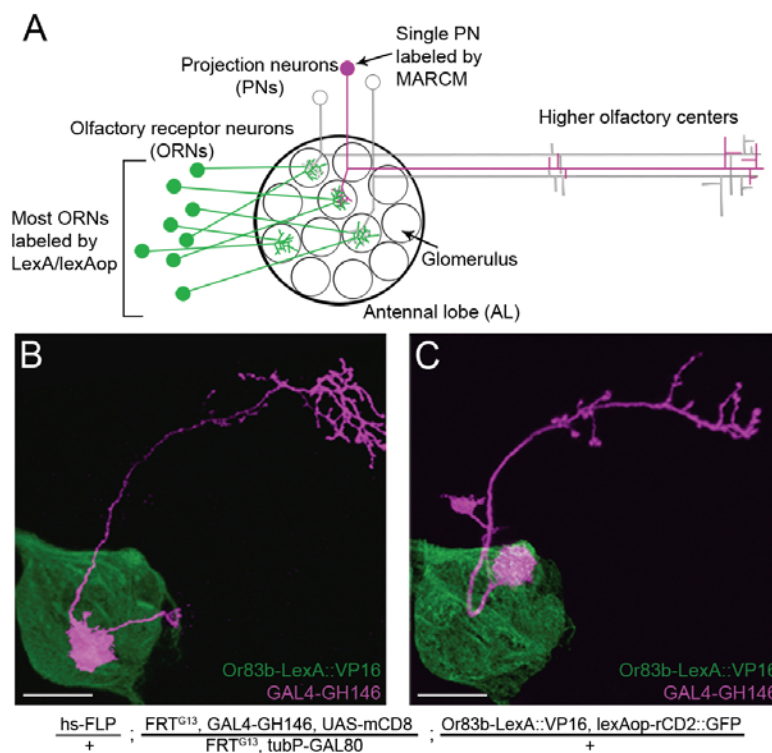


Figure 6. Differential expression of distinct transgenes in ORNs versus PNs

(A) Schematic illustration of the organization of the *Drosophila* olfactory circuitry. Distinct ORNs (green) project their axons to different glomeruli in the antennal lobe to form synapses with specific PNs (magenta and white). Note that LexA::VP16 can permit transgene induction in ORNs (green), independent of MARCM labeling of a single PN (magenta). (B–C) Composite confocal images of the adult ALs, in which ORN axons (green) and representative GAL80-minus single-cell PNs (magenta) were labeled by *Or83b-LexA::VP16*–dependent expression of *lexAop-rCD2::GFP* and *GAL4-GH146*–governed induction of *UAS-mCD8*, respectively. Scale bar, 50 μ m.

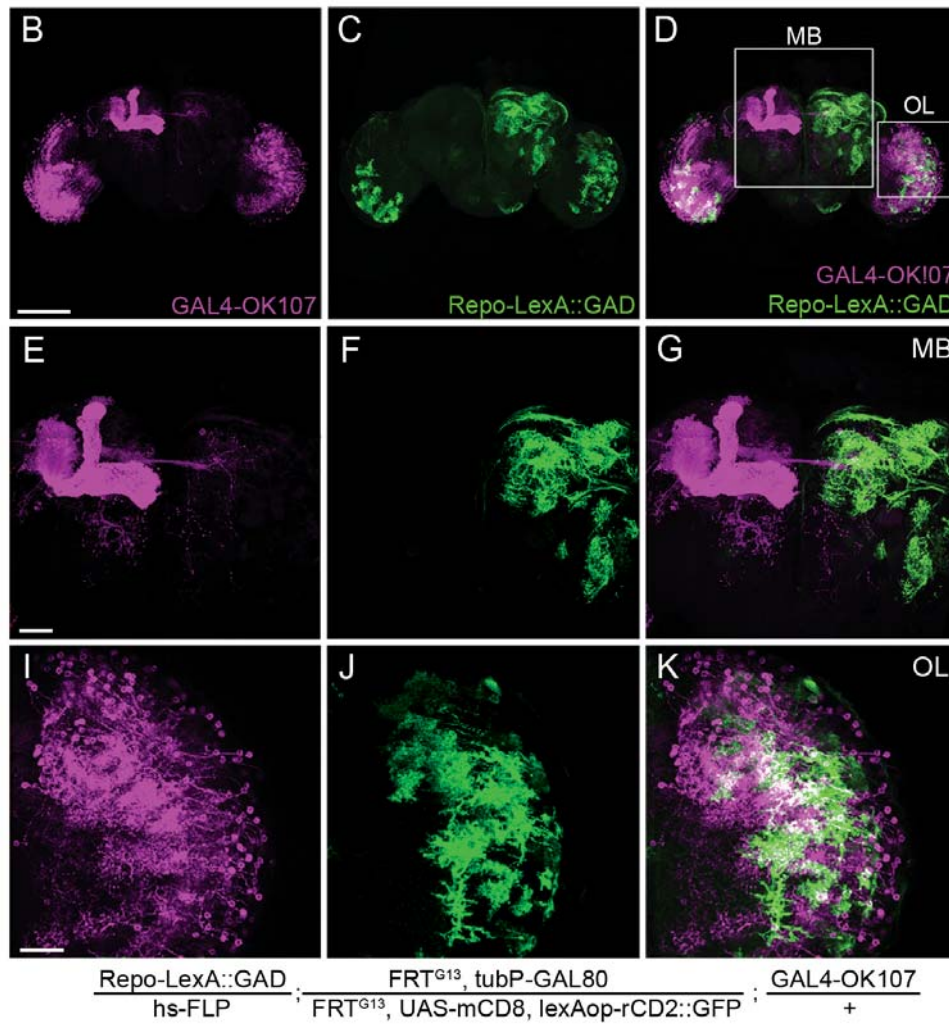
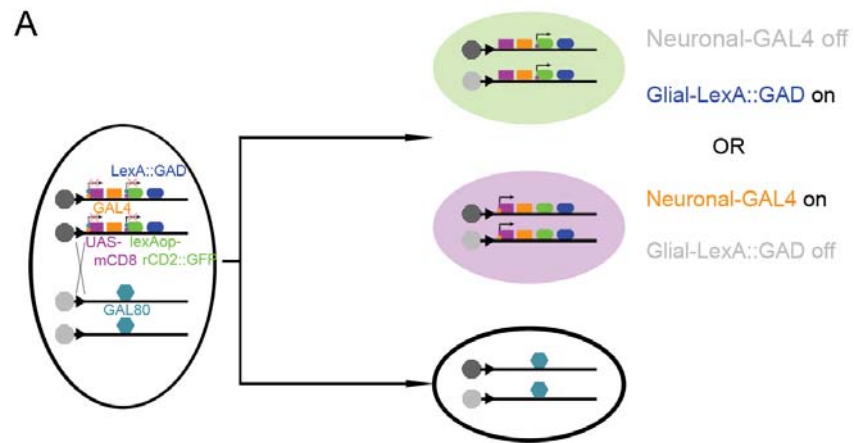


Figure 7. Labeling of GAL80-minus neurons and glia by dual-expression-control MARCM

(A) Schematic illustration of dual-expression-control MARCM. Mitotic recombination leads to loss of GAL80 in one of the two homozygous daughter cells. When glia and neurons express LexA::GAD and GAL4, respectively, LexA::GAD-positive GAL80-minus homozygous glia are labeled differentially from the GAL80-minus homozygous neurons expressing GAL4. (B–J) Composite confocal images of a mosaic adult fly brain, in which GAL80-minus neuronal and glial cells were differentially labeled by dual-expression-control MARCM. Mitotic recombination was induced in newly hatched larvae by brief activation of hs-FLP. The genotype was shown at the bottom. (B, E, H) GAL80-minus neuronal cells labeled by *GAL4-OK107*-driven expression of mCD8 (magenta). (C, F, I) GAL80-minus glial cells marked by *Repo-LexA::GAD*-mediated induction of rCD2::GFP (green). (D, G, J) Merged images. Close-up views of the boxed mushroom body and optic lobe regions in D are shown in E–G and H–J, respectively. There is no doubly labeled cell; the white regions in D, G and J result from merging magenta neurons with green glia from different focal planes. Note extensive mixing of magenta neurons and green glial cells in the optic lobe region (J) but no green glia in or around the large magenta mushroom body clone (G). Scale bar, 100 μ m in B, and 20 μ m in E and H.

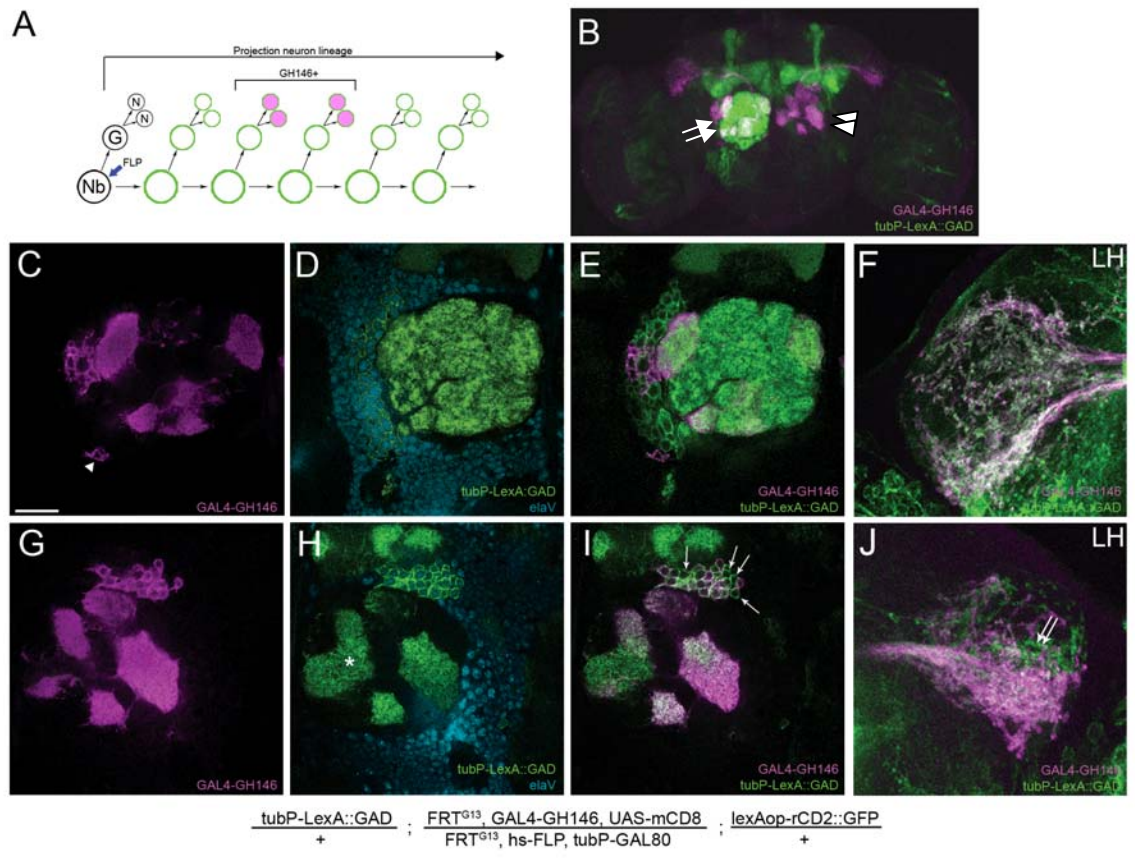


Figure 8. Dual-expression-control MARCM with *tubP-LexA::GAD* and *GAL4-GHI46*

(A) A hypothetical PN lineage yielding both *GAL4-GHI46*-positive (green-outlined pink circle) and *GAL4-GHI46*-negative (green-outlined circle) cells. By dual-expression-control MARCM, one can label all the GAL80-minus progeny using a ubiquitous *LexA::GAD* driver while marking cells of interest with a subtype-specific *GAL4* driver. (B) A mosaic adult brain in which *GAL4-GHI46* (magenta) selectively labels PN clones (double arrows and double arrowheads) while *tubP-LexA::GAD* (green) apparently marks all GAL80-minus cells. Close-up views of the ALs and the corresponding axon terminals in LH are shown in C–F and G–J, respectively. (C–J) Representative confocal images from individual single focal plane showing a lateral *GAL4-GHI46*-positive neuroblast clone (C–F) versus a dorsal *GAL4-GHI46*-positive neuroblast clone (F–J). The expression of *UAS-mCD8* (magenta), *lexAop-rCD2::GFP* (green), and endogenous *Elav* (cyan) are shown. Note the presence of additional *GAL4-GHI46*-positive cells (arrowhead) at the ventral end of the lateral cluster (C), apparent innervation of all the antennal lobe glomeruli by the lateral lineage (D), and few green only neurites at LH (F). Besides, there existed fewer but clear *GAL4-GHI46*-negative PNs in the dorsal lineage, as evidenced by several green-only cell bodies (arrows), one green-only glomerulus (asterisk), and many green only neurites at LH (G–J). In addition, no *Elav*-negative cell body could be found in the *GAL4-GHI46*-positive neuroblast clones (D, H). The genotype was shown at the bottom. Scale bar, 100 μm in B, and 20 μm in C and F.

CHAPTER III

LINEAGE ANALYSIS OF ANTENNAL LOBE NEURONS

Introduction

The *Drosophila* AL is the primary brain structure to integrate and process odor information (reviewed in Stocker, 1994). Studies with Golgi impregnation have identified two types of antennal lobe neurons, projection neurons (PN) which link to higher olfactory centers and local interneurons (IN) which connect between glomeruli (Stocker et al., 1990). The PNs and the INs have different functions in odor information processing. However, most of their origins and development are unclear (Stocker et al., 1995; Stocker et al., 1997; Jefferis et al., 2001).

The PNs exhibit huge morphological diversity and they are categorized by their projection patterns, such as unilateral monoglomerular, oligoglomerular and polyglomerular PNs (mPN, oPN and pPN, respectively) and bilateral projection neurons (B-PN). Most mPNs target their neurites into single glomeruli and extend axons to the MB and LH through inner antennal-cerebral tract (iACT), while some project axons to the LH through middle-ACT (mACT) and bypass the MB. Most of oPNs and pPNs arborize in multiple glomeruli and target axons to the LH via mACT. B-PNs form synapses in the AL, MB, LH and also other brain structures, such as suboesophageal

ganglion and deutocerebrum (Stocker et al., 1990). Different mPNs have been shown to form synapses with different classes of ORNs and these mPNs transmit the odor information to higher olfactory centers (Gao et al., 2000; Vosshall et al., 2000; Jefferis et al., 2001). Some of the oPNs and pPNs are GABAergic neurons and they are suggested to modulate mPNs' activity at the LH to further process the odor information (Tanaka et al., 2004; Jefferis et al., 2007).

LINs do not project processes outward the AL and the extensive arborizations of their neurites ramify the entire AL to form synapses in most of the glomeruli (Stocker et al., 1990). Functional studies have demonstrated that there are two types of INs, GABAergic inhibitory INs (iIN), and cholinergic excitatory INs (eIN). The iINs shape the odor-elicited spatial patterns in the AL by lateral inhibition (Wilson and Laurent, 2005). The eINs broaden the PN-receptive fields by depolarizing the PNs that are not directly elicited by activated ORNs. Although inhibitory and excitatory INs do not exhibit distinct morphologies (Shang et al., 2007), the molecular and functional difference demonstrates the diversity of INs.

How do these ALNs acquire their specific identities when they are born and achieve the diversified morphologies and functions during development? Studies show that each neuron acquires its unique spatial identity rooted in its precursor and temporal identity depending on its birth order and birth timing (Pearson and Doe, 2004). Neuron identities are also affected by cell-cell interactions between sibling neurons (e.g. Spana et al., 1996; Reddy et al., 1997; Skeath and Doe, 1998). To establish the lineage relationships of the ALNs will help us understand how ALNs are diversified.

The mPN lineages are the mostly well studied (Jefferis et al., 2001). Analysis by MARCM with mPN-specific enhancer trap line *GAL4-GHI46* (Stocker et al., 1997) show that *GAL4-GHI46*-positive PNs (*GHI46*-PNs) derive from three independent lineages, which position at the anterodorsal, lateral and ventral sides of the AL (Jefferis et al., 2001). Each *GHI46*-PN exhibits unique dendrite and axon projection patterns that are prespecified by its lineage and birth timing (Jefferis et al., 2001; Marin et al., 2002; Wong et al., 2002). However, lineage analysis of *GHI46*-PNs by dual-expression-control MARCM has shown that *GHI46*-PNs are subsets of the anterodorsal, lateral and ventral ALN lineages (adALN, lALN and vALN, respectively) (Lai and Lee, 2006) (Figure 8 in Chapter II). Most *GAL4-GHI46*-negative ALNs in the anterodorsal and ventral lineages probably obtain similar morphologies as *GHI46*-PNs while the *GAL4-GHI46*-negative ALNs in the lateral lineage may include local interneurons or atypical PNs (Chapter II) (Lai and Lee, 2006).

Several enhancer trap *GAL4* lines were collected to label the ALNs with the MARCM system. Dual-expression-control MARCM with these antennal-lobe-neuron-*GAL4*s (ALN-*GAL4*) and the ubiquitous driver *tubP-LexA::GAD* then determined the lineage relationships of these ALNs. Multiple distinct types of ALNs were observed to derive from one single lALN neuroblast. Single-cell and multicellular MARCM clone analyses in the lateral lineage showed that each type of lALNs was sequentially generated within specific developmental stages. Further genetic studies showed that the sibling ALNs derived from the same ganglion mother cells acquired different cell fates and Notch signaling-mediated cell-cell interactions determined the

sibling ALNs' fates. In addition, newly identified vALNs were observed to target their dendrites to single or multiple glomeruli in the AL and project their axons through mACT to the LH. The vALNs generated at different developmental stages exhibited preferential arborization patterns in both the AL and the LH.

Material and Methods

Generation of the enhancer trap line *LexA::GAD-GHI46*

A modified “transposon swap” strategy (Sepp and Auld, 1999) was used to generate the *LexA::GAD-GHI46* (*LG-GHI46*). The swapping P-element *P[LGawB]* was constructed by replacing *LexA::GAD* (Lai and Lee, 2006) with *GAL4* in *P[GawB]* (Brand and Perrimon, 1993) and then injected into y^-, w^- strain to generate transgenic flies according to standard procedures (Spradling and Rubin, 1982). Following stocks were used to generate the male flies for transposon swap: (1) *P[LGawB]; Pin/CyO*, (2) *GAL4-GHI46*, and (3) *Pin/CyO; Δ2-3, Sb/TM6B, Tb*. Each single male fly with the genotype *P[LGawB]/Y; GAL4-GHI46/CyO; Δ2-3, Sb/+* was then crossed with *UAS-EcR^{DN}* (Cherbas et al., 2003) to cause lethality of the flies carrying *P[GawB]*. The expression patterns were then examined by fluorescent microscopy in the progeny flies, which were produce from the cross of the male candidates and the reporter strain *lexAop-rCD2::GFP* (Lai and Lee, 2006).

MARCM clonal analysis

Larvae collected within 2-4 hours after hatching were cultured at the density of 80

larvae per vial at 25 °C. Wild-type or homozygous mutant MARCM Nb and/or single-cell clones were induced at various developmental stages by heat shock at 38 °C and then examined in adult brains. The fly strains used for various experiments were as follows: (i) dual-expression-control MARCM, (1)*Acj6-GAL4*, (2)*GAL4-GH146*; (3)*GAL4-GH298*, (4)*GAL4-KL107*, (5)*GAL4-MZ699*, (6)*GAL4-NP6115*, (7) *tubP-LexA::GAD;FRT^{G13},UAS-mCD8,lexAop-rCD2::GFP/CyO,Y*, (8)*FRT^{G13},hs-FLP,tubP-GAL80/CyO,Y*, (9)*hs-FLP,UAS-mCD8::GFP;FRT^{40A},tubP-GAL80/CyO*, and (10)*FRT^{40A},LG-GH146,lexAop-rCD2::GFP*; (ii) *notch* and *numb* clone analysis by MARCM, (1)*Acj6-GAL4*, (2)*GAL4-GH146*, (3)*GAL4-GH298*, (4)*GAL4-KL107*, (6)*GAL4-NP6115*, (9)*hs-FLP,UAS-mCD8::GFP;FRT^{40A},tubP-GAL80/CyO*, (11)*tubP-GAL4*, (12)*FRT^{19A},hs-FLP,tubP-GAL80;Pin/CyO*, (10)*FRT^{19A},UAS-mCD8::GFP*, (11)*FRT^{19A},UAS-mCD8::GFP,N^{55e11}/FM7C*, (12)*FRT^{19A},N^{55e11},Acj6-GAL4,UAS-mCD8::GFP/FM7C*, (13)*FRT^{19A},N^{55e11},GAL4-NP6115,UAS-mCD8::GFP/FM7C*, (14)*hs-FLP;FRT^{40A},tubP-GAL80/CyO*, (15)*hs-FLP;FRT^{40A},numb¹/CyO,Y*, (16)*FRT^{40A},numb¹,GAL4-GH146,UAS-mCD8::GFP/CyO,Y*, and (17)*Pin/CyO;UAS-mCD8,lexAop-rCD2::GFP*.

Immunohistochemistry and microscopy

Dissection, immunostaining and mounting of adult brains were carried out as described. Primary antibodies used in the study include rat monoclonal antibody to mCD8 (1:100, Caltag), rabbit antibody to GFP (1:100, Molecular Probes) and GABA (1:1000, Sigma), mouse monoclonal antibody to rCD2 (1:100), Acj6 (1:100, DSHB), nc82 (1:100, DSHB) and ChAT (1:100, DSHB). Immunofluorescent signals were collected by confocal microscopy and then processed using Adobe Photoshop.

Results

Characterization of antennal lobe neurons with various GAL4s

To characterize the antennal lobe neurons (ALNs), several GAL4 enhancer trap lines were collected (Figure 10). The GAL4 in these lines has been reported to express in the neurons which project their processes into ALs; these lines were thus named as *antennal-lobe-neuron-GAL4s* (*ALN-GAL4s*). The *ALN-GAL4s* were first examined if they labeled subsets of *GHI46*-PNs or mostly *GAL4-GHI46*-negative ALNs to avoid repetitive analysis of *GHI46*-PNs. The ALNs and *GHI46*-PNs were differentially labeled by various *ALN-GAL4s* and *LexA::GAD-GHI46* (*LG-GHI46*) in the presence of reporters *UAS-mCD8* and *lexAop-rCD2::GFP*. The *LG-GHI46* enhancer trap line was generated by a modified swap strategy and recapitulated the *GAL4-GHI46* expression pattern in the adult fly brains (Figure 10A-C). Among the *ALN-GAL4s*, *GAL4-GH298* (Stocker et al., 1997) (Figure 10D), *GAL4-KL107* (Shang et al., 2007) (Figure 10G), *GAL4-NP6115* (Figure 10J) and *GAL4-MZ699* (Figure 10R) did not label any *GHI46*-PNs. At the lateral

side, *Acj6-GAL4*-positive neurons (Suster et al., 2003; Jefferis et al., 2007) were observed to locate ventrally to the lateral *GHI46*-PNs (Figure 10M), and these lateral *Acj6*-positive antennal lobe neurons are named as *Acj6*-IALNs. At the anterodorsal side of the AL, *Acj6-GAL4* labeled anterodorsal *GHI46*-PNs as well as *GHI46*-negative cells (Figure 10M).

Various ALN-GAL4-positive neurons were then assigned to anterodorsal, lateral or ventral lineage by dual-expression-control MARCM (Lee and Lai, 2006; Chapter II) (Figure 9). The cell marker *Acj6* (Certel et al., 2000; Komiyama et al., 2003) was used to identify the three ALN lineages which were labeled by the ubiquitous driver *tubP-LexA::GAD*. In the anterodorsal lineage which contains about 73.2 ± 3.4 cells ($n = 4$), every neuron is *Acj6*-positive; in the lateral lineage which includes 193.3 ± 5.7 cells ($n = 8$), the neurons located at the ventral side are *Acj6*-positive; and none neuron in the ventral lineage (49.2 ± 6.2 cells, $n = 5$) is *Acj6*-positive (data not shown). The neuroblast clone which was induced mildly at early first-instar larva showed that the lateral lineage was labeled by *GAL4-GHI46* (Figure 8E in Chapter II), *GAL4-GH298* (Figure 10E), *GAL4-KL107* (Figure 10H), *GAL4-NP6115* (Figure 10K) and *Acj6-GAL4* (Figure 10N); entire anterodorsal lineage was labeled by *Acj6-GAL4* (Figure 10P); and *MZ699-GAL4* expressed in the ventral lineage (Figure 10S).

The cell number and projection pattern of the neuroblast clone labeled by various ALN-GAL4s were then further examined (Table I). The neurite targeting regions were identified on the basis of the new naming system of Otsuna and Ito (2006) (Figure 1 in Chapter I). The MARCM clones labeled by *GAL4-GHI46*, *GAL4-GH298*,

GAL4-KL107 and GAL4-MZ699 were examined in both male and female fly brains and no obvious sexual dimorphism was found (data not shown), consistent with Golgi impregnation (Stocker et al., 1990). Therefore, in the following studies, the MARCM clones were all obtained from adult female flies.

The lateral *GAL4-GH298*-positive neuroblast clone mainly includes about 21 local interneurons, and their neurites ramify throughout the entire ipsilateral AL. They do not extend out from the AL or across the midline to the contra-lateral AL (Figure 10F). The *GAL4-KL107*-positive neurons include nearly 50 local interneurons, and their neurites form apparent glomerular shapes in the ALs (Figure 10I). The neurites do not extend outside the ALs or across the midline to the contralateral AL (Figure 10I).

There are 13 *GAL4-NP6115*-positive ALNs, and they include multiple types of projection neurons (which are named as *NP6115*-PN). Their dendrites innervate the entire ipsi-lateral AL and innervation of the DA3 glomerulus is particularly intense (Figure 10L). Some dendrites cross the midline via the inter antennal connective (*in ant con*) (Strausfeld, 1976) (Figure 10L) and form connections at the ventral posterior side of the contralateral AL (arrow in Figure 10L). *NP6115*-PNs' axons project through the inner antennal-cerebral tract (iACT) to the posterior inferior protocerebrum (pipr) (Figure 10L). Some of the axons form synapses at the MB or LH, and some make a turn around the posterior inferior lateral protocerebrum (pilpr) and further project toward the ventral lateral protocerebrum (vlpr) (arrow in Figure 10L) and terminate in the deutocerebrum (de) (Figure 10L).

There are about 82 *Acj6*-1ALNs. Twelve *Acj6*-positive cells excluded from 1ALN

lineage were later determined to derive from an independent lineage residing lateral-ventrally to IALNs (data not shown). *Acj6*-ALNs comprise multiple types of neurons (Figure 10O). Both sides of ALs are innervated by *Acj6*-IALNs' neurites which pass through the *in ant con*. A process extending outward from the lateral side of the AL project through the outer antennal-cerebral tract (oACT) and terminates in the LH and the pilpr (arrow in Figure 10O). One thick fascicule passes through the great commissure (GC) which is located between the central complex and the oesophagus at the posterior side of the brain and the neurites terminates in both the lateral most ipsi- and the contralateral deutocerebra. At the ipsilateral side, the neurites have a broad innervation in de which includes the antennal mechanosensory and motor center (AMMC), while the neurites at the contra-lateral side are more concentrated (arrowhead in Figure 10O).

The anterior dorsal lineage labeled by *Acj6*-GAL4 is composed of about 75 cells and their projection patterns are identical to the *GHI46*-adPNs (Figure 10Q). Their dendrites innervate *GHI46*-adPN targeted glomeruli and other *GHI46*-adPN-negative glomeruli (for example, DA2, DL2, DP11, VC3, VC4, and Vm5v) in the ALs. The axons project through the iACT to form synapses in the MB and LH (Figure 10P). The 45 *GAL4-MZ699*-positive neurons have their dendrites innervating the entire AL, and their axons project through the middle ACT (mACT), bypass the MB and form synapses at the LH (Figure 10T).

Single cell analysis of lateral ALN lineage

Since the lateral ALN (IALN) lineage was observed to compose of multiple types

of neurons, these ALNs were further analyzed by MARCM to determine if each type of ALN was generated within a particular developmental stage. Because single-cell MARCM clones are the progeny generated from the precursors undergoing mitotic recombination, the birth timing of each type of neuron could be determined by the frequency of observed labeled single-cell MARCM clones which were induced at different developmental stages. Each ALN-GAL4 labeled multiple types of neuron (such as *GAL4-NP6115* in Figure 10L and *Acj6-GAL4* in Figure 10O) and certain types of cells were labeled by multiple ALN-GAL4s (such as ad-mPNs labeled by *GAL4-GHI46* and *Acj6-GAL4*). For consistency and simplicity, the ALNs in the following thesis were then classified and named by their morphologies. The neurons with the same dendrite and axon projection patterns were categorized as the same type and the number of single-cell MARCM clones of different types was tallied from the results of different *ALN-GAL4s*. The frequency of single-cell MARCM clones was normalized as the total number of MARCM clones per 100 brains (Figure 11). Notably, when *GAL4-KLI07* and *Acj6-GAL4* were used to label MARCM clones which were generated after first instar larva, the axons of ORNs could also be observed in the ALs and masked the projection patterns of *GAL4-KLI07*- and *Acj6-GAL4*-positive neurons (data not shown). Since earlier studies have demonstrated that stereotyped connections within the olfactory circuitry are not affected by the deprivation of olfactory input (Wong et al., 2002; Tanaka et al., 2004; Berdnik et al., 2006), the antennae and the maxillary pulps of newly eclosed adult flies are surgically removed and these treated flies were then kept in 25 °C for 7 days to allow the ORN axons to degenerate (Wong et al., 2002; Tanaka et al., 2004; Berdnik et al., 2006;

MacDonald et al., 2006) to reveal the morphology of these ALNs.

In the single-cell MARCM clone analysis (Figure 11), the neurites of *GH298-LIN* was observed to ramify throughout the entire AL. *KL107-GAL4* express in two types of AL interneurons. The morphology of the first type is the same as the *GH298-LIN*, and this type of interneuron is named as type I interneuron (type I IN). The neurites of the second type of *GAL4-KL107*-positive interneurons show obvious glomerular shapes and these interneurons are named as type II interneuron (type II IN). The type I INs are generated from the time of larva hatching and continues until mid-third instar larva stage. The type II INs are generated from late first instar larva (about 1 day after larval hatching) until mid-third instar larval stage. The early born type II INs form synapses with every glomerulus in the AL while some of the later born type II INs do not target their neurites to the entire AL (data not shown). It is not yet known if those later born type II INs form stereotyped connections with specific glomeruli.

GH146-IPNs are generated from second instar larva until middle third instar larva (Jefferis et al., 2001, Figure 11). *NP6115*-PNs are composed of multiple subtypes of PN. Some of them are mPNs, and their dendrites innervate the DA3 glomerulus and their axons form connections in the MB and LH (data not shown). They are born within the window when *GH146*-IPNs are generated (data not shown). Other *NP6115*-PNs have atypical projection patterns. For example, one type of atypical PN (aPN) targets dendrites to the posterior ventral side of both the ipsi- and contralateral AL, connected by the *in ant con*. This type of aPN projects its axon toward the pipr and then targets to the vlpr and the de (Figure 11). These *NP6115-GAL4*-positive aPNs are born at third instar larval stage

(Figure 11).

Acj6-IALNs include at least three different types of identifiable neurons. The first type of *Acj6*-IALN, which is named as type I *Acj6*-ALN, has neurites innervating the entire ipsi-lateral AL and no obvious glomerular shape is observed. A process was found to project from the AL through the oACT and to target the pilpr. The type I *Acj6*-ALN can only be generated by MARCM within the first two days after larva hatch (Figure 11). The second type of *Acj6*-ALN, which is named as type II *Acj6*-ALN, project their neurites to both sides of the ALs by passing through the *in ant con*, and the neurites are concentrated at the posterior ventral side of the ALs. The type II *Acj6*-ALNs are also born within first two days after larva hatch (Figure 11). The neurites from the third type of *Acj6*-ALNs do not innervate the AL at all even though these neurons are also derived from the IALN lineage, and this type of neuron is thus named as type III *Acj6*-positive neuron (type III *Acj6*-N). The type III *Acj6*-N has neurites innervating both ipsi- and contralateral de by passing through the GC. This type of neuron is generated from late second instar larva until late third instar larva and the single-cell MARCM clone is frequently labeled at mid-third instar larval stage (Figure 11).

After compiling the results of MARCM single-cell clone analysis, it drew our attention that type I INs, type II INs and mPNs were generated within the same 24-hour interval at second instar larva (boxed grey area in Figure 11). It is possible that these four types of neurons are generated sequentially, and the different developmental rate among different larva and the persistence of flipase activity affects our single-cell MARCM clone analysis. To address the issue, a complementary approach was taken. Here the

multicellular neuroblast clones which were generated at second instar larva were specifically labeled with two different types of neurons such as mPNs and INs, and these neuroblast clones were examined to determine the cellular composition. If one type of neuron (such as type I IN) finishes generation before the other type (such as mPN), the examined neuroblast clones should either contain only later born neurons (mPNs) or include both types of neurons in which there are fewer early born neurons (type I INs) and a complete set of later born neurons (mPNs). The fly strain which carries *LG-GH146/lexAop-rCD2::GFP* and *GAL4-GH298/UAS-mCD8* was therefore created to label mPN and type I IN simultaneously with dual-expression-control MARCM. In one of the three examined neuroblast clones ($n = 156$ brains) (Figure 12), there were 21 mPNs and 13 type I INs labeled (Figure 12D–F) and both types of cells were fewer than those in the neuroblast clones generated at early first instar larva (35 mPNs and 21 type I INs) (compared to Figure 12A–C). The reduction of mPNs was further confirmed by the disappearance of glomeruli which were specifically innervated by later mPNs (Figure 12D compared to 12A). The other two neuroblast clones included 30 mPNs and 18 type I INs, and 12 mPNs and 5 type I INs, respectively (data not shown). The simultaneous reduction of mPNs and type I INs in the later-generated MARCM neuroblast clones indicated that the generation of mPNs did not follow the completion of birth of type I INs.

Cellular and molecular mechanisms generating neuronal diversity in the IALN lineage

Several studies have demonstrated that during neurogenesis Notch signaling is a

fundamental mechanism to mediate cell fate decisions when sibling cells acquire different cell fates in the *Drosophila* CNS and PNS (Uemura et al., 1989; Spana and Doe, 1996; Skeath and Doe, 1998; Endo et al., 2007). If mPN and type I IN are derived from the same GMC, down-regulation or hyper-activation of notch activity would change the numbers of mPN and type I IN in the lALN lineage at the expense of their sibling cells. If the GMC generates two identical daughter cells in a variant sequence, manipulation of Notch activity would not alter the cell composition of the lALN lineage. An amorph allele N^{55e11} (Kidd et al., 1983) was used in the MARCM system with various ALN-GAL4s to label the *notch*^{-/-} neuroblast clones except *GAL4-KL107* (Figure 13). The *notch*^{-/-} lALN neuroblast clones could be labeled by *GAL4-GH146* (Figure 13A) and *GAL4-NP6115* (Figure 13B). It was noted that total cells labeled by *GAL4-GH146* in the *notch*^{-/-} lALN neuroblast clones increased ($n = 7$) when compared to the wild-type MARCM neuroblast clones (Figure 13A), and *GAL4-NP6115*-positive neurons also increased ($n = 3$) (Figure 13B). The projection patterns of the dendrites and axons from the *GAL4-GH146*- or *GAL4-NP6115*-labeled *notch*^{-/-} neuroblast clones were comparable to the wild type clones (compare Figure 13A to Figure 8B, and Figure 13B to 10L, respectively). In contrast, no *GAL4-GH298* ($n = 30$ brains), *GAL4-KL107* ($n = 28$ brains) or *Acj6-GAL4* ($n = 26$ brains) labeled neuroblast clones were observed to locate at the lateral side of ALs (data not shown). The disappearance of *Acj6*-ALNs was further confirmed by the observation that no cells in the *tubP-GAL4*-labeled *notch*^{-/-} lALN neuroblast clone were *Acj6*-positive ($n = 3$) (Figure 11C). In the mosaic brains with substantial reduction of *Acj6*-positive cells at the lateral-ventral side of AL, *GAL4-GH298*

($n = 4$) and *GAL4-KL107* ($n = 3$) did not label any cell in the IALN lineage (data not shown). Furthermore, the dendrites derived from the *tubP-GAL4*-labeled *notch*^{-/-} lateral neuroblast clone did not innervate the entire AL (Figure 13C) and only those glomeruli whose locations and shapes were pre-specified to be the targets of lateral mPN neurites were observed (Figure 13C). Their axons projected only through iACT and sprouted at the MB and LH (Figure 13D), and a thin process was also observed to target to vIpr (data not shown). These results also indicated that the mPNs and aPNs remained in the *notch*^{-/-} IALN neuroblast clone while INs and *Acj6*-ALNs disappeared.

Notch activity has been shown to be inhibited by the Numb protein, and the asymmetrical partitioning of Numb protein from the GMC into one daughter cell results in the sibling cell to acquire Notch signaling (reviewed in Guo et al., 1996). If Notch activity determines the cell fate of type I and type II INs and *Acj6*-ALNs, removal of Numb protein should make the Notch signaling active in all progeny and increase the cell number of INs and *Acj6*-ALNs. The amorphic allele *numb*¹ (Uemura et al., 1989) was thus used in the MARCM system to generate *numb*^{-/-} neuroblast clones. The neuroblast clones generated at early first instar larva could be labeled by *GAL4-GH298* (Figure 13E), and *GAL4-KL107* (Figure 13F). Counterstained with the cell marker *Acj6* in the above mosaic brains also showed the increase of *Acj6*-positive cells (Figure 13E&F). However, in the mosaic brains whose *Acj6*-positive cells located at the lateral side of AL were observed to increase, no lateral-*GHI46*-mPNs were found to ($n = 3$) (data not shown). These results further confirmed the involvement of Notch signaling in the ALN lineage diversification.

Ventral lineage analysis

Dual-expression-control MARCM showed that there are approximately fifty cells in the ventral lineage, and the entire lineage could be labeled by *GAL4-GHI46* and *GAL4-MZ699* (Table I). The general morphology of the *GAL4-MZ699*-positive ventral projection neurons (*MZ699*-vPNs) is similar to *GAL4-GHI46*-vPNs; *MZ699*-vPNs project their dendrites to the AL, target their axons toward the LH through mACT, and bypass the MB calyx (Figure 10T).

Serial single-cell MARCM clone analysis revealed that vPNs include mPNs, oPNs and pPNs. Each vPN born at a different developmental stage has its unique dendrite and axon projection pattern (Figure 14). For example, the early born vPN (approximate at first instar larval stage) innervates oligo-glomeruli without obvious glomerular shapes (Figure 14A). The vPNs born at early second instar larval usually innervate single glomerulus, such as DA1 (Figure 14B), VA2 (Figure 14C), V and VA11m (data not shown). Their axons spread in the LH and it has not been characterized if they have preferential areas in the LH. The vPNs born at early third instar larva target their dendrites evenly in the entire AL (Figure 14D), and their axons form synapses in the LH and further project anteriorly toward the midline to terminate in the anterior-inferior-medial protocerebrum (arrowhead in Figure 14D). The vPNs generated at mid-third and late-third instar larva both innervate their dendrites into oligo-glomeruli (for example, 14E and 14F, respectively) and no obvious glomerular shapes were observed. However, the terminal axonal processes are distinct. The axons derived from

the vPNs generated at mid-third instar larva project along the ventral side of the LH (arrow in 14E) while the later born vPNs' axons terminate at the dorsal side of the LH (double arrows in 14F). The results of lineage analysis showed that the vPNs born at different developmental stages acquire distinct neurite projection patterns.

Discussion

Diverse ALN lineages and spatial identity

The *Drosophila* ALs are formed by diverse neurons. Lineage analyses demonstrated that three ALNs lineages, which included *GHI46*-PNs, located anterodorsally, laterally and ventrally to the AL (Figure 10). Other lineages have also been found to participate in the formation of the AL, and they do not include *GHI46*-PNs (for example, Ng et al., 2004). Dual-expression-control MARCM with various enhancer trap GAL4 lines further showed the three lineages containing *GHI46*-PNs had distinct cellular compositions. The adALN lineage is composed of mPNs which form synapses with the MB and LH (Figure 10). The vALN lineage comprised mPNs, oPNs and pPNs, all of which project through mACT to target to the LH (Figure 14). The lALN lineage consists type I INs, type II INs, mPNs, aPNs, and Acj6-ALNs (Figure 10 & 11). The differences of these ALN lineages in the cellular composition indicate that each lineage is spatially specified based on their geographical position in the spatially patterned CNS.

It is noted that the same cell fate determinants may result in different types of cells in different lineages. Earlier studies have shown that anterodorsal *GHI46*-PNs require the transcription factor Acj6 to specify their cell identities (Komiyama et al.,

2003). However, Acj6-positive cells in the lateral lineage are not mPNs and have distinct projection patterns (Figure 10 & 11). Besides, both adALN and lALN lineages generate mPNs which project axons through the iACT to the MB and LH (Figure 10 and 11). Since adALN and lALN lineages are spatially specified, there might exist a common cell fate determinant, which is required for both lineages to determine mPN cell fates. However, mPNs from different lineages are prespecified to exhibit specific projection patterns (Jefferis et al., 2001; Marin et al., 2002; Wong et al., 2002). These results indicate a common feature for cell fate determination: the spatial identity rooted in each precursor set the tone for each lineage and other factors exert different effects based on the lineages to diversify the cell fates. How spatial identity and other cell fate determinants integrate to specify cell identity needs further investigations.

Temporal identity in the ALN lineages

How does the lateral lineage generate so many distinct cell-types? Single-cell analysis by the MARCM technique in the lateral lineage showed that the early-generated neurons were type I INs, type II INs and mPNs were born later, and type III Acj6-Ns and aPNs were born before pupae formation (Figure 11). Besides, vALNs born at different developmental stages also show preferential projection patterns (Figure 14). Earlier studies have also shown that anterodorsal *GHI46*-PNs born at different developmental stages acquire distinct cell fates. The results of the sequential generation of distinct types of cells within a lineage indicate that there exist temporal factors in each lineage, which are used to determine the temporal identities of the progeny.

Studies have characterized two types of temporal codes in the *Drosophila* CNS, the *Hunchback* (*Hb*) → *Krüppel* (*Kr*) → *Pdm* → *Castor* (*Cas*) signaling cascade and the Chinmo protein gradient. The *Hb* signaling cascade expresses in the Nbs and is inherited in the progeny. The cells inheriting different transcription factors acquire different temporal identities and exhibit different molecular properties (Isshiki et al., 2001; Pearson and Doe, 2004; Karcavich, 2005). Chinmo protein gradient has been shown to establish in the sequentially generated post-mitotic cells. The postmitotic neurons born at different timings follow their initial temporal cell fate specification to synthesize specific amounts of Chinmo protein (Zhu et al., 2006). The Chinmo protein is also synthesized in the anterodorsal *GHI46*-PNs to specify their identities (Zhu et al., 2006), however *Kr* does not involve the specification of *GHI46*-PNs (Komiya and Luo, 2007). Although these results suggest that ALN lineages do not use the *Hb* signaling cascade as the temporal code, the effects of *Kr* on other ALNs such as INs or *Acj6*-ALNs requires further study. Whether other ALNs also acquire their temporal identity by Chinmo protein is under investigation.

Proliferation model of the IALN lineage

Notch signaling has been shown as a generic mechanism to diversify sibling cell fates, one sibling has the active Notch signaling and acquires the 'A' fate, and the other sibling has no Notch signaling and acquires the 'B' fate (Artavanis-Tsakonas et al., 1999). The shift of cellular composition by manipulating Notch activity indicates that type I INs, type II INs and *Acj6*-ALNs need activated Notch signaling to acquire the A

fate, and for simplicity, these cells are called ‘series A cells’ (Figure 13E & F). In contrast, the B fates of mPNs and aPNs are determined when Notch signaling is down-regulated, and these cells are called ‘series B cells’ (Figure 13A-D). These results showed that the cell fates of lateral ALNs were also determined by Notch signaling-mediated cell-cell interaction between ALN progeny. However, whether Notch signaling also determines the cell identities in the adALN and vALN lineages is unknown.

Notably, there are more series A cells (about 140 cells) than series B cells (about 50 cells). The different cell number of these two series cells leads the proposal of two models of proliferation (Figure 15). In the first model, the lateral ALN neuroblast divides to generate one GMC, and the GMC gives rise to two cells with A or B fate which is determined by differential activity of Notch signaling. The unequal cell number leads us to hypothesize that many cells which require the down-regulation of Notch activity are not characterized in this study. However, the total cell number in the lateral lineage (approximate 200 cells) is near to the summation of series A cells and series B cells. This observation indicates that not many cells in the lateral lineage remain uncharacterized. Notch signaling has been shown to induce apoptosis in one of the two daughter cells in the *Drosophila* neuroblast 7-3 lineage (Lundell et al., 2003; Karcavich and Doe, 2005). This finding suggests that those unidentified cells could undergo apoptosis after birth or during metamorphosis (Figure 15A). By estimation, there are as many as 100 apoptotic cells in the lALN lineage. If the model is correct, it will be interesting to understand why so many cells undergo apoptosis during development.

In the other model, the lateral ALN neuroblast divides to generate one GMC, and

the GMC will divide asymmetrically once to produce a post-mitotic neuron and a secondary GMC. The secondary GMC divides one more time to generate two post-mitotic neurons, which means that at least three cells are generated per cycle of neuroblast division (Figure 15B). In this model, there are not many cells remaining uncharacterized. A similar model of proliferation has only been observed in the PNS progenitor cells (Bellaïche and Schweisguth, 2001). This unconventional model requires more evidence to support it. Furthermore, whether the Notch signaling is also used in the division of secondary GMC needs further study.

Several approaches should allow us to distinguish between these two models. For example, one can trace the lateral ALN neuroblast by live imaging to determine the number of cells generated during each cycle of neurogenesis. Alternatively, one can block apoptosis with apoptosis inhibitors such as P35 (Hay et al., 1994) or removal of apoptotic genes during development, and determine how many extra cells can be rescued in the lateral lineage. The other approach will require a more sophisticated genetic technique, which allows us to visualize both GAL80-plus and GAL80-minus clones by differential labeling. One can thus examine how many GAL80-plus cells associate with the GAL80-minus neuroblast clones in such a system and determine the proliferation model of the IALN lineage.

In summary, the lineage analyses of ALN lineages demonstrate how ALN precursor cells integrate spatial factor, temporal factor and cell-cell interaction to diversify the progeny. The precursor cells are specified by their spatial locations in the spatially patterned embryonic CNS when they are generated. These precursor cells then

use temporal codes to generate diverse nerve cells during neurogenesis in an invariant sequence. The lateral ALN lineage further partition Numb protein to one of the two ALNs to differentiate Notch signaling activity and diversify the cell identities of the progeny. The integration of all three mechanisms to diversify progeny within a lineage has been observed in the *Drosophila* embryonic CNS (Spana and Doe, 1996; Skeath and Doe; 1998; Schuldt and Brand, 1999; Karcavich and Doe, 2005), and it is first observed in the larval brain. Whether other lineages use the same strategies requires further detailed analyses of cell lineages.

As expected, the entire specification process requires the expression of unique genetic profiles at different stages in different cells. Studies have shown that each neuroblast in the late embryonic CNS expresses a unique combinatorial set of transcription factors (Urbach and Technau, 2003). *GHI46*-PNs within the same lineage also have been shown to express different cell fate determinants to specify their axon and dendrite projection patterns (Komiya and Luo, 2007). To understand how each progeny translates these cell fate determinants to acquire their mature morphologies and specific physiological functions is requisite in studying developmental neurobiology.

Neural diversity and olfaction in *Drosophila*

The multiple types of ALN neurons suggest that odor information processing is much more complicated than our current understanding. The spatial or temporal profile, which is suggested from various anatomical and functional studies, may oversimplify how fruit flies smell the environment (Hallem and Carlson, 2004; Olsen et al., 2007;

Shang et al., 2007). For example, some types II INs concentrate their neurites in certain glomeruli and these neurons may selectively enhance or attenuate odor signal. Further detailed descriptions of diverse ALNs may facilitate our understandings of olfaction. The type I *Acj6*-ALN and type II *Acj6*-ALN only innervate partial AL and these cells may confer different level of odor information to higher olfactory center via different pathways (Figure 11). Besides, the aPNs target their axons toward deutocerebrum rather than the MB and LH. The deutocerebrum has been shown the primary brain structure for mechanosensory system, such as auditory (Kamikouchi et al., 2006), and it would be interesting to understand if different sensory information influence each other and how they are integrated in the *Drosophila* CNS for different responses. These ALNs might also confer different information to different brain structures. Recent studies indicated that some ORNs in the coeloconic sensilla can detect humidity or amine (Yao et al., 2005), and one basiconic ORN is a sensor of carbon dioxide (Jones et al., 2007; Kwon et al., 2007). These specific ORNs are important for distinct physiological functions (Yao et al., 2005; Jones et al., 2007; Kwon et al., 2007). Whether these ALNs are specifically required for these unique sensors needs further anatomical and functional studies.

Table 1. Characterizations of ALN-GAL4s

Enhancer trap GAL4 line	Lineage ^a	Cell number Ave. \pm STD. (<i>n</i>)	Axonal Tract ^b	Neurotransmitter ^c
<i>GAL4-GH298</i>	Lateral	21.0 \pm 3.0 (7)	–	GABA
<i>GAL4-KL107</i>	Lateral	46.8 \pm 2.9 (6)	–	ACh, GABA
<i>GAL4-NP6115</i>	Lateral	13.0 \pm 0.9 (13)	iACT	ACh
<i>Acj6-GAL4</i>	Lateral	82.7 \pm 4.8 (7)	<i>int an c</i> , oACT, GC	ACh
	Anterodorsal	72.0 \pm 8.8 (7)	iACT	ACh
<i>GAL4-MZ699</i>	Ventral	45.2 \pm 5.2 (4)	mACT	GABA

^a Lineage was assigned by the result of dual-expression-control MARCM and their spatial location relative to the AL.

^b The axon is defined as the longest process extending from the cell body. No obvious long processes are observed in the ALN Nb clones labeled by *GAL4-GH298* and *GAL4-KL107*.

^c The neurotransmitters are determined by antibody to choline acetyltransferase (ChAT) and GABA.

Abbreviations: ACh, acetylcholine; GC, great commissure; iACT, mACT, oACT, inner/middle/outer antenno-cerebral tract; *int an c*, inter-antennal connective.

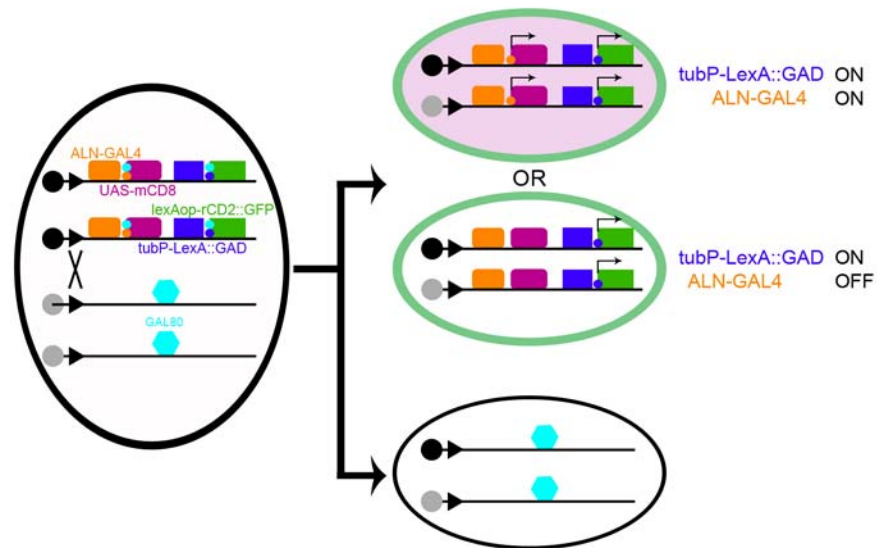


Figure 9. Dual-expression-control MARCM

Schematic illustration of the genetic basis of dual-expression-control MARCM. Every GAL80-minus cell will be labeled by *lexop-rCD2::GFP* which is driven by the ubiquitous driver *tubP-LexA::GAD* (green), while only GAL80-minus ALNs will also be labeled by *ALN-GAL4/UAS-mCD8* (pink).

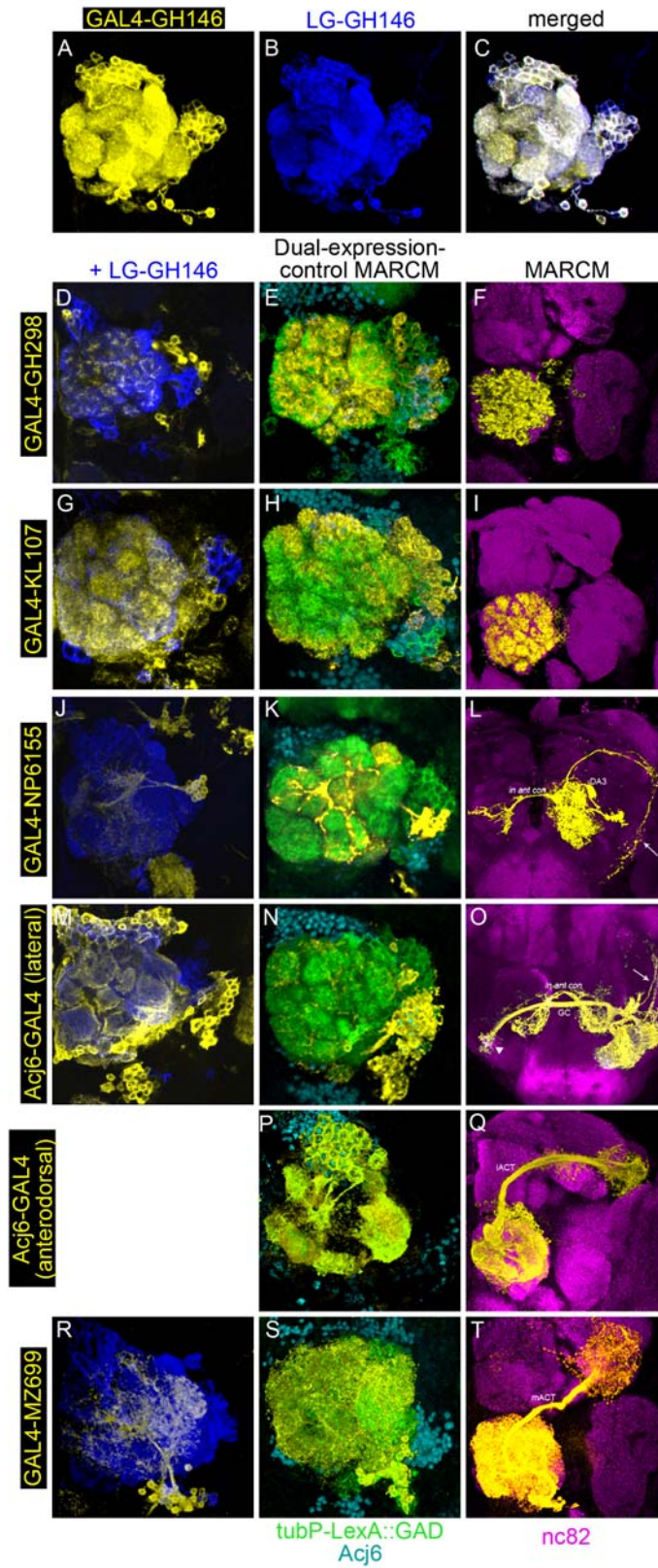


Figure 10. Characterization of antennal-lobe-neuron-GAL4s

(A-C) Stacked confocal images of *GAL4-GH146* (A) and *LexA-GAD-GH146* (*LG-GH146*) (B) which is generated by transposon swap strategy. (C: merged image from A and B). (D-T) Composite confocal images of various *ALN-GAL4s* and representative neuroblast clones labeled by dual-expression-control MARCM and MARCM. The name of each *ALN-GAL4s* is listed on the left. The left column (D, G, J, M&R) shows the merged images of *ALN-GAL4s* (yellow) in the presence of *LG-GH146* (blue). The middle column (E, H, K, N, P&S) shows the neuroblast clones labeled by *tubP-LexA::GAD* (green) and *ALN-GAL4s* (yellow) counterstained with the cell marker *Acj6* (cyan). Note the extra *Acj6*-positive cells in the anterodorsal side (P) are either born at embryonic stage or derived from different lineages. The right column (F, I, L, O, Q&T) shows the morphologies of ALN neuroblast clones (yellow) with nc82 antibody staining (magenta). Note the intensified DA3 glomerulus labeled by *GAL4-NP6115* (L) and the thin tract which projects outward AL to vilpr in the *Acj6-GAL4*-positive neuroblast clones (O). Abbreviations: GC, great commissure; iACT, inner antennal-cerebral tract; in ant con, inter antennal connective; mACT, middle antennal-cerebral tract.

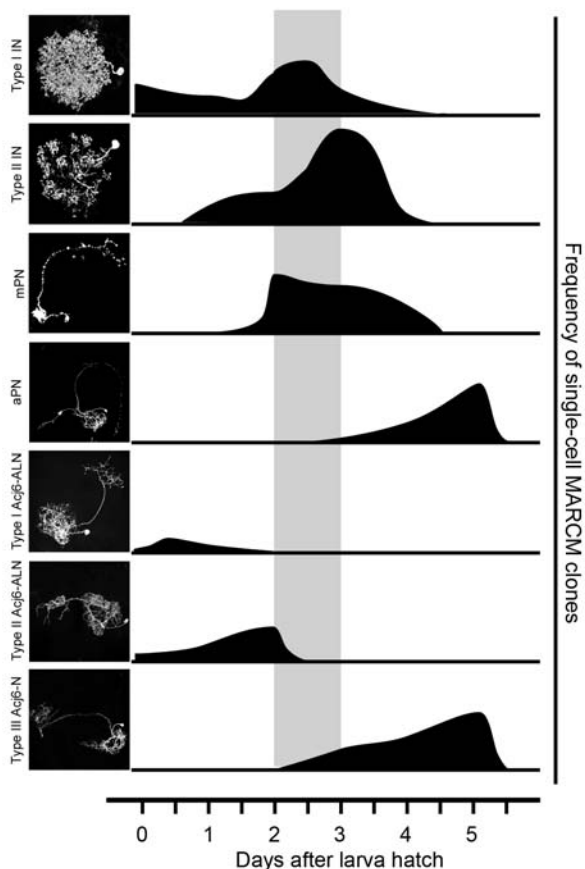


Figure 11. Single cell analysis of antennal lobe neurons

Summary of the labeling frequency of various lateral antennal lobe neurons (IALN) by the MARCM system during larval development. Eight types of ALNs were observed in the lateral ALN lineage (left side) and named by their morphology. The height of the silhouette at each point of developmental stage (horizontal axis) represents the calculated number of single cells per 100 brains (vertical axis) labeled by the MARCM system. Note the high frequency to observe type I IN, type II IN and mPN during the second instar larval stage (grey boxed area).

Abbreviations: ALN, antennal lobe neuron; aPN, atypical projection neuron; IN, interneuron; mPN, monoglomerular projection neuron; N, neuron.

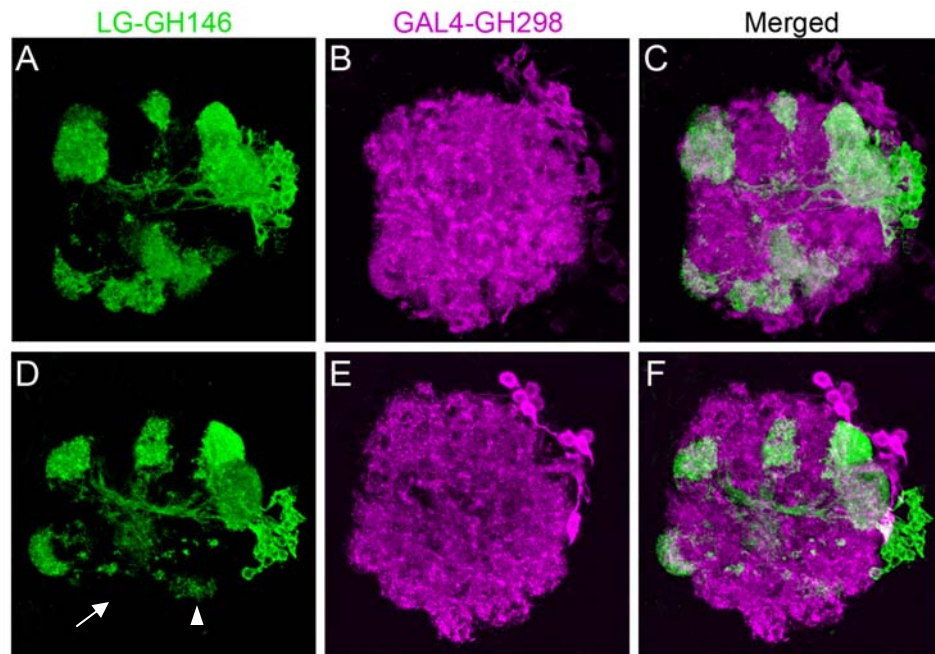


Figure 12. Simultaneous reduction of mPN and type I IN in the later-induced MARCM Nb clone

The dual-expression-control MARCM clones were generated at young first instar larva (A-C) and at mid-second instar larval stage (D-F). The neuroblast clones were labeled by *LG-GH146* (A&D) and *GAL4-GH298* (B&E) simultaneously in the same mosaic organism (merged images, C&F). Note the disappearance (arrow) or weakly labeling (arrowhead) of glomeruli located at the ventral AL labeled by *LG-GH146* (D).

Genotype: *hs-FLP,UAS-mCD8::GFP/+; FRT^{40A},LG-GH146,lexAop-rCD2::GFP/FRT^{40A},tubP-GAL80;GAL4-GH298/+.*

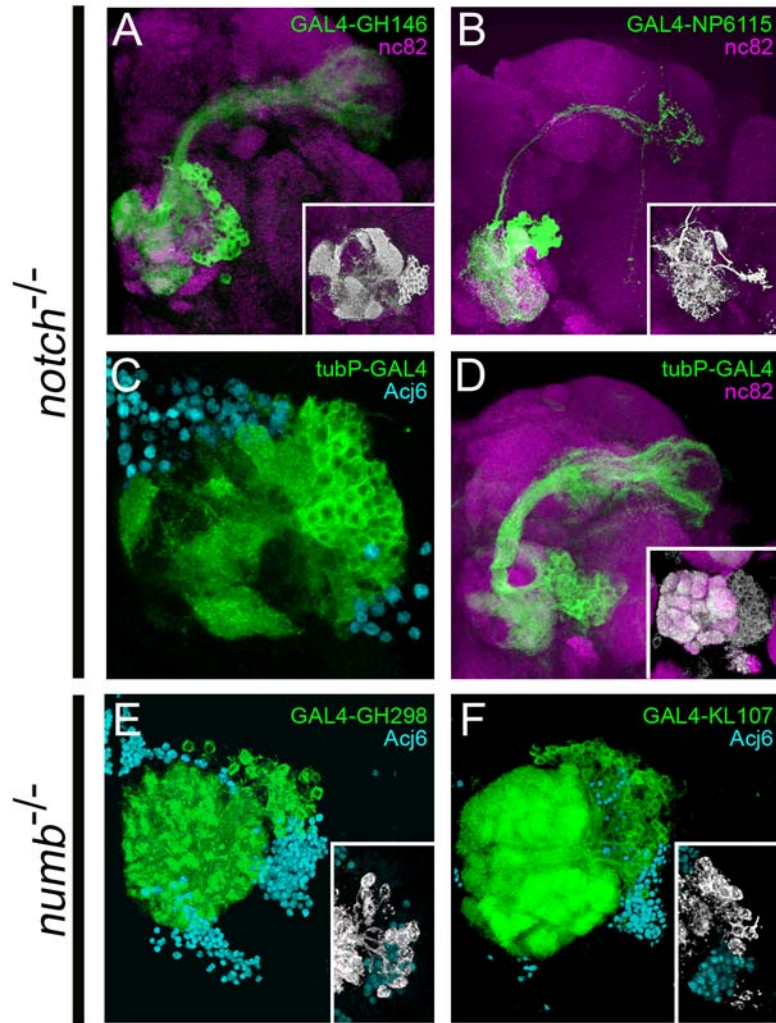


Figure 13. Notch signaling is involved in the generation of IALN neuronal diversity

(A-D) Lateral ALN *notch*^{-/-} MARCM neuroblast clones (green) labeled by *GAL4-GH146* (A), *GAL4-NP6115* (B) and *tubP-GAL4* (C&D), counterstained with nc82 antibody (magenta) (A, B&D) or cell marker *Acj6* (cyan) (C). The insets at the bottom-right corner are the wildtype MARCM clones (white) at the AL region (A, B&D). Note the comparable projection patterns of wildtype and *notch*^{-/-} MARCM clones (A, B&D) and the reduction of *Acj6*-positive cells in the *tubP-GAL4*-labeled *notch*^{-/-} MARCM clone (C). (E-F) Lateral ALN *numb*^{-/-} MARCM neuroblast clones (green) labeled by *GAL4-GH298* (E) and *GAL4-KL107* (F) counterstained with the antibody to cell marker *Acj6* (cyan). The insets at the bottom-right corner are the cell bodies of wildtyped MARCM clones (white) counterstained with antibody against *Acj6* (cyan). Note the difference of the cell number labeled by *GAL4-GH298* and *GAL4-KL107* and also the *Acj6*-positive cells located ventrally to the *GAL4-GH298*- and *GAL4-KL107*-positive neurons in the *numb*^{-/-} and wildtype MARCM neuroblast clones.

Genotype:(A)*FRT*^{19A},*UAS-mCD8::GFP,N^{55e11}/FRT*^{19A},*hs-FLP,tubP-GAL80*;
GAL4-GH146,UAS-mCD8::GFP/+; (B)*FRT*^{19A},*GAL4-NP6115,UAS-mCD8::GFP,N^{55e11}/FRT*^{19A},*hs-FLP,tubP-GAL80*; (C&D)*FRT*^{19A},*UAS-mCD8::GFP,N^{55e11}/FRT*^{19A},*hs-FLP,tubP-GAL80;tubP-GAL4/+*; (E)*hs-FLP,UAS-mCD8::GFP/+*;
FRT^{40A},*numb*¹/*FRT*^{40A},*tubP-GAL80*; *GAL4-GH298/+*; and
 (F)*GAL4-KL107/hs-FLP,UAS-mCD8::GFP;FRT*^{40A},*numb*¹/*FRT*^{40A},*tubP-GAL80*.

The MARCM clones are all induced at newly hatched larval stage.

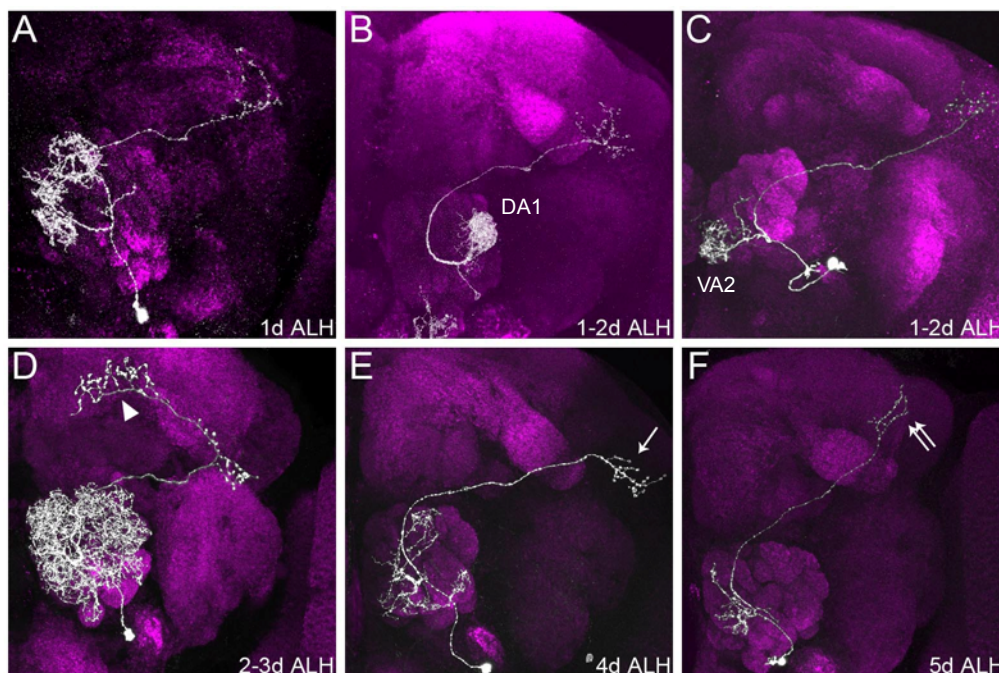


Figure 14. Sequential generation of different types of PN in the ventral lineage

Each type of single ventral projection neuron (white) labeled by the MARCM system is counterstained with the antibody nc82 (magenta). The preferential period to observe various vPN is dated at the bottom-right corner of each figure. Note the different dendritic and axonal projection patterns among the vPNs generated at different developmental stages. For example, vPNs may target their dendrites to specific glomeruli (B&C) or subset of glomeruli (A, E&F). The axons of vPNs may project outward the LH (arrowhead in D) or branch along the ventral side (arrow in E) or dorsal side (double arrows in F) of the LH.

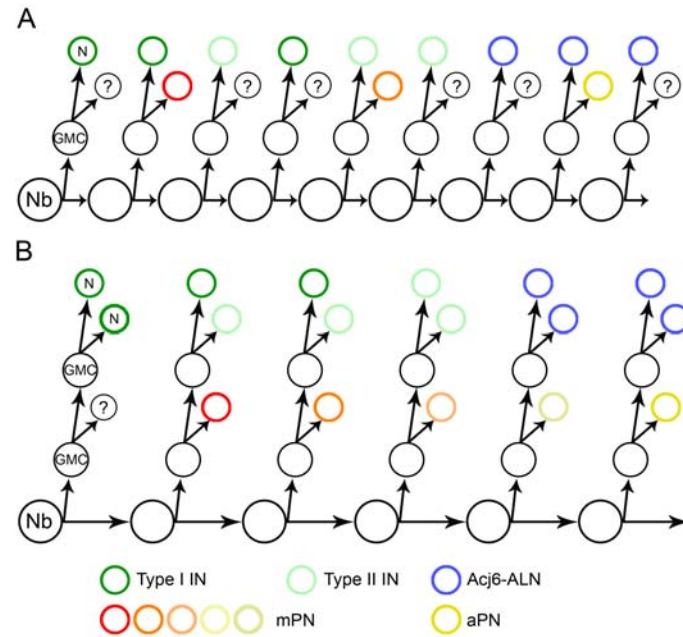


Figure 15. Two hypothetical proliferation models of lateral ALN lineage

Schematic illustrations of two hypothetical models of cellular mechanisms for lateral lineage neurogenesis. (A) During each cycle of neurogenesis, a neuroblast (Nb) divides to generate a ganglion mother cell (GMC). The GMC produces two postmitotic neurons (N) with different cell fates. The postmitotic neurons born at different developmental stages acquire different cell identities (circles with different colors). Note many cells are unidentified or apoptotic (black circle with question mark). (B) The neuroblast divides to produce one GMC. The GMC divides once to produce a postmitotic neuron and a secondary GMC. The secondary GMC divides one more time to produce two cells which acquire same or different identities. Postmitotic neurons born at different developmental stages by GMCs have different cell fates. Note that only the first pair of type I INs (dark green circles) has one unidentified sibling cell (black circle with question mark). Identities of different cells are present at bottom.

CHAPTER IV

GLIOGENESIS IN THE POSTEMBRYONIC *DROSOPHILA* BRAIN

Introduction

The glial cell is a major category of cell in the nervous system. It comprises around 50% of brain mass in primate, and 10% in invertebrate (Jones, 2001; Klambt et al., 2001). While developing, glial cells migrate extensively, change shape and also act as cues and substrates for neuronal migration and axon path-finding (Freeman and Doe, 2001; Freeman et al., 2003; Aigouy et al., 2004; Dearborn and Kunes, 2004; Edenfeld et al., 2007). After maturation, glial cells also support the structure of nervous systems, wrap and insulate neurons, buffer ions, pH and neurotransmitters to regulate synaptic efficacy and synaptogenesis, and form blood-brain barrier to isolate and protect neural tissues (reviewed in Jones, 2001; Freeman and Doherty, 2005).

In the *Drosophila* embryonic and early-larval CNS, glial cells can be generally classified as cortex glia, neuropile glia and surface glia based on spatial locations, morphologies and the expressions of different genetic profiles (Ito et al., 1995; Giangrande, 1996; Klambt et al., 1996; Jones, 2001; Freeman and Doherty, 2006). Cortex glia, also known as cell-body-associated glia, intermingle with the soma of neurons in cell cortex and are important for the nutrition supply of neurons. Neuropile glia ensheath neuropile to insulate axons or bundles of axons to fasciculate nerves and facilitate signal

propagation. Neuropile glia can be further classified as simple neuropile glia and complex neuropile glia based on their shapes (Oland et al., 1999). Surface glia isolate CNS from other tissues and form part of blood-brain barriers (Ito et al., 1995; Jones, 2001; Freeman and Doherty, 2005).

In the embryonic stage, nearly all glia in CNS originate from the neural stem cells, which delaminate from ectoderm and express a specific combinatorial set of transcription factors to specify their cell identity (Urbach and Technau, 2003). Three types of precursor cells, glioblast (GB), type 1 neuroglioblast (NGB) and type 2 NGB produce glial cells (Jacobs et al., 1989; Akiyama-Oda et al., 1999; Bernardoni et al., 1999; Udolph et al., 2001; Jones, 2001). Glioblasts give rise to only glial cells. Type 1 NGBs bifurcate at the first division to generate a GB and a neuroblast (NB), each of which restricts the types of their descendants as either glial cells or neurons. Type 2 NGBs behave like regular NBs: they generate a series of ganglion mother cells (GMCs) and the GMCs either divide to two daughter neurons or yield a neuron-glia sibling pair. These ectoderm-derived glia require the transcription factor encoded by the glial cell missing (*gcm*) gene (Hosoya et al., 1995; Jones et al., 1995) to activate downstream genes such as *repo*, *loco*, or *pnt* to promote their glial cell fate (Egger et al., 2002; Freeman et al., 2003).

However, our understandings of glial generation, diversification and development in post-embryonic stages remain rudimentary (Awad and Truman, 1997; Tix et al., 1997; Peraanu et al., 2005; Colonques et al., 2007). How do glial cells specify their cell fates? Are their cell fates related to their lineages or determined by their environment after migration and maturation? To answer these questions, it is important to perform glial

lineage analysis to lay the ground for the studies of their development.

Systematical post-embryonic glial lineage analysis with the MARCM technique reveals that surface glia and neuropile glia derive from separated glial precursor cells. Simple neuropile glia and complex neuropile glia in the antennal lobes also originate from separate glial precursors and their derivation is independent from antennal lobe neuronal lineages. By examining the size and cell numbers of glial MARCM clones, glial precursor cells use symmetrical division to proliferate neuropile glia and surface glia. The observations of glial lineage specificity and distinct proliferation pattern would provide different perspectives of the studies of glial development and functions.

Material and Methods

Fly stocks

(1) *hs-FLP;FRT^{G13},tubP-GAL80,Repo-GAL80/CyO* and (2) *Repo-GAL4;FRT^{G13},UAS-mCD8,UAS-nlsGFP/CyO* are used to generate glial MARCM clones. (3) *FRT^{G13},hs-FLP,tubP-GAL80/CyO*, *Y* is first crossed with (4) *Pin/CyO; tubP-GAL4/TM6B* (Lee and Luo, 1999) to obtain the temporary stock *FRT^{G13},hs-FLP,tubP-GAL80/CyO; tubP-GAL4/+*, which is then crossed with (5) *Repo-LexA::GAD;FRT^{G13},UAS-mCD8,lexAop-rCD2::GFP/CyO* (Lai and Lee, 2006) to study the lineage relationship of neurons and glia in the antennal lobes.

MARCM analysis of glia

Larvae which are collected within one hour after hatching are cultured at the density of

80 larvae per vial at 16 °C. MARCM clones are induced at various developmental stages by heat-shock at 38 °C for 10 minutes and then examined in adult brains.

Immunohistochemistry and confocal microscopy

Brains are dissected, fixed and stained as described before (Lai and Lee, 2006).

Antibodies used in this study include rat anti-mCD8 (Caltag, 1:100) and mouse anti-nc82 (DSHB, 1:50). Images are taken with Zeiss LSM510 or Zeiss Pascal confocal microscopy and processed with Adobe Photoshop.

Results

Lineage specificity of glial cells in the *Drosophila* brain

Different types of glial cells have been shown lineage specificity in the embryonic stage (Jacobs et al., 1989; Freeman and Doe, 2005). To extend the lineage analysis to the postembryonic stage, the MARCM technique is applied to label glial clones generated in larva. The specified glial lineage labeled by the MARCM technique would contain stereotyped glial cells at specific locations. In contrast, the non-specified glial lineages would include diverse types of glial cells and the composition of each multicellular MARCM clone will be distinct. *Repo-GAL4*, which has been demonstrated to label all Repo-positive glial cells in the adult brains (Lai and Lee, 2006), was used in the MARCM system to drive the expression of a membrane marker UAS-mCD8 (Lai and Lee, 2006) and a nuclear marker UAS-nlsGFP simultaneously (Shiga et al., 1996) to visualize the general morphology of glial cells and determine the cell numbers by

counting GFP-positive nuclei. Both surface glial clones and neuropile glial MARCM clones could be generated after embryogenesis, however, cortex glia clones were rarely observed. Few observation of cortex glia suggests that cortex glia are probably generated during embryogenesis, and our post-embryonic-generated glial clones analysis were thus focused on surface glia and neuropile glia.

When glial MARCM clones were mildly induced at the early larval stage (0-24 hours after larval hatch), big patches of surface glial cells (Figure 16A) or central brain (CB) neuropile glial cells (Figure 16E) could be observed. Surface glial clones were observed to form big patches and randomly cover various regions on the brain surface (43 clones in 93 brains) (Figure 16B-D). The CB neuropile glial clones outlined partial or entire various brain structures, such as mushroom bodies, central complexes or antennal lobes (ALs) (12 clones in 93 brains) (Figure 16F-H). These clones randomly distributed on the brain surface or in the brain, and there was also no correlation of their positions in different mosaic brains. Besides, the processes of surface glia and neuropile glia did not interweave or physically contact each other. Most of the mosaic brains contained only one type of glial clone (56 out of 93 brains), and the glial cells within each clone always tightly associated with each other (for example, Figure 16B-D and 16 F-H).

Similar phenomena were observed in the AL neuropile glial clones, which included simple neuropile glia and complex neuropile glia (Oland et al., 1999) (Figure 17). The somas of simple neuropile glial clones evenly surround the ALs, and their processes appear to wrap around entire ALs to separate ALs from other brain structures and border individual glomeruli within ALs (Figure 17A). The nuclei of complex

neuropile glia clones also locate outside ALs and their processes innervated various glomeruli and formed dendrite-like structures (Figure 17D). The cell bodies of both types of glial cells locate adjacent to each other and their processes interweave extensively. These two different types of glia, however, could be independently labeled in some mosaic brains, and the characteristic features of the other type of glia were not observed (Figure 17B&C, and E&F). Besides, the AL simple and complex neuropile glia did not outline or innervate other brain structures, and the glial cells wrapped other neuropiles did not target their processes into ALs (data not shown). All of the analyses showed that each type of glial cell could be independently labeled in the MARCM system .

Antennal lobe neurons and glia are derived from independent blast cells.

Earlier studies have shown that antennal lobe neurons are generated from at least three independent neuroblasts (Jefferis, 2001; Lai and Lee, 2006), and whether these neuroblasts also generate glial cells are unknown. The dual-expression-control MARCM technique was then used to label neurons and glial cells simultaneously in the same mosaic brains to study the relationship of gliogenesis and neurogenesis at the antennal lobes. If the AL neuropile glia were also derived from the AL neuroblasts, glial cells should also be labeled in ALN MARCM clones. Since there existed no enhancer trap GAL4 line which specifically labeled all of the ALNs (Chapter III), the ubiquitous driver *tubP-GAL4* and the glial specific driver *Repo-LexA::GAD* were used in the dual-expression-control MARCM system to label the entire neural lineage and glial cells, respectively. The MARCM clones were generated with low frequency when larvae

hatched and then were examined at the adult stage.

In the collected anterodorsal, lateral and ventral AL neuroblast MARCM clones, no glial cells were observed (for example, Figure 17G-I; data not shown). Besides, if AL neuropile glia were derived from AL neuroblasts, the chances to observe AL neuropile glial clone should equal to the AL neuroblast clones. By counting the numbers of the AL glial clone and neuroblast clones in the mosaic brains which were induced at newly hatch larvae, the frequency of observing AL neuroblast clones (average 59 clones in 100 brains) was higher than AL neuropile glial clones (average 0 clones in 100 brains). The AL neuropile glia clones could only be generated after first instar larvae, but the frequency (average 4 clones in 100 brains) was still much lower than AL neuroblast clones (average 68 clones in 100 brains). The results showed that AL neuropile glia and AL neurons were derived from separate lineages.

Proliferation pattern of gliogenesis

Neural precursor cells can divide asymmetrically or symmetrically for different purposes (reviewed in Lu et al., 2000). The precursor cells undergo asymmetrical division to produce two daughter cells with different cell fates or divide symmetrically to expand cell population with identical cell fates. How glial cells are generated from the precursor cells by what type of division remains unclear. This issue was addressed by analyzing different MARCM clones generated at different developmental stages.

A series of mosaic brains whose MARCM clones were generated at various developmental stages were collected, and the number of glial clones and the size of the

clones (numbers of glial cells within each clone) were counted. The glial clone, take surface glia as an example, was defined as a patch of glial cells which were physically attached together and each individual clone was substantially separated from each other. When MARCM clones were generated at early developmental stages (0-24 hours after larval hatch), two-cell glial clones were less observed (20%, n = 40), and most of the MARCM clones were big patches of glia which contained more than two glial cells (80%, n = 40). Compared to the mosaic brains induced at later stages, the percentage of two-cell glial clones increased to 41% (n = 73) when MARCM clones were induced at second instar larvae, and to 76% (n = 67) at late third instar larvae (Figure 19). The results showed that the ratio of two-cell clones to GB clones dynamically changed at various developmental stages.

The surface glial MARCM clones generated at any specific stage were then grouped as one-cell clone, two-cell clone and multi-cell clone (with more than two cells) (Figure 18). When MARCM clones were generated at 0-24 hours after larva hatched, five clones in average could be observed in every ten mosaic brains (n = 111 brains), and 93% of the clones contain multiple cells (n = 29 clones). If the MARCM clones were generated at second instar larvae, each mosaic brain contained 2.3 clones in average (n = 74 brains), and the percentage of multi-cell clones dropped to 38% while the percentage of one-cell and two-cell clones increased to 35% and 27%, respectively. The number of MARCM clones generated at early pupal stages tremendously increased to 20 clones per brain, and about 90% of the clones contained only one glial cell. The number of glial clones dropped to 3 clones per brain when mitotic recombination was induced 48 hours

after pupal formation and each clone contained only one glial cell (Figure 18). Notably, the morphology of the glial cells generated at early stage were not different from those generated at later stages (data not shown). These results suggested a proliferation pattern different from asymmetrical division.

Although the lack of obvious boundaries among different neuropile glial clones made it difficult to perform quantitative analysis, similar events were observed. The early-generated neuropile glial clones also contained multiple cells, and they wrapped around most regions of various brain structures. The later-generated neuropile glial clones were mainly composed of single glial cell, and they also spread around the entire brains and outlined partial various brain structures. In summary, the size (number of cells) of all types of glial clones decreased and the numbers of glial clones increased when they were generated at later developmental stages.

Discussion

Specified glial cell lineages have been demonstrated in mammalian CNS (Vaysse and Goldman, 1990), however, the phenomenon is less studied in *Drosophila* (Jacobs et al., 1989; Freeman et al., 2003) With the MARCM technique, surface glial cells, simple neuropile glia and complex neuropile can be independently labeled in different mosaic brains (Figure 16 and 17). If different types of glial cells are derived from the same precursors, the MARCM clones generated at early larval stages are expected to contain multiple types of glial cells. The independent labeling of different types of glial clones indicates that different types of glial cell derived from separated lineages and each

lineage produced only one kind of glia. Furthermore, the results from the studies by dual-expression-control MARCM showed that AL neuropile glia derived from specified glial precursor cells, which are independent of neuronal lineages (Figure 17G-I). All of these results indicate that different types of glial cells are specified on the basis of their lineage.

Notably, different types of glial cells which derive from different lineages can locate far away, such as neuropile glia and surface glia, or nearby, such as AL simple and complex neuropile glia (Figure 16 and 17). Since neuropile glia and surface glia do not intermingle their processes and they have distinct functions, and morphologies, these two lineages may be spatially specified. However, the simple neuropile glia and the complex neuropile glial cells distribute around the entire AL and juxtapose to each other. Although they have distinct morphologies, their processes wrap the same brain structure. It is thus unknown if simple and complex neuropile glial lineages are also spatially specified. One possibility is that the glial lineages are spatially specified when the precursor cells are generated, but the simple and complex neuropile glia migrate extensively during development as observed in other glia (e.g. Jacobs et al., 1989; Dearborn and Kunes, 2004). The other possibility is that these glial lineages do not have spatial identities, and they are specified by unknown temporal codes, cell-cell interaction between two precursor cells or uncharacterized mechanisms. If one can determine the glial precursor cells and identify their birth timing, it would help us understand how these two types of glial lineages are specified during development.

Neural precursor cells can divide asymmetrically or symmetrically for different

purposes (reviewed in Lu et al., 2000). The asymmetrical division allows the generations of two daughter cells with distinct cell identities while the symmetrical division results in two daughter cells with identical cell fates to expand the cell population. The glial proliferation pattern was determined by the glial MARCM clone analysis because the mosaic patterns labeled by the MARCM technique reflected how cells proliferated (Figure 19). For example, during neurogenesis, the NB divides asymmetrically to bud off a series of GMCs and renews itself for another division, and each GMC divides once to generate two postmitotic neurons. In neuronal lineage analysis with MARCM technique, the generation of NB- or two-cell- MARCM clones depends on which daughter cell loses the repressor GAL80 after mitotic recombination and is not related to the developmental stages. If the renewed NB loses the repressor, the rest of NB lineage will be labeled, and if GMC does not inherit the repressor, two-cell clone can be observed. The probability to label NB- or two-cell-MARCM clones in total mosaic brains should be 50% and 50%, respectively (Figure 2, Chapter I). If GB uses the same proliferation pattern, the ratio of MARCM-labeled GB clones and two-cell glial clones should also be close to 1 to 1 (Figure 19A). If the precursors use symmetrical division to proliferate descendants, each precursor will give rise to two precursors, and the number of descendants will increase exponentially during development. When MARCM clones are induced at various developmental stages, either daughter cell losing GAL80 will result in the labeling of half progenies, and the ratio of multi-cell clones to two-cell clones will not be 1 to 1 (Figure 19B). Besides, the early generated MARCM clones would contain abundant progenies and the numbers of glial clones would be not many. When the MARCM clones are

generated at later developmental stages, because of the increment of precursors by symmetrical division, the number of MARCM clones would massively increase due to the possible simultaneous events of mitotic recombination occurring in most precursors, and the cells within each clone would be expected to decrease (Figure 19B). As the results demonstrated, the unequal chance to observe early-generated GB and two-cell MARCM clones ruled out the possibility that GB used asymmetrical division to generate glial cells (Figure 18). Further quantitative analysis showed that the increment of one-cell clones and reduce of multi-cell clones were in accordance with the developmental stages, and the numbers of glial clones, which are generated at later larval stages, were much more than the early generated glial clones (Figure 18). These results support the model of symmetrical division during gliogenesis (Figure 19B), as previously observed in the optic lobes (Colonques et al., 2007).

The more direct evidence would be observing GAL80 homozygous and GAL80-minus clones simultaneously in the same mosaic brain and the comparison would tell us the correct model of glial proliferation. However, the current technique could not simultaneously label GAL80-plus and GAL80-minus clones, and a novel technique would be required to resolve the problem. Another possibility is that numerous GBs, which are quiescent at early developmental stages actively, generate one or two glial cells at later developmental stages. In the study of neurogenesis, BrdU incorporation experiments showed that embryonic-born neuroblasts will undergo quiescent before larval hatch, gradually reactivate during larval development and flourish the entire brain by the massive generation of neurons (Ito and Hotta, 1992). It is not clear yet if GBs also

undergo quiescence and reactivate later, and a detailed investigation of the GBs' behaviors during development will be required to address this issue.

The symmetrical division in glial cell proliferation and no obvious differences between early and later born glial cells also suggest that the glial cell fate may not be determined by temporal factors and cell-cell interactions. However, in the MARCM clonal analysis, single-cell clones can be observed through the entire developmental stages (Figure 18). This result indicates that the glial proliferation is not synchronized at a particular period during development. Although the glial cells born at different developmental stages do not display distinct morphologies, it requires further investigation to examine if they acquire different temporal identities and serve for different functions. Furthermore, several genes are observed to be spatially and temporally expressed in various glial lineages during embryogenesis (Freeman et al., 2003; Altenhein et al., 2006). How do these genes specify different lineages? Why do most glial lineage progeny not acquire temporal or spatial identities? Further studies of these questions will provide new perspectives to understand glial diversity and their development.

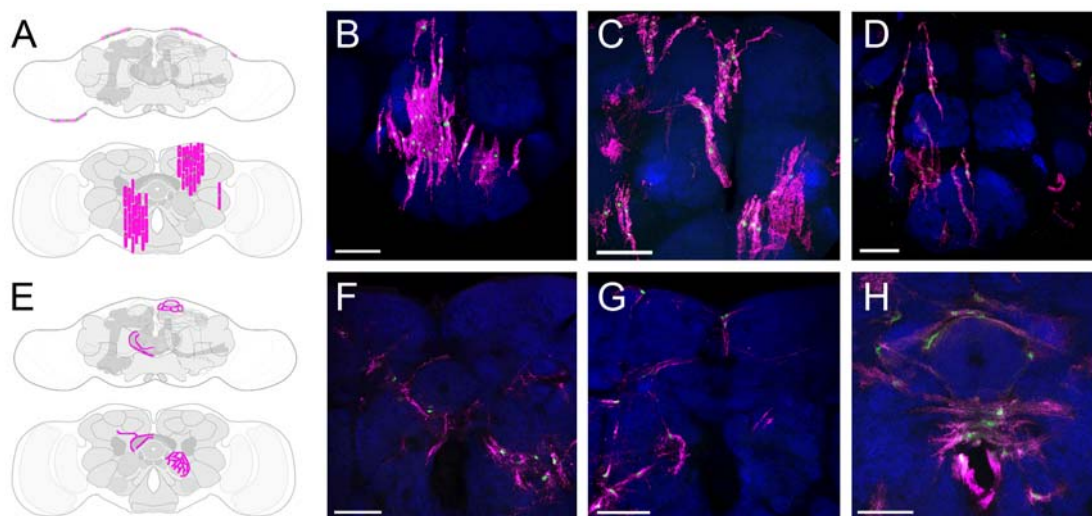


Figure 16. Independent labeling of surface and neuropile glial clones

Schematic illustrations and representative composite confocal images of surface (A-D) and neuropile glial clones (E-F). Schematic illustrations of surface glia (A) (pink) and neuropile glia (E) (pink) from the front view (upper panels) and horizontal view (lower panels) of the brains. The nuclei of each glia were shown (green). The representative glial clones are generated at newly-hatched larva (B, F), 3rd instar larva (C, G) or mid-pupal stages (D, H). The processes (magenta) and nuclei (green) of glial MARCM clones are shown with nc82 antibody staining (blue) (B-D, and F-H). Note the change of the size and number of randomly distributed surface glial MARCM clones at different developmental stages (B-D) and the wrapping of various partial brain structures by neuropile glial cells (F-H). Scale bars: 50 μ m.

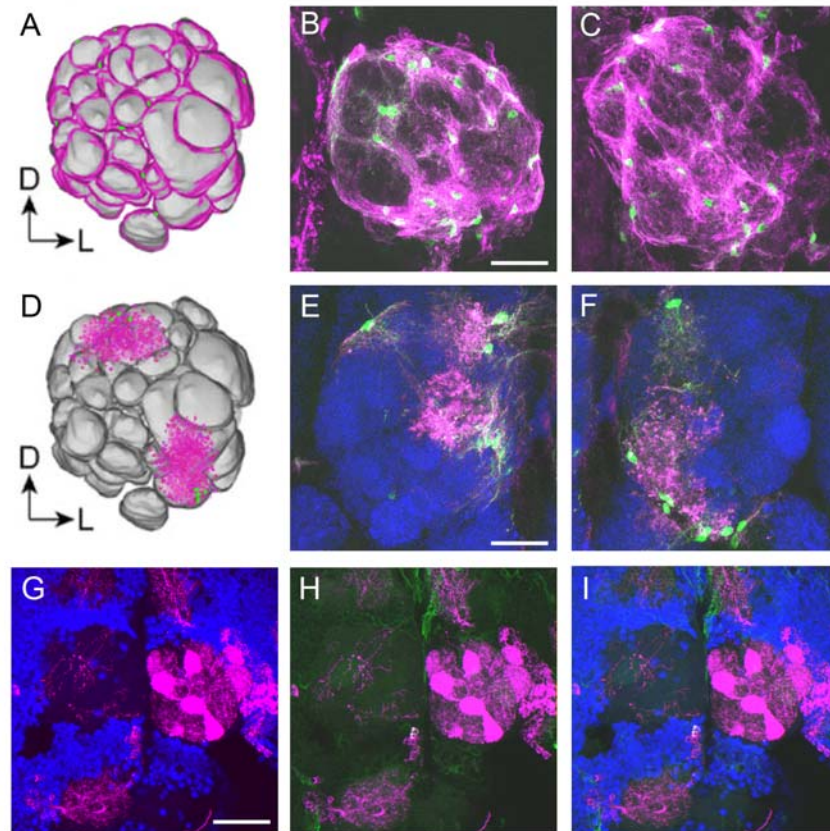


Figure 17. Separated antennal lobe glial lineages

(A-F) Schematic illustrations (A, D) and representative composite confocal images of simple and complex AL neuropile glial MARCM clones (B-C and E-F, respectively).

Glial processes (magenta) and nuclei (green) are shown with antibody nc82-stained AL (blue, E and F). The scheme of ALs (A&D) are modified from Couto et al., 2005. Note the proximate positions of the somas of simple and complex AL neuropile glia. (G-I)

Representative composite confocal images of a lateral ALN MARCM clone. Entire ALN clone (magenta) and few glial cells (green) are co-labeled with the neuronal marker Elav (blue). Scale bars: B&C, and E&F, 20 μm ; G-I: 50 μm .

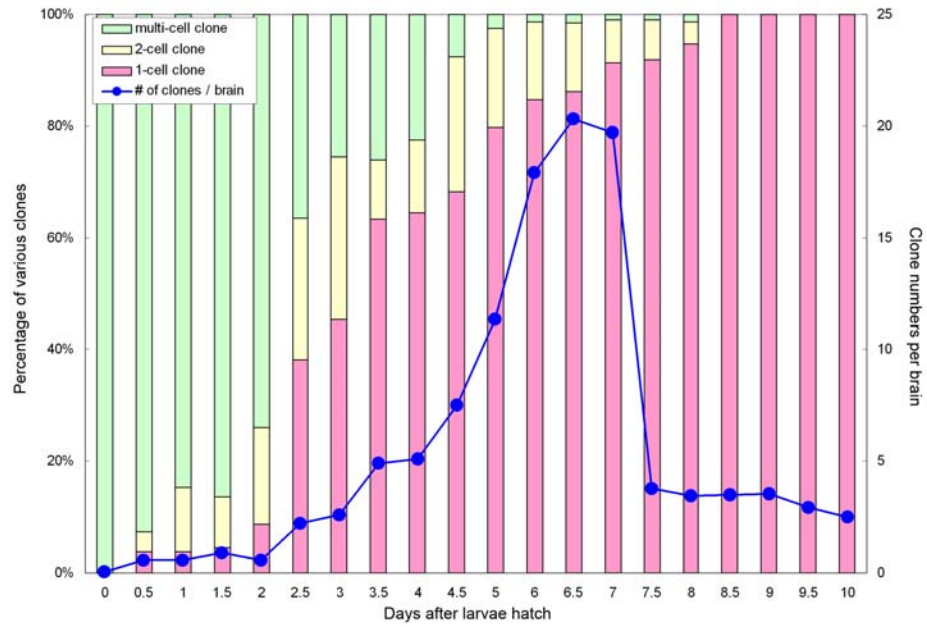


Figure 18. Surface glial MARCM clone analysis

Percentages of different size of clones in the total MARCM glial clones (stacked bars) and average numbers of clones in total MARCM-labeled mosaic brains (blue line). The glial clones are generated at various developmental stages with 0.5 day (12 hours) difference. Note the change of the ratios of two-cell (yellow bars) and multi-cell clones (green bars) during different developmental stages.

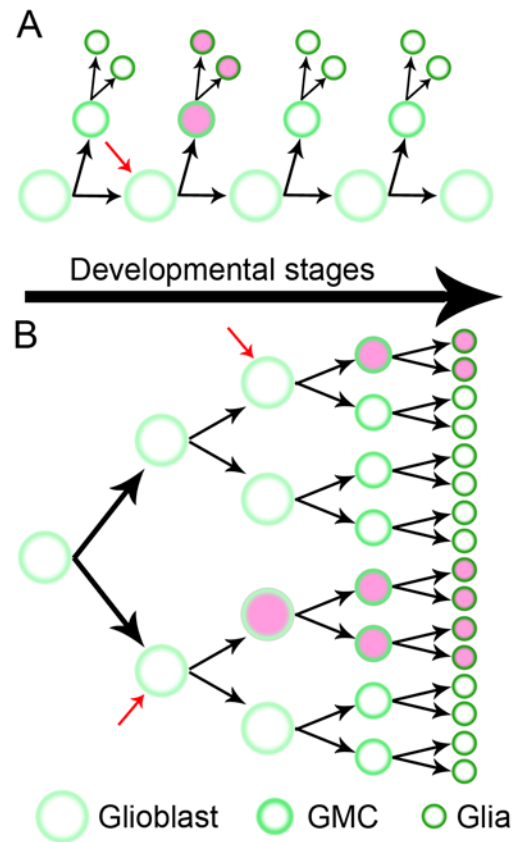


Figure 19. Proliferation models of gliogenesis

Schematic illustrations of two proliferation models, asymmetrical (A) and symmetrical (B) division of gliogenesis. Induction of MARCM clones (red arrows) generated at different developmental stages result in different labeling patterns (pink-colored circles).

CHAPTER V

MORPHOMETRIC ANALYSIS OF THE *DROSOPHILA* MUSHROOM BODIES

Introduction

Cell lineage analysis lays an important ground for molecular and genetic investigation of the mechanisms regulating the generation of cell diversity (for example, Guo et al., 1996; Isshiki et al., 2001; Zhu et al., 2006). MARCM technique is a powerful genetic tool for the detailed description of cell morphology with single-cell resolution (reviewed in Lee and Luo, 2001). Coupled with GAL4/UAS system and numerous antibodies, the identity of each single neuron can be determined on the basis of morphology and molecular marker (Zhu et al., 2003; Zhu et al., 2006). However, neuropiles in the *Drosophila* CNS are composed of dozens to hundreds of similar neurons which are organized in parallel. Sometimes, these neurons' morphologies are not obviously distinct from each other and there exist no subtype-specific GAL4s or cell markers to distinguish every neuron. Without further characterization of the neurons with similar morphologies, it is difficult to uncover the cellular and molecular mechanisms which are responsible for the generation of cell diversity during development.

Mushroom bodies (MB) are the *Drosophila* olfactory learning centers

(Heisenberg et al., 1985; Davis, 1993; de Belle and Heisenberg, 1994; Liu et al., 1999; Krashes et al., 2007). One MB is derived from four identical neuroblasts (Ito and Hotta, 1992; Ito et al., 1997; Zhu et al., 2003), and each neuroblast undergoes hundreds of asymmetrical divisions through developmental stages to produce identical ensembles of MBNs (MBN) populating all the 5 MB lobes (Crittenden et al., 1998). Detailed MARCM single-cell analysis with MB ubiquitous GAL4 driver (GAL4-OK107) shows that the γ lobe is formed by the MB γ neurons which are born before the mid-third instar larval stage (Lee et al., 1999; Zhu et al., 2006). The α' and β' lobes are formed by α'/β' neurons which are born at late larval stages (Lee et al., 1999; Zhu et al., 2006). The α and β lobes are composed of pioneer α/β neurons and α/β neurons, and the former are born before pupal formation while the latter are generated in the pupal stage (Lee et al., 1999; Zhu et al., 2006). Recent studies with subtype specific GAL4s further demonstrated that each subtype of MBNs project their dendrites into specific territories of the calyx (a domain formed by all MBN dendrites) (Zhu et al., 2003; Strausfeld et al., 2003; Tanaka et al., 2004; Lin et al., 2007). Systematic screening for mutants affecting the cellular composition of MB neuroblast clones by examining the cell morphology, revealed that chinmo (chronologically inappropriate morphogenesis) mutation causes the precocious development of later born pioneer α/β and reduction of γ and α'/β' neurons (Zhu et al., 2006). Without detailed investigation of cell composition of MBNs and description of cellular morphology with single-cell resolution, it will be challenging to characterize such mutants affecting neuronal diversity.

Each subtype of MBNs may contain as many as hundreds of neurons. Some types

of MBNs can be further classified by their morphology or different molecular markers, such as the characterization of core α/β neurons and two subtypes of α'/β' neurons by different enhancer trap GAL4 lines (Tanaka et al., 2004; Lin et al., 2007). Other types of MBNs have not been further classified with different subtypes. For example, all of ~ 200 γ neurons are generated in the embryonic and early larval stage (Lee et al., 1999), and these neurons show no obvious morphological distinction and no GAL4s are identified so far to distinguish them. It is thus unclear yet if there exists neuronal diversity within γ neurons. Besides, chinmo protein is highly expressed in γ neurons (Zhu et al., 2006), and whether chinmo also functions in γ neurons to diversify them can not be easily answered with current techniques and knowledge. Therefore, it is required to develop a computer algorithm to automatically characterize single MBNs' 3D morphologies and determine their spatial relationships within the whole MB in the help of determination of neuronal diversity.

The newly developed algorithm was built on the basis of morphological deformation and matching of irregular-shaped 3D objects (Guétat et al., 2006). This morphing system automatically computes dense point correspondences between a pair of 3D volumes and allows automatic morphing. Briefly, the algorithm uses various non-linear critical filters to reduce images' resolution without losing their global features. It then identifies rough point correspondences at coarse resolution levels followed by refinement of point correspondences at fine resolution levels. Point correspondences are established on the minimization of the morphing energy and each point correspondence is described using an affine matrix. This 3D morphing system compares two volumes'

shapes as well as their interiors throughout every single point (for technical details please see Appendix) (Guétat et al., 2006). The algorithm also provides local morphing energy as well as regional correspondence points morphing matrices as quantitative information about region-specific similarity and deviation between the two 3D objects of comparison (Guétat et al., 2006). The entire morphology of the MB is labeled by *247-LexA::VP16* which is specifically expressed in the MBs. The collected image data sets of MBs are then analyzed by the algorithm to construct a 3D virtual standard MB and also create a deviation chart to illustrate the regional deviation. *GAL4-NP7175*-positive core α/β neurons (Tanaka et al., 2004) are then spatially mapped within the MB via the algorithm and the results show that *GAL4-NP7175*-labeled axons but not dendrites occupied the same space in different MBs.

Material and Methods

New transgene and fly stock. *247-LexA::VP16* in *pCaSpeR4* was generated by subclone *LexA::VP16* (Lai and Lee, 2006) into the *pCaSpeR4* plasmid which contained MB specific enhancer *247* (Mcguire et al., 2001) and *SV40 tail*. The fly stock (1) *247-LexA::VP16,lexAop-rCD2::GFP/TM3,Sb* was then generated to outline the MBs. To independently label subsets of MBNs and whole MBs simultaneously, the fly stock (2) *FRT^{G13},hs-FLP,tubP-GAL80/CyO,y+* (Lee and Luo, 1999) was first crossed with *Pin/CyO,y+;GAL4-OK107* to generate a temporal stock *FRT^{G13},hs-FLP,tubP-GAL80;GAL4-OK107/+* which was then crossed with (3) *FRT^{G13},UAS-mCD8;247-LexA::VP16,lexAop-rCD2::GFP*. The flies for the spatial

mapping of core α/β neurons were generated by crossing (4) *UAS-mCD8; 247-LexA::VP16,lexAop-rCD2::GFP/TM6B* with (5) *GALA-NP7175*.

Fly rearing and the generation of MARCM clones. The MARCM clones were generated as described (Lee and Luo, 1999). In brief, the collected new-hatched larvae were heat-shocked at 38°C for 30 minutes and raised in 25°C until eclosion.

Brain dissection and confocal microscopy. Whole adult *Drosophila* brains were dissected and fixed as described. For GFP visualization, samples were mounted in the FocusClear reagent (Pacgen Biopharmaceuticals). For immunofluorescence, samples were stained with antibody against mCD8 (1:100, Caltag), subsequently labeled with Cy3-conjugated secondary antibody (1:200, Jackson Lab), and mounted in the same manner as for direct GFP visualization. Images of 20 female MBs from left hemisphere were collected under Zeiss LSM510 or Zeiss Pascal confocal microscopy with $512 \times 512 \times Z$ voxels with 8-bit intensity resolution; Z was depend on the thickness of MB. The voxel size of a data set is $0.45 \times 0.45 \times 1 \mu\text{m}$.

Results

The development of the algorithm for automatic morphometric analysis and the use of the algorithm described here were done by our collaborator Dr. Yoshihisa Shinagawa and his group.

Independent labeling of MBNs and the whole MB. The identification of individual MBNs involves locating MARCM-labeled single MBNs within the entire MB. It is thus essential to outline the entire MB when the subsets of MBNs are selectively labeled by MARCM. An isolated 247-bp genomic sequence when fused with GAL4 has been demonstrated to label large subsets of MBNs in the presence of UAS-marker (Zars et al., 2000; McGuire et al., 2001), and this 247-bp DNA fragment was then fused with LexA::VP16 to generate a putative MB specific driver *247-LexA::VP16* (Figure 20A&B). To investigate the number of MBNs labeled by *247-LexA::VP16,lexAop-rCD2::GFP*, the flies which also carry the marker *UAS-mCD8* (Lai and Lee, 2006) and *GAL4-OK107* are examined, and *GAL4-OK107* has been shown to express in all of the MBNs. The result shows that *247-LexA::VP16* labels every *GAL4-OK107*-positive MBN and drives no detectable expression outside MBs (Figure 20C-E). The binary system *247-LexA::VP16* and *lexAop-rCD2::GFP* was then used to label entire MB.

The driver *247-LexA::VP16* was then tested if it could work in conjunction with the MARCM system to independently label whole MBs and subsets of MBNs in the same mosaic organism (Figure 20F-H). The flies carrying the genotype of *FRT^{G13},UAS-mCD8/FRT^{G13},hs-FLP,tubP-GAL80; 247-LexA::VP16,lexAop-rCD2::GFP/+; GAL4-OK107/+* are generated and heat-shocked briefly at newly hatched larval stage to generate MARCM clones. Their brains are then examined at the adult stage. Single-cell and two-cell clones of GAL80-minus γ neurons are created and specifically labeled by *GAL4-OK107*-dependent expression of *UAS-mCD8* (Figure 20F). On the other hand, all MBNs are labeled by

lexAop-rCD2::GFP which is controlled by *247-LexA::VP16* (Figure 20G). The double labeling allows us to visualize small subsets of MBNs and the whole MB in the same organism (Figure 20H).

Creation of a virtual standard MB and computation of regional variation. To map individual MBNs into the MB, a virtual standard MB was required to morph various MARCM-labeled MBNs into a common reference (Figure 21). The standard MB was created by averaging the *247-LexA::VP16,lexAop-rCD2::GFP*-labeled MBs which were collected from right hemisphere of newly eclosed female brains with confocal microscopy. Twenty image data sets of MBs were first transformed individually in rigid and scale with a common coordinate system to compensate differences in position and orientation of the images. Every two MBs were then used to establish point-to-point correspondence and obtain morphing matrices for each point of correspondence (Figure 21A). The average morphing matrix then determined the normal spatial localization patterns of each point of correspondence from all the 20 MBs and constructed a digital three-dimensional virtual standard MB (Figure 21B).

For each point of correspondence, there existed variation for their spatial localization pattern, so it is important to establish the possible range of each point of correspondence in the standard MB to categorize the neurons with assorted morphologies. To determine the deviation of each point of correspondence within the standard MB, the morphing energy (pixels) which was used to morph each point of correspondence of every actual MB into the standard MB was computed. After comprehensive analysis, an

isosurface of the morphing energy was generated to graph the deviation of each point of correspondence among the MBs (Figure 22). The range of deviation was tinted for different colors, and the hot color (red and yellow) indicated big deviation and the cool color (green and blue) represented small deviation. When the deviation chart was rendered from cool color to hot color, the peduncle and the dorsal lobe of MB's isosurface gradually disappeared in the chart while the calyx and the medial lobe remained visible in hot color (Figure 22). The virtual standard MB and the deviation chart would be the foundation for the future mapping of every single MBN.

Spatial mapping of subsets of MBNs in the standard MB. The algorithm was first tested if it can morph the same MBNs from different organisms into the average virtual MB. GAL4-NP7175 has been shown to selectively label core α/β neurons (Tanaka et al., 2004). The soma of core α/β neurons clustered as four units, and their axon bundles merged beneath the calyx and fasciculated in the middle of the peduncle and lobes (Figure 23A). Spatial mapping of core α/β neurons into the standard virtual MB by automatic morphing should be able to tell if they constantly occupy the same space within the MB.

The newly eclosed flies carrying the genotype *GAL4-NP6115/+; UAS-mCD8/+; 247-LexA::VP16,lexAop-rCD2::GFP/+* were dissected and the image data sets of core α/β neurons within the entire MBs were collected with different channels (Figure 23B). Eight wild-type MBs labeled with *247-LexA::VP16*, in which *GAL4-NP7175*-positive core α/β neurons were differentially marked, were first individually morphed against

standard MB. The *GAL4-NP7175*-positive core α/β neurons (Figure 23C) were then warped into virtual MB with the same matrix (Figure 23D). To examine whether a similar set of voxels were involved after warping, all eight warped *GAL4-NP7175*-positive core α/β neurons were superimposed to the MBs and the use frequencies for individual voxels were calculated, i.e. each voxel was determined how many times were reached. For instance, all the voxels were contained in at least two and five out of eight times, respectively. The frequently shared voxels grossly constituted the entire axon bundles of *GAL4-NP7175*-positive core α/β neurons while the calyx was largely excluded (Figure 23E&F). The results suggested that *GAL4-NP7175*-positive core α/β neuron axons but not dendrites roughly occupy the same space in different MBs. This spatial mapping by automatic morphing would help build a cell-centered MB atlas.

Discussion

Structural studies of the nervous system provide us informative insights about their functions. Examination of structural changes in the nervous system when the organism experiences various environments can help us further identify the structures important for various brain functions. Further investigations of the neuronal connectivity help us understand how various information is transferred and processed. Several computer algorithms have been developed to quantitatively describe the brain structure and neuronal connectivity and they often involve the definition of reference points to generate a standard brain structure for further comparison (Rein, et al., 2002; Jefferis et al., 2007; Lin et al., 2007). Our newly developed algorithm also provides a new tool for the quantitative

description of brain structures, but our method uses automatic computation of point correspondences between a pair of irregular 3D shapes. Because the algorithm does not require any reference for registration process, the contour as well as the interior contents of any 3D object will not be distorted by manually or automatically specified feature correspondences during the morphing procedures. This program can recognize both common and unique features and also provide their quantitative information.

As shown of our MB morphometric analysis, the algorithm successfully creates a virtual standard MB and provides quantitative details of region deviation in the newly eclosed flies (Figure 21 & 22). As expected, the calyx where dendrites are concentrated is the most variable region within the MB, and the peduncle where axons fasciculate as one bundle is much more constant (Figure 22). Our analysis also shows that dorsal lobe which is required for long term memory is very stable while medial lobe which is important for short term memory is highly variable (Zars et al., 2000; Pascual and Preat 2001). Besides, output from different lobes has been shown involved in various stages of memory processing (Krashes et al., 2007). How morphological changes of different lobes relate to different types of memories requires further investigations.

Recent studies indicate that different projection neuron axons tend to form synapses at different domains in the MB calyx (Tanaka et al., 2004; Jefferis et al., 2007; Lin et al., 2007). Knowing if different types of MB neurons form synapses with particular types of PNs will provide insights about how odor information is transferred from the AL to the MB and further processed in the fly brains. However, there exist controversies if different types of MB neuorns target their dendrites to specific domains in the MB calyx

(Tanaka et al., 2004; Jefferis et al., 2007; Lin et al., 2007). The establishment of a virtual standard MB provides us another approach to map each single MBN in the MB. With the newly introduced LexA-based binary transcription system and the widely used MARCM technique, our results show that subsets of MBNs and the entire MB could be independently labeled in the same mosaic organism (Figure 20F-H, Figure 23). Spatial mapping of core α/β neurons in the MB with such dual-expression-control system showed that the axons of core α/β neurons have higher tendency to occupy the same region in the peduncle and lobes, while the dendrites do not have stereotyped projection patterns (Figure 23). The algorithm is currently under the process of improvement to help us to determine whether core α/β neurons tend to target their dendrites to specific domains in the calyx.

The results of the spatial mapping of core α/β neurons in the MB also show the possibility to create a cell-centered MB atlas. By generating serial single-cell MARCM clone at different developmental stages, each neuron should be able to be morphed into the MB with the algorithm and identified their particular spatial location. Such atlas of the MBNs will help to characterize the MBN diversity and provide an important resource for future phenotypic analysis at single-cell resolution to identify the genes involving the generation of neural diversity.

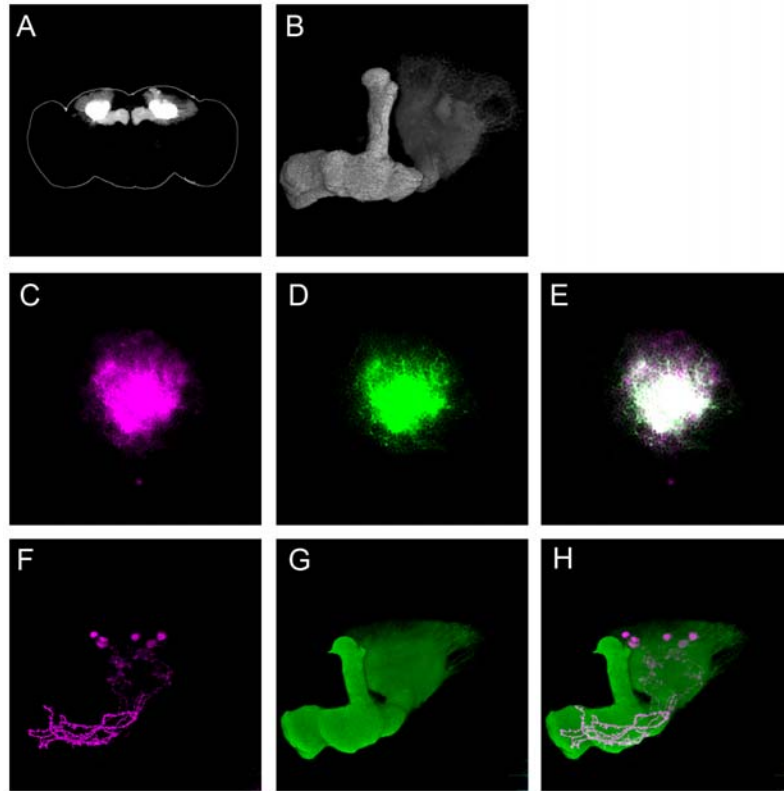


Figure 20. 247-LexA::VP16-labeled mushroom body

(A-B) Stacked confocal images of the expression pattern of *247-LexA::VP16* in the adult *Drosophila* brain (A) and the MB (B). (C-E) Soma of MBNs labeled by *GAL4-OK107,UAS-mCD8* (C) and *247-LexA::VP16, lexAop-rCD2::GFP* (D) in the same brain (E, merged image). (F-H) Independent labeling of *GAL4-OK107*-positive MARCM clone (F) in a *247-LexA::VP16*-positive MB (G) (merged image, H). Dorsal is at the top, medial to the left (B-H).

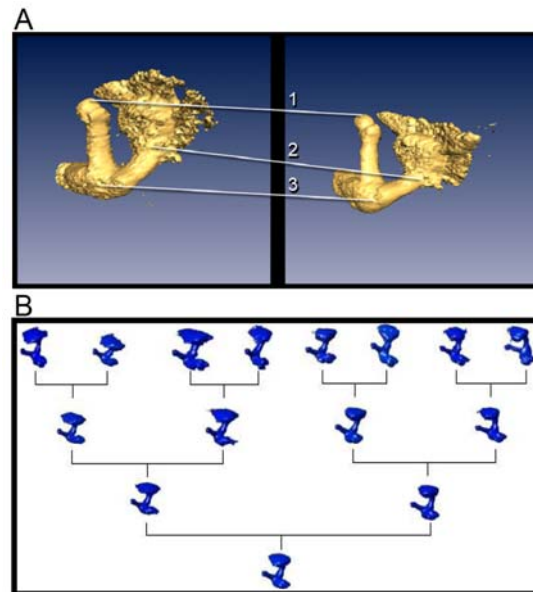


Fig 21. Generation of a virtual standard MB

(A) Visualization of two *247-LexA::VP16*-labeled MBs using AMIRA. Three hypothetical points of correspondences are indicated. (B) Flow chart of computing eight representative MBs (top) to generate the average MB (bottom).

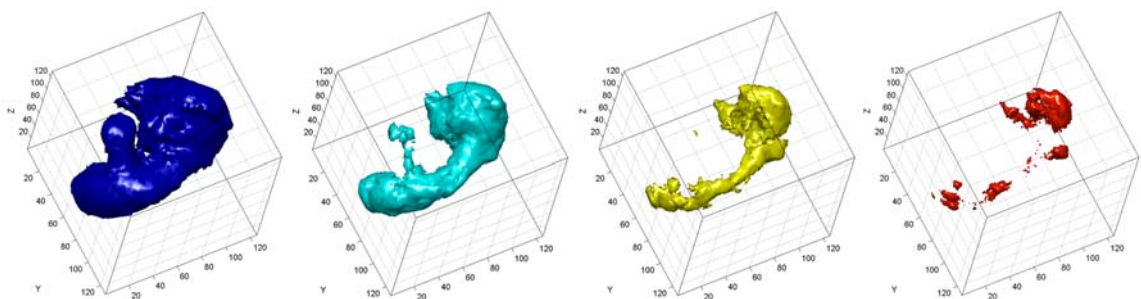


Figure 22. Deviation chart of MB

Various degrees of deviation of average newly eclosed MB are tinted with different colors.

Blue (left) represents the lowest deviation and red (right) shows the highest deviation.

Dorsal is at the top and medial to the left.

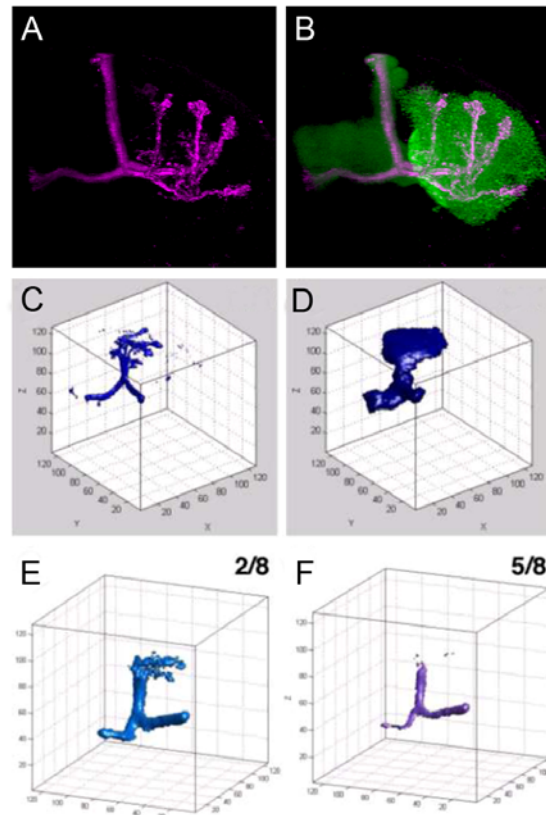


Figure 23. Spatial mapping of core α/β neurons in MBs

(A-D) Representative stacked confocal images of *GAL4-NP7175*-positive core α/β neurons alone (A) and in the presence of *247-LexA::VP16*-labeled MBs (green) (B). (C, D) Average 3D volume of *GAL4-7175*-positive core α/β neurons (C) and *247-LexA::VP16* (D) generated from the confocal images. (E-F) Shared voxels used at least two (E) or five (F) out of eight times when different *GAL4-NP7175*-positive core α/β neurons were warped into virtual average MB.

CHAPTER VI

CONCLUSIONS

Santiago Ramon y Cajal illustrated diverse neuronal morphologies in the organized nervous systems of various species a century ago. Neuroscientists since then are intrigued to investigate the mechanisms governing the generation of neural diversity. Detailed analysis of representative lineages followed by subsequent experimental studies has helped to characterize some cellular and molecular mechanisms in control of neural diversification.

The *Drosophila* olfactory circuitry is composed of diverse neurons and glial cells, and both of them have different functions in olfaction. Incomprehensive cell lineage analysis limits our understanding of the mechanisms to diversify the neurons and glial cells. To facilitate analysis of cell lineages and neural diversity in the olfactory circuitry, a new genetic technique, dual binary transcriptional systems, was developed by combining LexA/lexAop and GAL4/UAS systems. The inductions of GAL4/UAS and LexA/lexAop were comparable in quality and quantity. The incorporation of GAL80-suppressible transcription factor LexA::GAD contributed to the development of dual-expression-control MARCM, which was then used to facilitate the analysis of

complex cell lineages (Chapter II).

The concurrent use of different ALN-GAL4s and tubP-LexA::GAD in the dual-expression-control MARCM helped to characterize ALNs and also determined their lineage relationships. The results of the ALN lineage analyses showed that ALN lineages were first specified by their spatial locations in the CNS when the precursor cells were born. The ALN lineages then used temporal cues to sequentially generate different types of neurons. The lateral lineage further use partitioned Notch signaling to mediate cell-cell interactions between ALN progeny and diversify their cell fates. Many newly identified ALNs also provided new insights of olfaction and shed a light on the study of multisensory integration (Chapter III).

Glial cell lineage analysis by MARCM showed that functionally distinct and spatially distant surface glia and neuropile glia derived from independent lineages. Besides, two types of juxtaposed AL glial cells, simple AL glia and complex AL glia, were also generated by separate glial lineages. Dual-expression-control MARCM further revealed that the glial cells wrapping MBNs and ALNs derived from independent glial lineages. Glial precursor cells were demonstrated to use symmetrical division to proliferate glial cells during development. The model of symmetrical division suggested that the glial cells may not be further diversified by temporal factors and cell-cell interactions (Chapter IV).

To provide another aspect of MBN diversity, an algorithm was developed to perform automatic morphometric analysis to quantitatively describe spatial locations of individual MBNs within the entire MB. Two independent binary transcriptional systems

were introduced to independently label individual MBNs with the MARCM technique and label the entire MB simultaneously. The preliminary results of spatial mapping of core α/β MBNs in the virtual standard MB created by the algorithm demonstrated that axons but not dendrites roughly occupy the same region in the MB (Chapter V).

During the development of *Drosophila* larval cerebrum, estimated 85-100 neuroblasts are actively dividing to generate about 300,000 neurons in the adult fly brain (Strausfeld, 1976; Ito and Hotta, 1992). Several studies have identified the molecular markers for each neuroblast and axonal tracts of each neuropile during development (e.g Urbach and Techanu, 2003; Younossi-Hartenstein et al., 2006; Poreanu and Hartenstein, 2006), and exquisite computer algorithms have also been developed by independent groups to build the standard atlas of the adult fly brain (Rein et al., 2002; Jefferis et al., 2007; Lin et al., 2007). These studies provide us valuable information and useful approaches to characterize neural diversity. In this thesis work, the detailed cell lineage analysis by the MARCM and dual-expression-control MARCM systems and neuronal morphometric analysis by the computer algorithm also show the possibility to identify each neuron up to single cell resolution based on the combination of the morphology, cell marker, spatial location within a neuropile, and connectivity. These newly developed methods greatly facilitate the analysis of neural diversity, and the results establish the foundation for future genetic and molecular experiments to uncover the underlying cellular and molecular mechanisms governing the generation of neural diversity in the *Drosophila* olfactory circuitry.

REFERENCES

- Aigouy B, Van de Bor V, Boeglin M, Giangrande A. (2004). Time-lapse and cell ablation reveal the role of cell interactions in fly glia migration and proliferation. *Development* 131, 5127-5138.
- Akiyama, Y., Hosoya, T., Poole, A. M., and Hotta, Y. (1996). The *gcm*-motif: a novel DNA-binding motif conserved in *Drosophila* and mammals. *Proc. Natl. Acad. Sci. U.S.A.* 93, 14912-14916.
- Akiyama-Oda Y, Hosoya T, Hotta Y. (1999). Asymmetric cell division of thoracic neuroblast 6-4 to bifurcate glial and neuronal lineage in *Drosophila*. *Development* 126, 1967-1974.
- Altenhein, B., Becker, A., Busold, C., Beckmann, B., Hoheisel J.D., and Technau, G.M. (2006). Expression profiling of glial genes during *Drosophila* embryogenesis. *Dev. Biol.* 296, 545-560.
- Anderson, D.J. (1992). Molecular control of neural development. In *An Introduction to Molecular Neurobiology*, Z.W. Hall, ed. (Sunderland, Mass. : Sinauer Associates), pp. 355-387.
- Armstrong, J.D., de Belle, J.S., Wang, Z., and Kaiser, K. (1998). Metamorphosis of the mushroom bodies; large-scale rearrangements of the neural substrates for associative learning and memory in *Drosophila*. *Learn Mem.* 5, 102-114.
- Artavanis-Tsakonas, S., Rand, M.D., and Lake, R.J. (1999). Notch signaling: cell fate control and signal integration in development. *Science* 284, 770-776.
- Awad, T.A., and Truman, J.W. (1997). Postembryonic development of the midline glia in the CNS of *Drosophila*: proliferation, programmed cell death, and endocrine regulation. *Dev. Biol.* 187, 283-297.
- de Belle, J.S., and Heisenberg, M. (1994). Associative odor learning in *Drosophila* abolished by chemical ablation of mushroom bodies. *Science* 263, 692-5.
- Bellaïche, Y., and Schweisguth, F. (2001). Lineage diversity in the *Drosophila* nervous system. *Curr. Opin. Genet. Dev.* 11, 418-423.
- Berdnik D., Chihara, T., Couto, A., and Luo, L. (2006). Wiring stability of the adult *Drosophila* olfactory circuit after lesion. *J. Neurosci.* 26, 3367-3376.
- Bernardoni R, Kammerer M, Vonesch JL, Giangrande A. (1999). Gliogenesis depends on glide/*gcm* through asymmetric division of neuroglioblasts. *Dev. Biol.* 216, 265-275.
- Blair, S.S. (2003). Genetic mosaic techniques for studying *Drosophila* development. *Development* 130, 5065-5072.
- Bourbon, H.M., Gonzy-Treboul, G., Peronnet, F., Alin, M.F., Ardourel, C., Benassayag, C., Cribbs, D., Deutsch, J., Ferrer, P., Haenlin, M., Lepasant, J.A., Noselli, S., and Vincent, A. (2002). A P-insertion screen identifying novel X-linked essential genes in *Drosophila*. *Mech. Dev.* 110, 71-83.
- Brand, A.H., and Perrimon, N. (1993). Targeted gene expression as a means of altering cell fates and generating dominant phenotypes. *Development* 118, 401-415.
- Brent, R., and Ptashne, M. (1985). A eukaryotic transcriptional activator bearing the DNA specificity of a

- prokaryotic repressor. *Cell* 43, 729-736.
- Calleja, M., Moreno, E., Pelaz, S., and Morata, G. (1996). Visualization of gene expression in living adult *Drosophila*. *Science* 274, 252-255.
- Certel, S.J., Clyne, P.J., Carlson, J.R., and Johnson, W.A. (2000). Regulation of central neuron synaptic targeting by the *Drosophila* promoter, Acj6. *Development* 127, 2395-2405.
- Cherbas, L., Hu, X., Zhimulev, I., Belyaeva, E., and Cherbas, P. (2003). EcR isoforms in *Drosophila*: testing tissue-specific requirements by targeted blockade and rescue. *Development* 130, 271-284.
- Colonques, J., Ceron, J., and Tejedor, F.J. (2007). Segregation of postembryonic neuronal and glial lineages inferred from a mosaic analysis of the *Drosophila* larval brain. *Mech. Dev.* 124, 327-340.
- Connolly, J.B., Roberts, I.J., Armstrong, J.D., Kaiser, K., Forte, M., Tully, T., and O'Kane, C.J. (1996). Associative learning disrupted by impaired Gs signaling in *Drosophila* mushroom bodies. *Science* 274, 2104-2107.
- Couto, A., Akenius, M., and Dickson, B.J. (2005). Molecular, anatomical, and functional organization of the *Drosophila* olfactory system. *Curr. Biol.* 15, 1535-1547.
- Crittenden, J.R., Skoulakis, E.M., Han, K.A., Kalderon, D., and Davis, R.L. (1998). Tripartite mushroom body architecture revealed by antigenic markers. *Learn. Mem.* 5, 38-51.
- Davis, R.L. (1993). Mushroom bodies and *Drosophila* learning. *Neuron* 11, 1-14.
- Dearborn, R., Jr., and Kunes, S. (2004). An axon scaffold induced by retinal axons directs glia to destinations in the *Drosophila* optic lobe. *Development* 131, 2291-2303.
- Doe, C.Q. and Technau, G.M. (1993). Identification and cell lineage of individual neural precursors in the *Drosophila* CNS. *Trends Neurosci.* 16, 510-514.
- Doe, C.Q., and Goodman, C.S. (1985a). Early events in insect neurogenesis: I. Development and segmental differences in the pattern of neuronal precursor cells. *Devl. Biol.* 111, 193-205.
- Doe, C.Q., and Goodman, C.S. (1985b). Early events in insect neurogenesis: II. The role of cell interactions and cell lineage in the determination of neuronal precursor cells. *Devl. Biol.* 111, 206-219.
- Duffy, J.B. (2002). GAL4 system in *Drosophila*: A fly geneticist's swiss army knife. *Genesis* 34, 1-15.
- Edenfeld, G., Altenhein, B., Zierau, A., Cleppien, D., Krukkert, K., Technau, G., and Klambt, C. (2007). Notch and Numb are required for normal migration of peripheral glia in *Drosophila*. *Dev Biol.* 301, 27-37.
- egger, B., Leemans, R., Loop, T., Kammermeier, L., Fan, Y., Radimerski, T., Strahm, M.C., Certa, U., and Reichert, H. (2002). Gliogenesis in *Drosophila*: genome-wide analysis of downstream genes of *glial cells missing* in the embryonic nervous system. *Development* 129, 3295-3309.
- Endo, K., Aoki, T., Yoda, Y., Kimura, K., and Hama, C. (2007). Notch signal organizes the *Drosophila* olfactory circuitry by diversifying the sensory neuronal lineages. *Nat. Neurosci.* 10, 153-160.

- Estojak, J., Brent, R., and Golemis, E.A. (1995). Correlation of two-hybrid affinity data with in vitro measurements. *Mol. Cell Biol.* *15*, 5820-5829.
- Frank, E., and Sanes, J.R. (1991) Lineage of neurons and glia in chick dorsal root ganglia: analysis in vivo with a recombinant retrovirus. *Development* *111*, 895-908.
- Freeman, M.R., Delrow, J., Kim, J., Johnson, E., and Doe, C.Q. (2003). Unwrapping glial biology: Gcm target genes regulating glial development, diversification, and function. *Neuron* *38*, 567-580.
- Freeman, M.R., and Doe, C.Q. (2001). Asymmetric Prospero localization is required to generate mixed neuronal/glial lineages in the *Drosophila* CNS. *Development* *128*, 4103-4112.
- Freeman, M.R., and Doherty, J. (2006). Glial cell biology in *Drosophila* and vertebrates. *Trends Neurosci.* *29*, 82-90.
- Gao, Q., Yuan, B., and Chess, A. (2000). Convergent projections of *Drosophila* olfactory neurons to specific glomeruli in the antennal lobe. *Nat Neurosci* *3*, 780-785.
- Giangrande, A. (1996). Development and organization of glial cells in *Drosophila melanogaster*. *Int. J. Dev. Biol.* *40*, 917-927.
- Gimlich, R.L. and Cooke, J. (1983). Cell lineage and the induction of a second nervous system in amphibian development. *Nature* *306*, 471-473.
- Godement, P., Vanselow, J., Thanos, S., and Bonhoeffer, F. (1987). A study in developing visual systems with a new method of staining neurones and their processes in fixed tissue. *Development* *101*, 697-713.
- Golic, K.G., and Lindquist, S. (1989). The FLP recombinase of yeast catalyzes site-specific recombination in the *Drosophila* genome. *Cell* *59*, 499-509.
- Goulding, S.E., zur Lage, P., and Jarman, A.P. (2000). *amos*, a proneural gene for *Drosophila* olfactory sense organs that is regulated by *lozenge*. *Neuron*, *25*, 69-78.
- Greenwald., I. (1985). The genetic analysis of cell lineages in *Caenorhabditis elegans*. *Phil. Trans. R. Soc. Lond. B* *312*, 129-137.
- Guétat, G., Maitre, M., Joly, L., Lai, S.-L., Lee, T., and Shinagawa, Y. (2006). Automatic 3D grayscale volume matching and shape analysis. *IEEE Trans. Inf. Technol. Biomed.* *10*, 362-76.
- Guo, M., Jan L.Y., and Jan, Y.N. (1996). Control of daughter cell fates during asymmetric division: interaction of numb and notch. *Neuron*, *17*, 27-41.
- Hallem, E.A., and Carlson, J.R. (2004). The odor coding system of *Drosophila*. *Trends Genet.* *20*, 453-459.
- Hay, B. A., Wolff, T., and Rubin, G.M. (1994). Expression of baculovirus P35 prevents cell death in *Drosophila*. *Development* *120*, 2121-2129
- Heisenberg, M., Borst, A., Wagner, S., and Byers, D. (1985). *Drosophila* mushroom body mutants are deficient in olfactory learning. *J. Neurogenet.* *2*, 1-30.
- Hosoya, T., Takizawa, K., Nitta, K., and Hotta, Y. (1995). *glial cells missing*: a binary switch between neuronal and glial determination in *Drosophila*. *Cell* *82*, 1025-1036.

- Isshiki, T., Pearson, B., Holbrook, S., and Doe, C.Q. (2001). *Drosophila* neuroblasts sequentially express transcription factors which specify the temporal identity of their neuronal progeny. *Cell*, *106*, 511-521.
- Ito, K., Awano, W., Suzuki, K., Hiromi, Y., and Yamamoto, D. (1997a). The *Drosophila* mushroom body is a quadruple structure of clonal units each of which contains a virtually identical set of neurones and glial cells. *Development* *124*, 761-771.
- Ito, K., and Hotta, Y. (1992). Proliferation pattern of postembryonic neuroblasts in the brain of *Drosophila melanogaster*. *Dev. Biol.* *149*, 134-148.
- Ito, K., Sass, H., Urban, J., Hofbauer, A., and Schneuwly, S. (1997b). GAL4-responsive UAS-tau as a tool for studying the anatomy and development of the *Drosophila* central nervous system. *Cell Tissue Res.* *290*, 1-10.
- Ito, K., Urban, J., and Technau, G.M. (1995). Distribution, classification, and development of *Drosophila* glial cells in the late embryonic and early larval ventral nerve cord. *Roux's Arch. Dev. Biol.* *204*, 284-307.
- Jacobs, J.R., Hiromi, Y., Patel, N.H., and Goodman, C.S. (1989). Lineage, migration, and morphogenesis of longitudinal glia in the *Drosophila* CNS as revealed by a molecular lineage marker. *Neuron* *2*, 1625-1631.
- Jacobson, M., and Hirose, G. (1978). Origin of the retina from both sides of the embryonic brain: A contribution to the problem of crossing over at the optic chiasma. *Science* *202*, 637-639.
- Jefferis, G.S., and Hummel, T. (2006). Wiring specificity in the olfactory system. *Semin. Cell Dev. Biol.* *17*, 50-65.
- Jefferis, G.S.X.E., Marin, E.C., Stocker, R.F., and Luo, L. (2001). Target neuron prespecification in the olfactory map of *Drosophila*. *Nature* *414*, 204-208.
- Jefferis, G.S.X.E., Potter, C.J., Chan, A.M., Marin, E.C., Rohlfsing, T., Maurer, C.R., and Luo, L. (2007). Comprehensive maps of fly higher olfactory centres: spatially segregated fruit and pheromone representation. *Cell* *128*, 1187-203.
- Jessell, T.M., and Sanes, J.R. (2000). The generation and survival of nerve cells. In *Principles of Neural Science* 4/e, E.R. Kandel, J.H. Schwartz, and T.M. Jessell, ed. (New York : McGraw-Hill, Health Professions Division), pp. 1041-1062.
- Jhaveri, D., Sen, A., Reddy, G.V., and Rodrigues, V. (2000). Sense organ identity in the *Drosophila* antenna is specified by the expression of the proneural gene *atonal*. *Mech. Dev.* *99*, 101-111.
- Jones, B.W. (2001). Glial cell development in the *Drosophila* embryo. *Bioessays* *23*, 877-887.
- Jones, B.W., Fetter, R.D., Tear, G., and Goodman, C.S. (1995). *glial cells missing*: a genetic switch that controls glial versus neuronal fate. *Cell* *82*, 1013-1023.
- Jones, W.D., Cayirlioglu, P., Kadow, I.G., and Vosshall, L.B. (2007). Two chemosensory receptors together mediate carbon dioxide detection in *Drosophila*. *Nature* *445*, 86-90.

- Kamikouchi, A., Shimada, T., and Ito, K. (2006). Comprehensive classification of the auditory sensory projections in the brain of the fruit fly *Drosophila melanogaster*. *J. Comp. Neurol.* *20*, 317-356.
- Karcavich, R.E. (2005). Generating neuronal diversity in the *Drosophila* central nervous system: a view from the ganglion mother cells. *Dev. Dyn.* *232*, 609-616.
- Karcavich, R.E., and Doe, C.Q. (2005). *Drosophila* neuroblast 7-3 cell lineage: a model system for studying programmed cell death, Notch/Numb signaling, and sequential specification of ganglion mother cell identity. *J. Comp. Neurol.* *481*, 240-251.
- Kidd, S., Lockett, T.J., and Young, M.W. (1983). The Notch locus of *Drosophila melanogaster*. *Cell* *34*, 421-433.
- Kidd, S., Lieber, T., and Young, M.W. (1998). Ligand-induced cleavage and regulation of nuclear entry of Notch in *Drosophila melanogaster* embryos. *Genes Dev.* *12*, 3728-3740.
- Klambt, C., Hummel, T., Granderath, S., and Schimmelpfeng, K. (2001). Glial cell development in *Drosophila*. *Int. J. Dev. Neurosci.* *19*, 373-378.
- Klambt, C., Hummel, T., Menne, T., Sadlowski, E., Scholz, H., and Stollewerk, A. (1996). Development and function of embryonic central nervous system glial cells in *Drosophila*. *Dev. Genetics* *18*, 40-49.
- Komiyama, T., Johnson, W., Luo, L., and Jefferis, G.S.X.E. (2003). From lineage to wiring specificity: POU domain transcription factors control precise connections of *Drosophila* olfactory projection neurons. *Cell* *112*, 157-67.
- Komiyama, T., and Luo, L. (2007). Intrinsic control of precise dendritic targeting by an ensemble of transcription factors. *Curr. Biol.* *17*, 278-85.
- Krashes, M.J., Keene, A.C., Leung, B., Armstrong, J.D., and Waddell, S. (2007). Sequential use of mushroom body neuron subsets during *Drosophila* odor memory processing. *Neuron* *53*, 103-15.
- Kwon, J.Y., Dahanukar, A., Weiss, L.A., and Carlson, J.R. (2007). The molecular basis of CO₂ reception in *Drosophila*. *Proc. Natl. Acad. Sci. U. S. A.* *104*, 3574-8.
- Laemmli U.K. (1970). Cleavage of structural proteins during the assembly of the head of bacteriophage T4. *Nature* *227*, 680-685.
- Lai, S.-L., and Lee, T. (2006). Genetic mosaic with dual binary transcriptional systems in *Drosophila*. *Nat. Neurosci.* *9*, 703-709.
- Laisue, P.P., Reiter, C., Hiesinger, P.R., Halter, S., Fischbach, K.F., and Stocker, R.F. (1999). Three-dimensional reconstruction of the antennal lobe in *Drosophila melanogaster*. *J. Comp. Neurol.* *405*, 543-552.
- Lee, T., Marticke, S., Sung, C., Robinow, S., and Luo, L. (2000a). Cell-autonomous requirement of the USP/EcR-B ecdysone receptor for mushroom body neuronal remodeling in *Drosophila*. *Neuron* *28*, 807-818.

- Lee, T., Lee, A., and Luo, L. (1999). Development of the *Drosophila* mushroom bodies: sequential generation of three distinct types of neurons from a neuroblast. *Development* 126, 4065-4076.
- Lee, T., and Luo, L. (1999). Mosaic analysis with a repressible cell marker for studies of gene function in neuronal morphogenesis. *Neuron* 22, 451-461.
- Lee, T., and Luo, L. (2001). Mosaic analysis with a repressible cell marker (MARCM). for *Drosophila* neural development. *Trends Neurosci.* 24, 251-254.
- Lee, T., Winter, C., Marticke, S.S., Lee, A., and Luo, L. (2000b). Essential roles of *Drosophila* RhoA in the regulation of neuroblast proliferation and dendritic but not axonal morphogenesis. *Neuron* 25, 307-316.
- Lin, H.H., Lai, J.S., Chin, A.L., Chen, Y.C., and Chiang, A.S. (2007). A Map of Olfactory Representation in the *Drosophila* Mushroom Body. *Cell* 128, 1205-1218.
- Liu, L., Wolf, R., Ernst, R., and Heisenberg, M. (1999). Context generalization in *Drosophila* visual learning requires the mushroom bodies. *Nature* 400, 753-6.
- Lohs-Schardin, M., Sander, K., Cremer, C., Cremer, T., and Zorn, C. (1979). Localized ultraviolet laser microbeam irradiation of early *Drosophila* embryos: fate maps based on localization and frequency of adult defects. *Devl. Biol.* 68, 533-545.
- Lu, B., Jan, L., and Jan YN. (2000). Control of cell divisions in the nervous system: symmetry and asymmetry. *Annu. Rev. Neurosci.* 23, 531-556.
- Lundell, M.J., Lee, H.K., Pérez, E., and Chadwell, L. (2003). The regulation of apoptosis by Numb/Notch signaling in the serotonin lineage of *Drosophila*. *Development* 130, 4109-4121.
- Luo, L. (2007). Fly MARCM and mouse MADM: Genetic methods of labeling and manipulating single neurons. *Brain Res. Rev.* [in press].
- Ma, J., and Ptashne, M. (1987). The carboxy-terminal 30 amino acids of GAL4 are recognized by GAL80. *Cell* 50, 137-142.
- MacDonald, J.M., Beach, M.G., Porpiglia, E., Sheehan, A.E., Watts, R.J., and Freeman, M.R. (2006). The *Drosophila* cell corpse engulfment receptor Draper mediates glial clearance of severed axons. *Neuron* 15, 869-81
- Manseau, L., Baradaran, A., Brower, D., Budhu, A., Elefant, F., Phan, H., Philp, A.V., Yang, M., Glover, D., Kaiser, K., Palter, K., and Selleck, S. (1997). GAL4 enhancer traps expressed in the embryo, larval brain, imaginal discs, and ovary of *Drosophila*. *Dev. Dyn.* 209, 310-322.
- Marin, E.C., Jefferis, G.S., Komiyama, T., Zhu, H., and Luo, L. (2002). Representation of the glomerular olfactory map in the *Drosophila* brain. *Cell* 109, 243-255.
- Masuda-Nakagawa, L.M., Tanaka, N.K., and O'Kane, C.J. (2005). Stereotypic and random patterns of connectivity in the larval mushroom body calyx of *Drosophila*. *Proc Natl Acad Sci U S A.* 102, 19027-19032.

- McGuire, S.E., Le, P.T., and Davis, R.L. (2001). The role of *Drosophila* mushroom body signaling in olfactory memory. *Science* 293, 1330-1333.
- Ng, J., and Luo, L. (2004). Rho GTPases regulate axon growth through convergent and divergent signaling pathways. *Neuron* 44, 779-93.
- Oland LA, Pott WM, Higgins MR, Tolbert LP (1998). Targeted ingrowth and glial relationships of olfactory receptor axons in the primary olfactory pathway of an insect. *J. Comp. Neurol.* 398, 119-138.
- Olsen, S.R., Bhandawat, V., and Wilson, R.I. (2007). Excitatory interactions between olfactory processing channels in the *Drosophila* antennal lobe. *Neuron* 54, 89-103.
- Orban, P.C., Chui, D., and Marth J.D. (1992). Tissue- and site-specific DNA recombination in transgenic mice. *Proc. Natl. Acad. Sci. U.S.A.* 89, 6861-6865.
- Otsuna, H., and Ito, K. (2006). Systematic analysis of the visual projection neurons of *Drosophila melanogaster*. I. Lobula-specific pathways. *J. Comp. Neurol.* 497, 928-958.
- Pascual, A., and Preat, T. (2001). Localization of long-term memory within the *Drosophila* mushroom body. *Science* 294, 1115-1117.
- Pearson, B.J., and Doe, C.Q. (2003). Regulation of neuroblast competence in *Drosophila*. *Nature* 425, 624-628.
- Pereanu, W., and Hartenstein, V. (2006). Neural lineages of the *Drosophila* brain: a three-dimensional digital atlas of the pattern of lineage location and projection at the late larval stage. *J. Neurosci.* 26, 5534-5553.
- Pereanu, W., Shy, D., and Hartenstein, V. (2005). Morphogenesis and proliferation of the larval brain glia in *Drosophila*. *Dev. Biol.* 283, 191-203.
- Ptashne, M. (1988). How eukaryotic transcriptional activators work. *Nature* 335, 683-689.
- Reddy, G.V., Gupta, B., Ray, K., and Rodrigues, V. (1997). Development of the *Drosophila* olfactory sense organs utilizes cell-cell interactions as well as lineage. *Development*, 124, 703-712.
- Rein, K., Zöckler, M., Mader, M.T., Grübel, C., and Heisenberg, M. (2002). The *Drosophila* standard brain. *Curr. Biol.* 12, 227-231.
- Robinow, S., and White, K. (1991). Characterization and spatial distribution of the ELAV protein during *Drosophila melanogaster* development. *J. Neurobiol.* 22, 443-461.
- Sanes, J.R. (1989) Analyzing cell lineage with a recombinant retrovirus. *Trends Neurosci.* 12, 21-28.
- Sepp, K.J., and Auld, V.J. (1999). Conversion of lacZ enhancer trap lines to GAL4 lines using targeted transposition in *Drosophila melanogaster*. *Genetics* 151, 1093-1101.
- Schudt, A., and Brand, A. (1999). Mastermind acts downstream of notch to specify neuronal cell fates in the *Drosophila* central nervous system. *Dev. Biol.* 205, 287-295.
- Skeath J.B., and Doe, C.Q. (1998). Sanpodo and Notch act in opposition to Numb to distinguish sibling neuron fates in the *Drosophila* CNS. *Development* 125, 1857-1865.

- Shang, Y., Claridge-Chang, A., Sjulson, L., Pypaert, M., and Miesenböck, G. (2007) Excitatory local circuits and their implications for olfactory processing in the fly antennal lobe. *Cell* 128, 601-612.
- Shiga, Y., Tanaka-Matakatsu, M., and Hayashi, S. (1996). A nuclear GFP/ beta-galactosidase fusion protein as a marker for morphogenesis in living *Drosophila*. *Dev. Growth Diffn.* 38, 99-106.
- Spana E.P., and Doe, C.Q. (1996) Numb antagonizes Notch signaling to specify sibling neuron cell fates. *Neuron* 17, 21-26.
- Spradling, A.C., and Rubin, G.M. (1982). Transposition of cloned P elements into *Drosophila* germ line chromosomes. *Science* 218, 341-347.
- Sternberg, P.W., and Horvitz, H.R. (1984). The genetic control of cell lineage during nematode development. *Ann. Rev. Genet.* 18, 489-524.
- Stocker, R.F., Lienhard, M.C., Borst, A., and Fischbach, K.F. (1990). Neuronal architecture of the antennal lobe in *Drosophila melanogaster*. *Cell Tissue Res.* 262, 9-34.
- Stocker, R.F. (1994). The organization of the chemosensory system in *Drosophila melanogaster*: a review. *Cell Tissue Res.* 275, 3-26.
- Stocker, R.F., Tissot, M., and Gendre, N. (1995). Morphogenesis and cellular proliferation pattern in the developing antennal lobe of *Drosophila melanogaster*. *Roux's Arch. Dev. Biol.* 205, 62-72.
- Stocker, R.F., Heimbeck, G., Gendre, N., and de Belle., J.S. (1997). Neuroblast ablation in *Drosophila* P[GAL4] lines reveals origins of olfactory interneurons. *J. Neurobio.* 32, 443-456.
- Strausfeld, N.J. (1976). Atlas of an insect brain. Berlin: Springer.
- Strausfeld, N.J., Sinakevitch, I., and Vilinsky, I. (2003). The mushroom bodies of *Drosophila melanogaster*: an immunocytological and golgi study of Kenyon cell organization in the calyces and lobes. *Microsc. Res. Tech.* 62, 151-69
- Sulston, J.E., Schierenberg, E., White, J.G., and Thomson, J.N. (1983). Embryonic cell lineage of the nematode *Caenorhabditis elegans*. *Devl. Biol.* 100, 64-119.
- Suster, M.L., Martin, J.R., Sung, C., and Robinow, S. (2003). Targeted expression of tetanus toxin reveals sets of neurons involved in larval locomotion in *Drosophila*. *J. Neurobiol.* 55, 233-246.
- Szuts, D., and Bienz, M. (2000). LexA chimeras reveal the function of *Drosophila* Fos as a context-dependent transcriptional activator. *Proc. Natl. Acad. Sci. U. S. A.* 97, 5351-5356.
- Taghert, P.H., and Goodman, C.S. (1984). Cell determination and differentiation of identified serotonin-immunoreactive neuron in the grasshopper embryo. *J. Neurosci.* 4, 989-1000.
- Tanaka, N.K., Awasaki, T., Shimada, S., and Ito, K. (2004). Integration of chemosensory pathways in the *Drosophila* second-order olfactory centers. *Curr. Biol.* 14, 449-457.
- Tix, S., Eule, E., Fischbach, K.F., and Benzer, S. (1997). Glia in the chiasmata and medulla of the *Drosophila melanogaster* optic lobes. *Cell Tissue Res.* 289, 397-409.

- Triezenberg, S.J., Kingsbury, R.C., and McKnight, S.L. (1988). Functional dissection of VP16, the trans-activator of herpes simplex virus immediate early gene expression. *Genes Dev.* 2, 718-729.
- Truman, J., and Bate, M. (1988). Spatial and temporal patterns of neurogenesis in the central nervous system of *Drosophila melanogaster*. *Dev. Biol.* 125, 145-157.
- Udolph, G., Rath, P., and Chia, W. (2001). A requirement for Notch in the genesis of a subset of glial cells in the *Drosophila* embryonic central nervous system which arise through asymmetric divisions. *Development*, 128, 1457-1466.
- Uemura, T., Shepherd, S., Ackerman, L., Jan, L.Y., and Jan, Y.N. (1989). *numb*, a gene required in determination of cell fate during sensory organ formation in *Drosophila* embryos. *Cell* 58, 349-360.
- Underwood, E.M., Caulton, J.H., Allis C.D., and Mahowald, A.P. (1980) Developmental fate of pole cells in *Drosophila melanogaster*. *Devl. Biol.* 74, 286-301.
- Urbach, R., and Technau, G.M. (2003). Molecular markers for identified neuroblasts in the developing brain of *Drosophila*. *Development* 130, 3621-3637.
- Vaysse, P.J.-J., and Goldman, J.E. (1990). A clonal analysis of glial lineages in neonatal forebrain development *in vitro*. *Neuron* 5, 227-235.
- Vojtek, A.B., Hollenberg, S.M., and Cooper, A.J. (1993). Mammalian Ras interacts directly with the serine/threonine kinase Raf. *Cell* 74, 205-214.
- Vosshall, L.B., Wong, A.M., and Axel, R. (2000). An olfactory sensory map in the fly brain. *Cell* 102, 147-159.
- Wang, J., Ma, X., Yang, J.S., Zheng, X., Zugates, C.T., Lee, C.-H.J., and Lee, T. (2004). Transmembrane/juxtamembrane domain-dependent Dscam distribution and function during mushroom body neuronal morphogenesis. *Neuron* 43, 663-672.
- Wang, J., Zugates, C.T., Liang, I.H., Lee, C.H., and Lee, T. (2002). *Drosophila* Dscam is required for divergent segregation of sister branches and suppresses ectopic bifurcation of axons. *Neuron* 33, 559-571.
- Wang, J.W., Wong, A.M., Flores, J., Vosshall, L.B., and Axel, R. (2003). Two-photon calcium imaging reveals an odor-evoked map of activity in the fly brain. *Cell* 112, 271-282.
- Weisblat, D.A., Sawyer, R.T., Stent, G.S. (1978). Cell lineage analysis by intracellular injection of a tracer. *Science* 202, 1295-1298.
- Wilson, R.J., and Laurent, G. (2005). Role of GABAergic inhibition in shaping odor-evoked spatiotemporal patterns in the *Drosophila* antennal lobe. *J. Neurosci.* 25, 9069-9079.
- Wong, A.M., Wang, J.W., and Axel, R. (2002). Spatial representation of the glomerular map in the *Drosophila* protocerebrum. *Cell* 109, 229-241.
- Xiong, W.C., and Montell, C. (1995). Defective glia induce neuronal apoptosis in the *repo* visual system of *Drosophila*. *Neuron* 14, 581-590.

- Xu, T., and Rubin, G.M. (1993). Analysis of genetic mosaics in developing and adult *Drosophila* tissues. *Development* *117*, 1223-1237.
- Yang, M.Y., Armstrong, J.D., Vilinsky, I., Strausfeld, N.J., and Kaiser, K. (1995). Subdivision of the *Drosophila* mushroom bodies by enhancer-trap expression patterns. *Neuron* *15*, 45-54.
- Yao, C.A., Ignell, R., and Carlson, J.R. (2005). Chemosensory coding by neurons in the coeloconic sensilla of the *Drosophila* antenna. *J. Neurosci.* *25*, 8359-8367
- Yeh, E., Gustafson, K., and Boulianne, G.L. (1995). Green fluorescent protein as a vital marker and reporter of gene expression in *Drosophila*. *Proc. Natl. Acad. Sci. U. S. A.* *92*, 7036-7040.
- Younossi-Hartenstein, A., Nguyen, B., Shy, D., and Hartenstein, V. (2006). Embryonic origin of the *Drosophila* brain neuropile. *J Comp, Neurol.* *497*, 981-998.
- Zars, T., Fischer, M., Schulz, R., and Heisenberg, M. (2000). Localization of a short-term memory in *Drosophila*. *Science* *288*, 672-675.
- Zheng, X., Wang, J., Haerry, T.E., Wu, A.Y., Martin, J., O'Connor, M.B., Lee, C.H., and Lee, T. (2003). TGF- β signaling activates steroid hormone receptor expression during neuronal remodeling in the *Drosophila* brain. *Cell* *112*, 303-315.
- Zhu, S., Chiang, A.S., and Lee, T. (2003). Development of the *Drosophila* mushroom bodies: elaboration, remodeling and spatial organization of dendrites in the calyx. *Development* *130*, 2603-2610.
- Zhu, S., Lin, S., Kao, C.-F., Awasaki, T., Chiang, A.-S., and Lee, T. (2006). Gradients of the *Drosophila* chinmo BTB-zinc finger protein govern neuronal temporal identity. *Cell* *127*, 409-422
- Zong, H., Espinosa, J.S., Su, H.H., Myzumdar, M.D., and Luo, L. (2005). Mosaic analysis with double markers in mice. *Cell* *121*, 479-492.
- Zugates, C.T., and Lee, T. (2004). Genetic mosaic analysis in the nervous system. *Curr. Opin. Neurobiol.* *14*, 647-653.

APPENDIX

The following work is reprinted from the IEEE Transactions of Information Technology in Biomedicine article as titled “Automatic 3D grayscale volume matching and shape analysis” published on April, 2006 (Guétat et al., 2006). The work and the body of the text were done by the group lead by Dr. Yoshihisa Shinagawa.

Overview of the algorithm

In this algorithm, the mapping between the two volumes is computed according to a multiresolutional and multifiltering approach. We use the maximum, minimum and the averaging filters to capture the characteristics of the objects at coarser resolution levels and to construct multiresolution hierarchies for each 3D object. We also compute edge intensities along each direction at the different levels of resolution. The corresponding point of each voxel is then chosen by minimizing an energy function. It is essential to compute the point correspondences at different levels of resolution to make the computation feasible: rough point correspondences found at coarse levels allow us to limit the search extent efficiently at finer levels.

A. Global registration

Even if this approach handles large and plastic displacements, it cannot compensate for global motions which include large rotations. Such global motions often happen when object poses are unknown during scanning. Estimating them directly in the optimization procedure would lead to a major increase in computational time due to the overwhelming dimension of the search space.

Instead, we propose to compensate for global motions using a preprocessing step. A

set of very sparse correspondences is found, either using the isolation measure or object segmentation, from which an affine motion is computed. This motion model is simple, easily invertible and versatile enough to register the two objects.

B. Critical-point filters for constructing multiresolution hierarchy

As stated previously, voxel intensities may differ from image to image due to, for example, different conditions of staining samples. It is known that linear filters, such as Gaussian filter, smooth out features at coarse resolution levels and make it difficult to find correct point correspondences.

For example, a Gaussian filter changes the brightness and the positions of pixels with peak intensities, which leads to wrong point correspondences. For this reason, to be robust against such changes, we employ the nonlinear Critical-Point Filters (CPF) to locate the critical points such as peaks, pits and saddle points of pixels intensities in the objects at coarser resolution levels. To limit the amount of computation, we chose to use only the peak and pit filters (out of the eight possible critical-point filters) in association with the linear averaging filter to compensate for the fact that peak and pit filters are more noise-sensitive. This combination well balances the noise-sensitivity while preserving salient features. We use these three intensity filters to construct multiresolution pyramids.

C. Multiresolutional and multifiltering approach

The mapping is computed according to a multiresolution and multifiltering framework. It consists of a succession of mappings computed between the objects resulting from the different filters and resolutions. The algorithm starts by mapping the volumes at the lowest resolution; having a small number of voxels, the number of

possible mappings is extremely low. Then, it calculates a mapping at the next finer level of resolution. At each level, the order in which the filters are applied is permuted to equally consider each characteristic of the objects. The correspondences found in one mapping are then used to constrain the computation and guide the next mapping.

D. Mapping of a voxel: energy minimization

The algorithm uses the correspondences established by the previous mapping to define a limited search area for the corresponding position of each voxel in the next mapping. This region is called the *inherited volume* and contains a small number of voxels. To find the best match, the algorithm computes a weighted sum of several energies taking into account the previous mappings, intensity difference and edge intensities, and the general smoothness of the mapping for each destination voxel in this inherited volume. The resulting correspondence is the one whose total energy is the minimum.

E. Refinement using the inverse mapping

A pair of volumes are mapped bidirectionally. The inverse mapping is useful to correct errors of point correspondences in the forward direction (from the first volume to the second); *i.e.*, the backward mapping (from the second volume to the first) should be in the opposite direction of the forward mapping unless there are errors or occlusions. For this purpose, we compute the forward and backward mappings f and g independently first, and then we refine them taking both mappings into account, to obtain more reliable correspondences.

The algorithm in details

A. Global registration

The goal of global registration is to estimate an affine motion which compensates for the possibly different poses of the matched objects. Nevertheless, this preprocessing step is not always necessary, especially when the pose of the volumes is already known, like in CT or MR volumes, or when the volumes differ widely in shape, where a global registration would be meaningless. The global registration is however very meaningful regarding volumes with similar shapes obtained using confocal microscopes because these cannot determine the pose of the objects. Finding the characteristics of the affine transformation requires the extraction of at least four correspondence pairs.

Indeed, an affine transformation is fully characterized by a 3×3 matrix (for rotation, dilation and shear) along with a 3×1 vector (for translation), *i.e.* 12 unknowns total; the 12 equations needed to solve for these unknowns are provided by the four correspondence pairs, each pair providing three equations (one equation for each dimension). When we have more than four correspondence pairs, we solve for these unknowns in a Minimum Norm Least Square (MNLS) sense. The affine transformation, defined by a matrix A and a translation vector t , is then applied in the following way:

$$\begin{pmatrix} x_{preproc} \\ y_{preproc} \\ z_{preproc} \end{pmatrix} = \begin{pmatrix} a_{11} & a_{12} & a_{13} \\ a_{21} & a_{22} & a_{23} \\ a_{31} & a_{32} & a_{33} \end{pmatrix} \begin{pmatrix} x_{ini} \\ y_{ini} \\ z_{ini} \end{pmatrix} + \begin{pmatrix} t_x \\ t_y \\ t_z \end{pmatrix}$$

with

$$I_{preproc} \begin{pmatrix} x_{preproc} \\ y_{preproc} \\ z_{preproc} \end{pmatrix} = I_{ini} \begin{pmatrix} x_{ini} \\ y_{ini} \\ z_{ini} \end{pmatrix}$$

where $I_{preproc}$ and I_{ini} are the intensity values in the preprocessed object and the initial object respectively.

We propose two different techniques to extract points of interest in the volumes, one using the isolation measure, the other based on segmentation using the Expectation-Minimization (EM) Algorithm. The former is applicable to any kinds of volumes and is robust against big variations of shapes; the latter provides more precise results but requires that the volumes to be mapped can be approximated by sets of ellipsoids. The correspondences between the extracted points can then be done either manually, or more interestingly using a standard LS criterion or *a priori* information about the volumes.

1) *Isolation measure*: The isolation measure is the average distance from a given point to all the points of the object (it was originally defined for object surfaces). Thus, a point close to the object center has a low isolation measure whereas a point close to an extremity of the object will have a high isolation measure. This paper proposes the expansion of the isolation measure for grayscale volumes. The mathematical definition of the proposed isolation measure μ of a given voxel \vec{v} is:

$$\mu(\vec{v}) = \frac{\int_X w(\vec{v}, \vec{p}) d_{min}(\vec{v}, \vec{p}) d\vec{p}}{\int_X w(\vec{v}, \vec{p}) d\vec{p}}$$

$$w(\vec{v}, \vec{p}) = \frac{1}{|I(\vec{v}) - I(\vec{p})| + 1}$$

$$d_{min}(\vec{v}, \vec{p}) = \min_{all\ paths\ P} \sum_{i=0}^{N_P-1} d(\vec{v}_i, \vec{v}_{i+1})$$

where \vec{v}_i 's are located on the path P from $\vec{v}_0 = \vec{v}$ to $\vec{v}_{N_P} = \vec{p}$ (N_P is the number of voxels on the path P from \vec{v} to \vec{p}). Thus, the function returns $d_{min}(\vec{v}, \vec{p})$ the shortest distance between every pair of points \vec{v} and \vec{p} in the volume X . $I(\vec{v})$ is the voxel intensity at point \vec{v} . The distance d between \vec{v} and neighboring point \vec{v}_1 in the coordinate lattice is defined by

$$d(\vec{v}, \vec{v}_1) = \alpha |I(\vec{v}) - I(\vec{v}_1)| + \|\vec{v} - \vec{v}_1\|$$

where $\|\vec{v} - \vec{v}_1\|$ is the Euclidean distance between \vec{v} and \vec{v}_1 .

We implement a discrete version of this algorithm. When we set the intensity of voxels located on the surface to 1 and the intensity of other points to 0, *i.e.*:

$$I(\vec{v}) = \begin{cases} 1 & \vec{v} \in Surface \\ 0 & otherwise \end{cases},$$

and make α approach ∞ , so that a path going through zerovoxels will also have a length approaching ∞ , this isolation measure coincides with that of the previous work defined for object surfaces.

Finally, by considering the local extrema of the isolation measure in the object, we can define several characteristic points. Regarding two similar objects, these points are consistent and can be used to define the affine transformation we are looking for. Therefore, we do not need to use any *a priori* information about the shape of the volumes to be mapped. An example of the isolation measure for objects called *mushroom bodies* (located in fly brains) is displayed in Figure 1.

Algorithm 1 Gaussian mixture estimation

inputs: K, K_{goal} (if known), $\{P(\omega_k)\}, \{\mu_k\}, \{\Sigma_k\}, \{\vec{p}_i\}$
while MML criterion not satisfied or $K > K_{goal}$ **do**
 while \mathcal{L} decreases and not too many iterations **do**
 $\forall (k, i), P(\omega_k | \vec{p}_i) = \frac{1}{Z_{0i}} \mathcal{N}(\mu_k, \Sigma_k)(\vec{p}_i) P(\omega_k)$
 $\forall k, P(\omega_k) = \frac{1}{Z_1} \max(0, \sum_i P(\omega_k | \vec{p}_i) - 9)$
 Remove ellipsoids with $P(\omega_k) \approx 0$
 $\mathcal{L} = \sum_i \log Z_{0i}$
 $\forall k, \mu_k = \frac{1}{Z_{2k}} \sum_i P(\omega_k | \vec{p}_i) \vec{p}_i$
 $\forall k, \Sigma_k = \frac{1}{Z_{2k}} \sum_i P(\omega_k | \vec{p}_i) (\vec{p}_i - \mu_k)(\vec{p}_i - \mu_k)^t$
 Remove component with smallest $P(\omega_k)$

2) *Object segmentation*: When objects can be approximated by sets of ellipsoids, as it is for instance the case with mushroom bodies, rough correspondences required for global registration can be obtained by matching ellipsoids between volumes and pairing their centers and extremities, based on their relative dimensions and relative locations.

The ellipsoidal approximation is recasted into a Gaussian mixture model estimation, which is solved using the modified Expectation-Maximization (EM) algorithm. The standard EM algorithm tends to converge to local minima, which makes its initialization critical. To alleviate this issue, Figueiredo and Jain proposed to cover the space by more ellipsoids than necessary and remove the less likely ones until the Minimum Message Length (MML) criterion is satisfied. When the object geometry is roughly known a-priori, like it is the case with mushroom bodies, it is better to remove ellipsoids until a predefined number of them is reached; this avoids the problem of having to reduce the number of ellipsoids in both volumes to a common number at the end of the algorithm. The algorithm is detailed in Algorithm 1 where p_i denotes the i^{th} voxel coordinates, $P(\omega_k)$ the probability of the Gaussian component ω_k , μ_k its mean, Σ_k its covariance matrix, K the number of ellipsoids, K_{goal} the final number of ellipsoids and L the data loglikelihood. The normalizing constants Z_{0i} , Z_l and Z_{2k} are defined such that $\sum_k P(\omega_k|\vec{p}_i) = 1$, $\sum_k P(\omega_k) = 1$, and $\sum_i P(\omega_k|\vec{p}_i) = 1$ respectively. The 3-dimensional Gaussian probability distribution function has the classical equation

$$\mathcal{N}_{(\mu_k, \Sigma_k)}(\vec{p}_i) = \frac{1}{\sqrt{(2\pi)^3 |\Sigma_k|}} e^{-\frac{1}{2}(\vec{p}_i - \mu_k)^t \Sigma^{-1} (\vec{p}_i - \mu_k)}$$

The process is initialized by assuming that all ellipsoids are equiprobable, *i.e.* . The $P(\omega_k) = \frac{1}{K}$ set of voxel coordinates $\{\vec{p}_i\}$ is obtained by thresholding voxel intensities.

Ellipsoids are initialized by spheres, *i.e.* $\{\Sigma_k = \sigma_k \times I\}$ where I is the identity matrix and σ_k is a positive scalar. Their centers $\{\mu_k\}$ and scalars $\{\sigma_k\}$ are chosen so that the volume is evenly covered.

Figure 2 shows the major steps of such a process. The final segmentation is obtained by assigning classes to voxels in a maximum likelihood fashion.

We have proposed in this section two different algorithms to segment 3D volumes and extract points of interest from them, so as to be able to perform a global registration. The method based on the EM algorithm uses the assumption that the objects can be approximated by sets of ellipsoids, like it is the case for the mushroom bodies. Using such information about the shape of the objects improves the quality of the registration. However, we can not always make such assumptions, and in such cases the use of the segmentation based on the isolation measure is recommended. A comparison of the results can be seen in Figure 3.

B. Filtering using CPFs and edge detection

To recognize global structures within 3D data, a great number of multiresolutional filters have been proposed. They are classified into two groups: linear filters and nonlinear filters. The former have a long history and include the Fourier transformation, Gaussian filter, or wavelets. Such filters are equivalent to convolving the data with discretized kernels. However, when used for image matching (2D or 3D), linear filters blur extrema, making their location ambiguous and modifying their intensity. Moreover, linear filters filter out textured regions, thus losing precious information. Thus, we use nonlinear filters called the Critical Point Filters (CPF). These filters preserve intensities and locations of critical point of the 3D volumes while reducing the resolution at the same time. We can define eight critical-point filters to detect minima, maxima and saddle points but we restrain our work to the pit and peak filters because of the large amount of data we already have to deal with using only these two filters.

The maximum (or peak) filter compares eight voxels in a cube of size $2 \times 2 \times 2$, and chooses the voxel with maximum intensity. The minimum (or pit) filter is similar

except that it chooses the minimum. Both filters reduce the resolution by a factor of two along each direction and keep the brightness of the critical points. However, because the CPFs rely on computation of minima and maxima, they are sensitive to noise, especially at coarsest levels. Therefore we also use an averaging filter, less noise-sensitive, to keep information on the global shape of our volumes. The introduction of this standard linear filter well balances the noise-sensitivity while CPFs preserve salient features. At the lowest resolutions especially, the volumes obtained using the averaging filter convey more information than those obtained using CPFs, which might have a very low Signal to Noise Ratio.

All the three filters generate a coarser lattice by grouping eight voxels at the original resolution into a single voxel: the latter is called the parent and its coordinates are given by:

$$parent(i, j, k) = \overline{(i, j, k)} = \left(\left\lfloor \frac{i}{2} \right\rfloor, \left\lfloor \frac{j}{2} \right\rfloor, \left\lfloor \frac{k}{2} \right\rfloor \right)$$

where $\lfloor i \rfloor$ is the largest integer that does not exceed i . Its intensity depends on the filter we are currently using. Three multiresolution pyramids are constructed by applying the maximum, minimum and the averaging filters to the input volumes recursively. Edges are also an important part of the information contained in volumes. They give us a general shape and are often well located and may be defined very precisely. To compute the edge intensity, a Sobel-like 3D edge detector [32] is applied to the pyramid obtained by the averaging filter. This detector provides three values of edge intensity corresponding to each direction:

$$E = \frac{1}{16} H * I$$

where I is the 3D volume and H is one of the following filters:

$$H_x(:, :, \pm 1) = \begin{pmatrix} -1 & 0 & 1 \\ -1 & 0 & 1 \\ -1 & 0 & 1 \end{pmatrix}, H_x(:, :, 0) = \begin{pmatrix} -1 & 0 & 1 \\ -8 & 0 & 8 \\ -1 & 0 & 1 \end{pmatrix}$$

H_z and H_y are obtained from H_x by permuting the directions.

C. Inherited volume

In what follows, we call the first volume the *source* volume and the second the *destination* volume following the tradition of. The subvolume of the destination object in which the correspondence is searched (we call it the *inherited volume*) is defined as the bounding box containing all the correspondents of its neighboring voxels found at the previous mapping (Figure 4). This definition is straightforward when the previous mapping has been calculated at the same resolution. When we change the level of resolution, we need to estimate the position of the corresponding voxels at the current resolution level with a coarser mapping. The estimation can be done with the following formula where $f(i, j, k)$ is the corresponding 3D position in the fine lattice we are looking for and $f_p(i, j, k)$ is the original corresponding position found by the previous mapping (coarser resolution):

$$f(i, j, k) = f_p(\overline{(i, j, k)}) + f_p(\overline{(i, j, k) + (1, 1, 1)})$$

$$f(i, j, k) = f_p(\lfloor \frac{i}{2} \rfloor, \lfloor \frac{j}{2} \rfloor, \lfloor \frac{k}{2} \rfloor) + f_p(\lfloor \frac{i+1}{2} \rfloor, \lfloor \frac{j+1}{2} \rfloor, \lfloor \frac{k+1}{2} \rfloor)$$

D. Scanning Order

The mapping is computed according to a multiresolution and multifiltering framework. It consists of a succession of mappings computed between the objects resulting from the different filters and resolutions. The algorithm starts by mapping the volumes at the lowest resolution; having a small number of voxels, the number and the complexity of possible mappings are extremely low. Then, it will keep finding the point correspondences at the next finer level of resolution. At each level, the order in which the filters are applied has to be permuted to equally consider each characteristic

of the objects. Indeed, we avoid scanning them always in the same order so that all filters have an equal importance. Scanning them always first with the pit filter and then with the peak filter, for instance, would give much more weight to the pit filter. Correspondences found in one mapping are then used to constrain the computation and guide the following mapping. The same observation is made to scan the voxels of each filtered image. The first voxels scanned have indeed more freedom to move than the last ones, so keeping a unique scan order would give too much weight to the first ones. As voxels along edges are often easier to map and convey most of the information about the optical flow, we map the voxels according to the descending order of their edge intensity. The first voxels to be mapped are located at the object frontiers and are less constrained by the smoothness energy term compared with the voxels in the flat areas that are mapped afterward. This approach improves the mapping especially in the case where the positions of the two objects are quite different. More precisely, we classify the voxels into four groups of equal population according to their edge intensity, defined as the L^2 norm of the gradients along the three dimensions. The algorithm starts by mapping the voxels inside the first group (with high edge intensity), one after the other, following monotonic variations of the coordinates, then it does the same thing with the second group, and so on. By not respecting the exact descending order, we avoid the situation where the scanning is too scattered spatially. Just note that we still map the borders to themselves to initialize the algorithm.

E. Energy of the forward mappings

The algorithm can use the correspondences established by the precedent submapping to define a limited search area for the corresponding position of each

voxel. This region is called the inherited volume. To find the best match, the algorithm computes several energies taking into account the precedent mappings, the difference of brightness and edge intensities, and the general smoothness of the mapping for each destination voxel in this inherited volume. The resulting correspondence is the one whose total energy is the minimum. For the forward mapping f from the source object to the destination object and its inverse g , an energy is first computed for each destination voxel in the inherited volume, and then the candidate with the minimum energy is chosen. This energy is defined as a weighted sum of different energies taking into account all the measurements calculated on the 3D objects and the previous mapping.

The first group of energy terms consists of the differences of each measure between the candidate destination voxel \vec{q} and the source voxel \vec{p} the intensity (or brightness) obtained either from the minimum, maximum or averaging filter

$$E_I = |I_1(\vec{p}) - I_2(\vec{q})|,$$

and the edge intensities

$$E_E = \frac{1}{3} (|E_{x_1}(\vec{p}) - E_{x_2}(\vec{q})| + |E_{y_1}(\vec{p}) - E_{y_2}(\vec{q})| + |E_{z_1}(\vec{p}) - E_{z_2}(\vec{q})|)$$

where E_x , E_y and E_z are the edge intensities. The energy related to the smoothness of the mapping compares the movements of the neighboring voxels with the movement of the voxel to be mapped. Some of its neighbors are already mapped (set V_m) and the other half not yet (set V_n). We will consequently consider the previous mapping to compute their movements but the energy due to these movements will be weighted by $\alpha_n < 1$ to take into account the lack of precision:

$$E_S = \frac{1}{\#(V_m)} \left(\sum_{i \in V_m} |(\|\vec{p} - \vec{q}\| - \|\vec{p}_i - f(\vec{p}_i)\|)| \right) + \frac{\alpha_n}{\#(V_n)} \sum_{i \in V_n} |(\|\vec{p} - \vec{q}\| - \|\vec{p}_i - g(\vec{p}_i)\|)|$$

where f and g are the current and previous mappings, and $\#(V)$ is the number of voxels in V .

We also define an energy related to the Euclidean distance between the candidate voxel and the corresponding destination voxel found at the previous mapping f_p to transmit the information from the previous mapping to the next mapping:

$$E_D = \|\vec{q} - f_p(\vec{p})\|$$

For E_S and E_D , two cases arise when considering the former mapping: it was calculated either at the same resolution with a different filter or at the coarser level of resolution. For the latter, we extend the correspondence found at the coarser level to the current resolution. Finally, we weight these different energies. In particular, the smoothness and distance energies are based on Euclidean distances: their weight is halved each time the algorithm goes to a finer level of resolution because the physical distances are doubled. The final energy is given by:

$$E_T = \alpha_I E_I + \alpha_E E_E + \alpha_D E_D + \alpha_S E_S.$$

As said previously, for each voxel of the source volume, the total energy is computed for each candidate voxel in the inherited area of the destination volume, and the one with minimum energy is chosen as the corresponding point to the current point in the source volume. The parameters α_I , α_E , α_D and α_S are multiplicative coefficients that enable to add energies with very different meanings and units (distance, intensity, gradient magnitude); their values are chosen to balance the characteristics they correspond to.

F. Refining the mappings

As the forward mapping may not be perfect, we want to refine it by using the backward mapping. The inverse mapping is useful to correct errors of point correspondences; *i.e.*, in theory, the backward mapping should be in the opposite direction of the forward mapping unless there are errors or occlusions. To check this,

we compute the forward and backward mappings f and g , and we then refine them to obtain more reliable correspondences for each mapping. We consider all the voxels of the inherited volume again and compute a refinement energy as the sum of two distances; the first one is simply the Euclidean distance between the candidate voxel \vec{q} and the correspondent $f(\vec{p})$ chosen by the forward mapping. The second one uses the backward mapping to compute the distance between the current source voxel \vec{p} to be mapped and the corresponding voxel $g(\vec{q})$ of the destination candidate voxel in the source object. If the correspondence is correct, the two mappings should be similar and this distance be small. Otherwise, it shows that there are errors. The resulting mappings f' and g' are computed by choosing the destination voxel with the minimum refinement energy within the inherited volume as is shown in Figure 6. Thus, the final correspondence is obtained by minimizing the cost energy:

$$E_R = \|\vec{q} - f(\vec{p})\| + \|\vec{p} - g(\vec{q})\| .$$

G. Oversampling

As the two objects are not identical, it is impossible to obtain a one-to-one mapping; *i.e.*, we cannot find correspondences from all the source voxels to all the destination voxels. For this reason, we oversample the voxel grid with a factor of two in the destination object, *i.e.*, allowing the source voxel to be mapped to intermediate half-integer positions between the existing destination voxels. The measurements (brightness and edge intensity) and their movements are expanded by linear interpolation. However, we add a penalty to the total energy of the correspondence in this case so that the source voxel is mapped to an intermediate position only when the intensity difference is significant. Contrary to the weights in the computation of the total energy, this penalty is not a multiplicative constant but an offset added to the total energy.

H. Occlusions

The portions of an object that exist in one volume but do not in the other volume are called *occlusions*. Currently, we handle occlusions in the following way: if voxels in the source volume are occluded in the destination volume, those voxels are mapped to a small portion in the destination volume. In other words, those voxels are squeezed. This is acceptable due to two factors: first, the smoothness energy leads to the fact that these occluded voxels are not randomly mapped but instead have the same correspondents as their neighbors; second, the number of voxels occluded is usually very small compared to the number of voxels in the volume.

I. Undoing the registration

We have to be careful with the fact that, in most cases, we use registered images as inputs for our algorithm. Thus, in order to obtain the mapping between our two original volumes, we have to undo the registration, which is feasible as we used an affine transformation, invertible, to do the registration. The mapping between the two preprocessed volumes is characterized by a 3D array V of motion vectors $\vec{v}_{i,j,k}$ which is of same size as the input volumes. Each vector describes the difference of position between the source voxel $\vec{p} = (i\ j\ k)^T$ and its correspondent $\vec{q} = f(\vec{p}) = (i_{dest}\ j_{dest}\ k_{dest})^T$, *i.e.* $\vec{v}_{i,j,k} = \vec{q} - \vec{p}$. Then, given that we used the affine transformation defined by the matrix A and the translation vector \vec{t} to process the destination volume, the new move vector for voxel \vec{p} is given by:

$$\vec{v}_{new} = (A^{-1} - I) \vec{p} - A^{-1} (\vec{v}_{i,j,k} + \vec{t})$$

J. Shape and volume analysis

Once we have obtained the standard volume, average of a given group of similar objects, we want to conduct an analysis on how much each object in the group differs from the standard one. In order to achieve this goal, we need to define a new plasticity measure, which describes how plastic a region of the volume is. When comparing two objects, this measure corresponds to how different the first one is from the second one according to the mapping, after global motion compensation. That is, we compute the mapping f between the two volumes, and we also compute an affine transformation A which will compensate for the global motion. In order to compute the affine transformation, we can reuse the segmentation or the isolation measure studied previously which gave us some characteristic points of the objects. Then, the measure of plasticity is defined as follows for each nonzero voxel:

$$m_{plasticity}(\vec{p}) = \|f(\vec{p}) - A(\vec{p})\|^2 \quad \text{with} \quad \vec{p} = \begin{pmatrix} i \\ j \\ k \end{pmatrix}$$

With this definition, we can detect which parts of the volumes are the most plastic and have a quantitative measure of their plasticity; indeed, even if the plasticity is computed independently for each voxel, whole neighborhoods will appear to have a higher plasticity. This phenomenon can be emphasized by applying a lowpass filter to the volume to keep track only of the main differences in plasticity between the different parts of the volume.

Then, from this definition, we can try to determine which parts of the object are the most plastic within a given group of volumes. In order to do this, we have to map the average object with each of the volumes, compute the plasticity in each case, and finally compute the average plasticity.

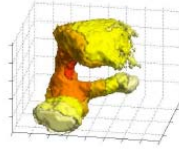


Fig. 1. Isolation measure (yellow: high, red: low).

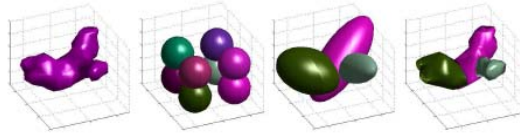


Fig. 2. Example of object segmentation: mushroom body without calyx (a), initial Gaussian mixture (isosurfaces at 3σ) (b), final mixture (same isosurfaces) (c), and segmentation (d).

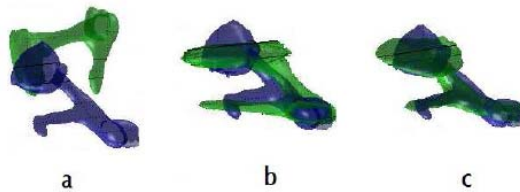


Fig. 3. Comparison of global registration techniques: a - volumes before registration b - after registration using the isolation measure c - after registration based on the EM algorithm.

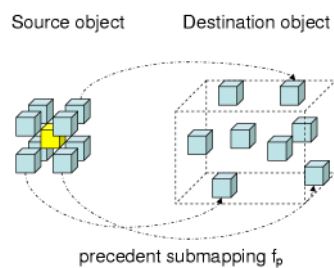


Fig. 4. Inherited Volume.

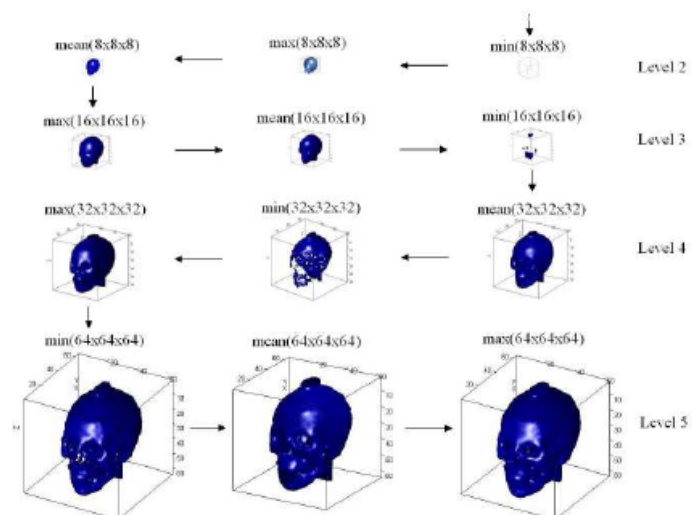


Figure 5. A Mapping Process.

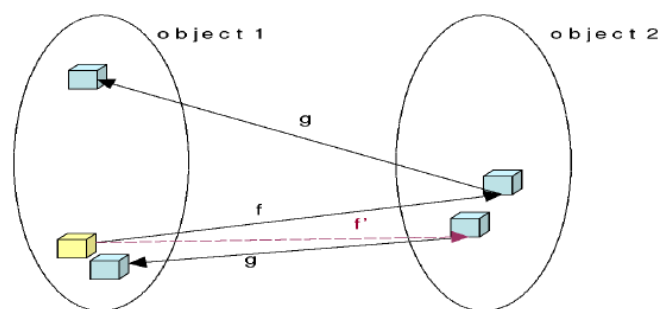


Fig. 6. Refinement by modifying f to f'